THE PETROLOGY OF BASEMENT ROCKS AND ASPECTS OF GOLD MINERALIZATION IN KUTCHERI AREA, WONAKA SCHIST BELT, NORTHWESTERN NIGERIA.

By

Abdulgafar Kayode AMUDA, BSc GEOLOGY (UNILORIN), 2005
(M.Sc./Scie/00568/2009-2010)

A THESIS SUBMITTED TO THE SCHOOL OF POSTGRADUATE STUDIES, AHMADU BELLO UNIVERSITY, ZARIA; IN PARTIAL FULFILMENT OF THE REQUIREMENTS FOR THE AWARD OF AMASTER OF SCIENCE DEGREE IN GEOLOGY

DEPARTMENT OF GEOLOGY
FACULTY OF SCIENCE
AHMADU BELLO UNIVERSITY, ZARIA
NIGERIA

MAY, 2014

DECLARATION

I declare that the work in this thesis entitled “The petrology of basement rocks and aspects of gold mineralization in Kutcheri area, Wonaka schist belt, northwestern Nigeria” has been carried out by me in the Department of Geology, Ahmadu Bello University, Zaria. The information derived from the literature has been duly acknowledged in the text and a list references provided. No part of this thesis was previously presented for another degree or diploma at this or any other Institution.

Name of Student	Signature	Date

CERTIFICATION

This thesis entitled **"**THE PETROLOGY OF BASEMENT ROCKS AND ASPECTS OF GOLD MINERALIZATION IN KUTCHERI AREA, WONAKA SCHIST BELT, NORTHWESTERN NIGERIA" by AMUDA, ABDULGAFAR KAYODE meets the regulations governing the award of the degree of Master of Science of the Ahmadu bello University, Zaria, and is approved for its contribution to knowledge and literary presentation.

(Name)	(Signature)	Date
Chairman, Supervisory Committee (Name)	(Signature)	Date
Member, Supervisory Committee (Name)	(Signature)	Date
Head of Department (Name)	(Signature)	Date
Dean, School of Postgraduate Studies (Name)	(Signature)	Date

ACKNOWLEDGEMENTS

Foremost, I give thanks to uncreated creator (ALLAH) of all that exist. Moreover, I would like to express my indebtedness to the following staff of the Department of Geology, Ahmadu Bello University, Zaria:

The Head of Department, Prof. U.A. Danbatta for facilitating the Vice Chancellors approval for me to undertake this postgraduate study and for allowing me to use field mapping and laboratory facilities of the Department.

My supervisors Prof. U.A. Danbatta and Dr. T. Najime for their mentorship in the undertaking of this project. They were instrumental to title and painstakingly corrected, edited, constructively criticized and proffer solution to lapses in the work.

All staff that expressed memorable support while hospitalized for my recent automobile accident that necessitated differing an academic session.

Lecturers Prof. E.C. Ike, Prof. U.A. Danbatta, Dr. E.A. Bala, Dr. E. Ikpokonte, Dr. P.O. Ogunleye, Dr. T. Najime, Dr. A.A. Ibrahim for impacting knowledge during my course work.

Technical staffs Mr. E. Animashawun, Mr. J.O. Eka, Mr. R. Lamja, Mr J. Yashe, Mr. U. Muhammed and Mr. K. Ishaku who provided support at various stages of the project.

Mr. S.M. Elaktipo for constructive discussions and putting me through the basics of use of GCD toolkit for my geochemical analysis.

Mr. S. Ekwuribe, Manager of Multi-User Science Research Laboratory, ABU, Zaria and Mal. B. Musa for help with laboratory facilities for sample pre-treatment and analysis.

My heartfelt gratitude also goes to my parents Mr. and Mrs. H.K. Amuda for their patience, understanding and support both financially and morally. Same goes to my siblings Mr. F. Adam, Mr. M. Abubakar, Mr. L. Shuaib and Mrs. D. Memunat. Other family members like uncle(s) Mr. Y. Abdulganeey and Mr. Y. Zakariyyah for their financial support, Mr. Y. Salihu, Mr. Y.

Abdulraheem are deeply appreciated. Also, my dear cousins Mr. Y. Ibrahim for being my field assistance on my 3rd trip, Miss. Y. Rashidat, Mr. O. Nazeemdeen and others.

My resounding gratitude goes to my wife Mrs. T.R. Sanni and my three precious and dear gifts from Allah, Mal. A. Abdullah, Hajiya A. Maryam and Hajiya A. Aasiya. I would not have been able to get this far with this work safe their understanding and support. I deeply appreciate your invaluable contributions. It will not be too much to have your names as author on cover page safe for obvious reasons.

My profound gratitude geos to senior colleagues in the Department of Geology and Centre for Energy Research and Training, Dr. V. Obiosio and Dr. P.O. Ogunleye for their consistent, unalloyed career advice. Also, Dr. A.A. Ibrahim and Mal. S.S. Magaji for their help during my seminar presentation and project proposal.

Am also grateful to Village Head Gidan Chido and Kutcheri who accommodated me and supported during field work. Also Mal. M. Abdullahi, Head of Kutcheri Co-operative and Mining for granting me unreserved access to their mining sites.

I give thanks to my dear friend Mr. A. Akeem for his assistance during my reconnaissance field work with his car. Also, Mr. A. Rasheed and Mr. J. Kamaldeen for being my field assistance on second trip. My in-law in Alberta, Canada, Mr. A.K. Sanni that facilitated payment for my geochemical analysis in ACME laboratories. Professional colleagues Mr. W.T. Andongma, Mr. U.J Adoze, Mr. I. Mustapha and Miss. J.U. Akoh for their contribution and encouragement.

Finally, I wish to thank all those people that have assisted in one way or another but their names are not mentioned.

ABSTRACT

The study area forms part of the Precambrian to Early Paleozoic Nigerian Basement complex. Multispectral images from Landsat 7 ETM+ were utilized to complement lithological mapping, elucidate lineaments and clearly outline alteration zones.

Field mapping in Faskari and Chafe was carried out using topographical map of Funtua NW sheet 78 on a scale 1: 50, 000 and the area of gold mineralization around Kutcheri were further mapped on a scale of 1: 25, 000 to study it in more detail. Petrographic studies of 16 samples were conducted using transmitted light microscope. The geochemical analysis of 10 representative samples for major and trace elements was carried out using X-ray fluorescence technique, inductively coupled sector field mass spectrometry. Also, 13 quartz vein samples were analysed for target (Au) and pathfinder elements (Pb, Hg, Cu, Ag and Zn) using Atomic Absorption Spectrophotometer.

The dominant rock types are gneisses, metasediments, granites and serpentinite with minor quartz-tourmaline rock, aplite dyke, quartzofeldspathic and quartz veins. Petrographic studies have shown that the gneisses include banded gneiss, porphyroblastic and granite gneiss that mainly composed of quartz, feldspar, biotite ± pyroxene. The metasediments include biotite schist and phyllite that are composed of quartz, biotite, feldspar, ± muscovite, ± chlorite. The granites include medium to coarse grained to porphyritic varieties and are mainly composed of quartz, feldspar and biotite.

These rocks have been deformed; sheared with joints and foliation. The dominant foliation trend NNE-SSW to NE-SW, follows the general trend of structures resulting from Pan-African Orogeny. Traces of other trend directions thought to be pre-Pan African are also observed.

Exfoliation and tectonic joints with non-orthogonal joint pattern are observed. Both dextral and sinistral strike slip faults are observed on granites. Folds mainly had NNE-SSW axial trend.

Geochemical analyses results show that SiO_2 in gneisses range from 72.2-64.2 wt.%, and metasediments from 68.5-58.0 wt.%. The K_2O in gneisses ranges from 5.32-1.52 wt.% and metasediments from 5.42-1.98 wt.%. The Na_2O is generally higher in gneisses 5.18-3.39 wt.% than in the metasediment 3.35-0.71 wt.%. The CaO content of all lithologies overlaps (1.07-2.86 wt%) except for phyllite (0.61 wt%). The alkali and alkali earth elements are enriched in the gneisses with Sr varying from 574.0-103.1 ppm, Rb from 336.9-67.6 ppm and Ba from 1415-215 ppm compared with the metasediments with Sr varying from 213.1-60.0 ppm, Rb from 170.4-58.9 ppm and Ba from 1155-419.0 ppm respectively. Similar trend occurred in rare earth element being significantly enriched in the gneisses with La from 392.3-14.2 ppm, Ce from 690.5-29.0 ppm, Eu from 2.55-0.74 ppm and Lu from 0.72-0.15 than in the metasediments with La from 29.0-20.2 ppm, Ce from 60.3-41.8 ppm, Eu from 1.31-1.08 and Lu from 0.50-0.36 ppm respectively.

Moderate to high mobility of alkali elements K and Na confirms low grade metamorphism for the metasediments (greenschist facies) and low to medium grade for the gneisses (greenschist to lower amphibolite facies). The gneisses are of igneous parentage except granite gneiss that may be sedimentary. The gneisses have granitic to granodioritic composition related to granite that originated from magma enriched in alumina relative to alkalis. Paleoweathering estimates point to relatively moderate to intense chemical weathering of the metasedimentary source rocks that are immature.

Normalised trace element shows a striking parallelism with upper continental crust for the metasediments while the gneisses are more evolved. Relative depletion of HREE and enrichment of LREE with significant negative Eu anomaly in the gneisses and metasediments shows that plagioclase feldspar fractionates. Negative Ce anomaly in granite gneiss indicates absence of zircon while negative Ce anomaly characteristics of the metasediments indicates anoxic to suboxic condition during metamorphism.

Alluvial/elluvial gold grains with pristine, modified and reshaped morphology occur in sediments while primary gold mineralization is presumed to occur in quartz veins. Geochemical investigation for target (Au) and some pathfinder elements (Pb, Hg, Cu, Ag and Zn) show Au concentration to range between < 1-4.8 ppm, Pb (<2-28 ppm), Hg (<0.5 ppm), Cu (6.2 to 61.4 ppm), Ag (<0.5 ppm) and Zn (8.8 to 39 ppm). There is no significant statistical difference between the Au, Pb, Cu, Ag and Zn content in Dutsen Burka and Gidan Boss area. Pearson correlation coefficient shows Cu and Pb are indicator elements for Au in the area.

TABLE OF CONTENTS

TITLE **PAGE**

Title page……i

Declaration……..ii

Certification……iii

Acknowledgement……..iv

Abstract……...vi

Table of contents……ix

List of Tables……...xiv

List of Figures……..xv

List of Plates……xviii

List of Appendices……..xxv

List of Maps……xxvi

CHAPTER ONE

GENERAL INTRODUCTION..... 1

1.1 THE NIGERIAN BASEMENT COMPLEX 1

1.2 LOCATION AND ACCESSIBILITY 3

1.3 RELIEF AND DRAINAGE..... 4

1.4 CLIMATE AND VEGETATION..... 4

1.5 PREVIOUS WORK 5

1.6 PRESENT WORK 6

1.6.1 Aim and Objectives..... 6

1.7 JUSTIFICATION OF STUDY 7

1.8 MATERIALS AND METHODS 7
1.8.1 Preamble 7
1.8.2 Remote Sensing Interpretation 7
1.8.3 Fieldwork and Sampling 9
1.8.4 Panning 10
1.8.5 Map Digitization 10
1.8.6 Laboratory Analysis 10
1.8.7 Data Interpretation 11

CHAPTER TWO

REGIONAL GEOLOGY 12
2.1 PREAMBLE 12
2.2 NIGERIAN BASEMENT COMPLEX 12
2.2.1 Lithology 12
2.2.2 Evolution of the Nigerian Basement 18
2.2.3 Structures 19
2.2.4 Geochemistry 20
2.2.5 Sediment maturity and Source area weathering of metasediments 22
2.2.6 Gold Mineralization 24

CHAPTER THREE

REMOTE SENSING AND SPECTRAL ANALYSIS 27
3.1 PREAMBLE 27
3.2 DIGITAL ELEVATION MODEL 27
3.3 BAND RATIOING 29

3.4 COLOUR COMPOSITES 31
3.4.1 Chica-Olmo ratio 31
3.4.2 Kaufmann ratio 32
3.5 AUTOMATIC LINEAMENTS EXTRACTION 33

CHAPTER FOUR

FIELD GEOLOGY, PETROGRAPHY AND STRUCTURES 37
4.1 PREAMBLE 37
4.2 PORPHYROBLASTIC GNEISS AND GRANITE GNEISS 39
4.2.1 Field relationships 39
4.2.2 Petrography of Porphyroblastic Gneiss 39
4.3 BANDED GNEISS 42
4.3.1 Field relationships 42
4.3.2 Petrography of banded gneiss 43
4.4 BIOTITE SCHIST 46
4.4.2 Petrography of biotite schist 46
4.5 PHYLLITE 50
4.5.1 Field relationships 50
4.5.2 Petrography of phyllite 51
4.6 PORPHYRITIC BIOTITE GRANITE 52
4.6.1 Field relationships 52
4.6.2 Petrography of porphyritic biotite granite 54
4.7 MEDIUM-COARSE GRAINED BIOTITE GRANITE 56
4.7.1 Field relationship 56
4.7.2 Petrography of medium-coarse grained biotite granite 56

4.8 SERPENTINITE 57
4.8.1 Field relationships 57
4.8.2 Petrography of serpentinite 58
4.9 MINOR LITHOLOGIES 59
4.9.1 Field relationships 59
4.10 SUPERFICIAL DEPOSITS 60
4.10.1 Laterites 60
4.10.2 Alluvium deposit 61
4.11 STRUCTURES 62
4.11.1 Foliation 62
4.11.2 Joints 64
4.11.3 Faults 67
4.11.4 Folds 68

CHAPTER FIVE

GEOCHEMISTRY 70
5.1 MAJOR ELEMENTS DISTRIBUTION IN THE GNEISSES AND METASEDIMENTS 70
5.2 TRACE ELEMENT DISTRIBUTION IN GNEISSES AND METASEDIMENTS 72
5.3 RARE EARTH ELEMENTS DISTRIBUTION IN GNEISSES AND METASEDIMENTS 74
5.4 GEOCHEMICAL CHARACTERIZATION 76
5.4.1 Harker Diagram 76
5.4.2 Alumina variation for gneisses 78
5.4.3 Evolution Indices (Discriminant Function) of gneisses 79
5.4.4 Crustal discrimination for gneisses 79

5.4.6 Protolith precursor diagrams 81
5.4.7 Paleoweathering conditions and degree of maturity of metasediments 85
5.4.8 Spider diagrams for normalised trace elements 86
5.4.9 Chondrite normalised REE pattern 89

CHAPTER SIX

GOLD MINERALIZATION 93
6.1 GEOLOGICAL SETTING 93
6.2 GOLD OCCURRENCES 96
6.3 SAMPLE COLLECTION AND ANALYSIS 99
6.3.1 Sediment sampling 99
6.3.2 Panning and grain morphology 99
6.3.3 Chemical analysis and statistical relation 100

CHAPTER SEVEN

SUMMARY, CONCLUSION AND RECOMMENDATION 106
7.1 SUMMARY AND CONCLUSION 106
7.2 RECOMMENDATION 108
REFERENCES 109
APPENDIXES 118

LIST OF TABLES

TABLE		PAGE
Table 1.1:	Summary of literally known band ratio composites	9
Table 3.1:	Default parameters for LINE module for linearment extraction	34
Table 4.1:	Modal composition of minerals in major lithologies in the study area	38
Table 5.1:	Major element content of gneisses and metasediments	71
Table 5.2:	Trace element content of gneisses and metasediments	73
Table 5.3:	Rare Earth Element (REE) contents of gneisses and metasediments	75
Table 5.4:	Chemical Index of Alteration and Index of Compositional Variability of metasediments.	85
Table 5.5:	Chondrite normalised values of Nakamura, 1978 showing significant ratios for rocks in the study area	89
Table 6.1:	Concentration of target and pathfinder elements around Gidan Boss and statistical relations	101
Table 6.2:	Concentration of target and pathfinder elements around Dutsen Burka and statistical relations	102

LIST OF FIGURES

FIGURES		PAGE
Fig. 1.1:	Location of Nigerian sector of the Pan-African Province of West Africa (After Turner, 1983).	1
Fig. 1.2:	Schematic section across the West African margin showing the effects of Pan-African event in the basement of Western Nigeria (modified from Burke and Dewey, 1972 *in* Danbatta, 2008).	2
Fig. 1.3:	Study area within a Geological sketch map of Nigeria showing the major geological components; Basement, Younger Granites, and Sedimentary Basins (after Obaje, 2009).	3
Fig. 1.4:	Methodology diagram for processing and enhancement of LandSat Thematic image (after Amuda *et al.,* 2014)	8
Fig. 2.1:	Basement Geology of Nigeria: The Migmatite-Gneiss Complex (mgn), the Schist Belts (sb) and the Older Granites (og). (Wright, 1985)	13
Fig. 2.2:	Schist belt localities within the context of the Geology of Nigeria (After Woakes *et al.,* 1987)	15
Fig. 2.3:	Areas of Gold mineralization in Nigeria (after Garba, 2000).	24
Fig. 2.4:	Gold production potential in Nigeria (Ajayi, 2003)	25
Fig. 3.1:	ASTER GDEM draped on topographic map of the study area.	28
Fig. 3.2:	ETM+ band ratio 5/7 of the study area showing granite and gneisses with high tone white to mist grey.	30
Fig. 3.3:	ETM+ band ratio 3/1 of the study area showing granite and gneisses show dark grey tone	31
Fig. 3.4:	Colour composite (Chica-Olmo ratio) which include the combination of ETM+ band ratios 5/7 (R) for granitic rocks, 5/4 (G) for iron minerals and 3/1 (B) for ferric oxides	32
Fig. 3.5:	Colour composite (Kaufmann ratio) which include the combination of ETM+ band ratios 7/4, 4/3 and 5/7 displayed as RGB showing areas of mineral alteration	33

Fig. 3.6:	Automatic extracted lineament trends (default setting) of structures in the study area	35
Fig. 3.7:	Rose (azimuth-frequency) diagram of lineaments orientations	36
Fig. 4.1:	Rose diagram of foliation trends in gneisses	63
Fig. 4.2:	Rose diagram of foliation trends in metasediments	63
Fig. 4.3:	Rose diagram of longer axis trends of phenocrysts in porphyritic biotite granite	64
Fig. 4.4:	Rose diagram of joint trends in gneisses within of the study area	66
Fig. 4.5:	Rose diagram of joint trends in metasedimants within the study area	66
Fig. 4.6:	Rose diagram of showing trends of joints in granite within the study area	67
Fig. 5.1:	Binary variation plots of SiO_2 with the other major oxides in gneisses	76
Fig. 5.2:	Binary variation plots of SiO_2 with the other major oxides in metasediments	77
Fig. 5.3:	Binary plot of molecular ratio of alumina to alkalis [$Al_2O_3/(Na_2O+K_2O)$] versus alumina to lime and alkalis $Al_2O_3/(CaO+Na_2O+K_2O)$] of Shand (1943) showing chemical classification of the gneisses	78
Fig. 5.4:	Ternary Plot of K_2O-TiO-P_2O_5 of Pearce *et al.*, 1975 showing crustal discrimination of gneisses and quartz-tourmaline rock in the study area	80
Fig. 5.5:	Ternary ACF plot of James *et al.*, 1978 showing compositional variation in the gneisses, quartz-tourmaline rock and metasediments	81
Fig. 5.6:	Bivariate (Al_2O_3 versus MgO) discrimination diagrams of Marc, 1992 with line that seperate paragneiss from orthogneiss for gneisses in the study area	82
Fig. 5.7:	Bivariate discrimination plot of SiO_2 versus $Na_2O=K_2O$ of Cox *et al.*, 1979, showing chemical classification and nomenclature of gneisses and quartz-tourmaline rock	83
Fig. 5.8:	Bivariate (TiO_2 versus SiO_2) discrimination diagram of Tarney, 1977 with a line that separates Igneous from Sedimentary fields for the rocks in the study area	84

Fig. 5.9: Comparison of trace element of metasediments content with estimates of Taylor and McLennan (1995) normalised to upper continental crust of Taylor and McLennan (1995) 87

Fig. 5.10: Comparison of trace element estimate of Taylor and McLennan (1995) with gneisses content normalised to bulk continental crust of Taylor and McLennan (1995) 88

Fig. 5.11: Chondrite normalised (Nakamura, 1974) showing rare earth elements (REE) pattern in metasediments in the study area 90

Fig. 5.12: Chondrite normalised (Nakamura, 1974) showing rare earth elements (REE) pattern in gneisses and quartz-tourmaline rock in the study area 91

Fig. 6.1: Standard deviation plot for samples around Gidan Boss and Dutsen Burka 103

Fig. 6.2: Bivariate plot of Au against other trace element (Hg, Zn, Cu, Pb and Ag) 105

LIST OF PLATES

PLATES		PAGES
Plate I:	Photograph of PGn with white coloured porphyroblasts at 11° 50□′ 22.4″N and 7° 11′ 14.0″ E	39
Plate II:	Photograph of feldspathic porphyroblasts in PGn and boudins of Feldpathic veins (4 cm width) perpendicular to the NE-SW (040°) trend of host rock at 11° 50′ 2.4″ N, 07° 09′ 12.2″E	39
Plate III:	Photomicrograph of PGn showing brown pyroxene with two direction cleavages	40
Plate IV:	Photomicrograph of PGn with red to green interference colours in pyroxene	40
Plate V:	Photomicrograph of PGn with myremekitic intergrowth texture (M) in microcline	41
Plate VI:	Photomicrograph of PGn showing pyroxene with deep pink interference colour	41
Plate VII:	Photomicrograph of GGn with subidioblastic light green chlorite (Chl) and opaque minerals (Opq)	42
Plate VIII:	Photomicrograph of GGn with cracks (C) in quartz and grey microcline	42
Plate IX:	Photograph of BGn 1 with joints mainly trending parallel to the direction of the bands with few perpendicular to it at 11° 45′ 33″ N and 07° 08′ 25″ E	43
Plate X:	Photograph of Bgn 2 with alternating light and dark coloured bands that are slightly folded in places around Tanimu at 11° 49′ 10″ N and 7° 14′ 22″ E	43
Plate XI:	Photomicrograph of BGn 1 showing foliated brown coloured Biotite	44

Plate XII:	Photomicrograph of BGn 1 showing plagioclase feldspar predominates the feldspar	44
Plate XIII:	Photomicrograph of BGn 1 with colourless quartz with low relief	44
Plate XIV:	Photomicrograph of BGn 1 with small scaled tartan twinning in microcline	44
Plate XV:	Photomicrograph of BGn 2 with lineated and folded brown biotite minerals	45
Plate XVI:	Photomicrograph of BGn 2 showing grey coloured plagioclase feldspar	45
Plate XVII:	Photomicrograph of BGn 2 with foliated dark brown biotite and light green coloured chlorite (Chl)	45
Plate XVIII:	Photomicrograph of BGn 2 with myrmekitic intergrowth texture (Myr) in plagioclase and its alteration to sericite in places	45
Plate XIX:	Photograph of parallel and perpendicular leucocratic vein in biotite schist at 11° 57′ 46″ N and 07° 13′ 21″ E	46
Plate XX:	Photograph of biotite schist in a river channel with parallel quartzofeldspatic veins at 11° 57′ 30″ N and 7° 6′ 50″ E	46
Plate XXI:	Photomicrograph of BSch 1 showing lineated brown coloured biotite with weak pleichroism	47
Plate XXII:	Photomicrograph of BSch 1 showing yellow to brown interference colour in biotite	47
Plate XXIII:	Photomicrograph of BSch 2 with brown coloured biotite with pleichroic halo in places. It has moderate relief	48
Plate XXIV:	Photomicrograph of BSch 2 showing biotite display different interference colours	48
Plate XXV:	Photomicrograph of BSch 3 with colourless muscovite and brown biotite that have moderate relief and perfect cleavage	48
Plate XXVI:	Photomicrograph of BSch 3 with mica (biotite and muscovite). The micas display different interference colour	48

Plate XXVII: Photomicrograph of BSch 4 with lepidoblastic foliation pattern and colourless equigranular quartz with low relief 49

Plate XXVIII: Photomicrograph of BSch 4 with plagioclase feldspar (Pl) and biotite with grey and brown interference colour 49

Plate XXIX: Photomicrograph of BSch 5 with foliation of subidioblastic biotite with moderate relief, alteration to chlorite and inclusion of opaque minerals in places 49

Plate XXX: Photomicrograph of BSch 5 showing xenoblastic quartz with wavy extinction on some grains 49

Plate XXXI: Photomicrograph of Bsch 6 showing brown coloured granoblastic biotite with opaque inclusions 50

Plate XXXII: Photomicrograph of Bsch 6 showing porphyroblastic quartz and orthoclase feldspar in fine grained groundmass 50

Plate XXXIII: Photograph of light grey coloured phyllite near Yankuzua at 11° 57′ 51.9″ N and 07° 05′ 39.8″ E 51

Plate XXXIV: Photograph of phyllite with tarnished and brown appearance trend at the banks of an ephemeral stream channel at 11° 58′ 00″ N and 07° 06′ 23.5″ E 51

Plate XXXV: Photomicrograph of Phy 1 showing brown to faint yellow biotite with wavy slaty texture and pleichroic 52

Plate XXXVI: Photomicrograph of Phy 1 2nd order light to dark brown interference colour 52

Plate XXXVII: Photomicrograph of Phy 2 with slaty foliation pattern in biotite and quartz 52

Plate XXXVIII: Photomicrograph of Phy 2 showing light brown polarization colour in biotite 52

Plate XXXIX: Photograph showing relic raft brown coloured BSch in contact with PBG at 11° 55′ 05″ N and 07° 10′ 02″ E 53

Plate XL: Photograph of a closer view to the sharp intrusive contact between PBG and BSch at the foot of PBG stock at 11° 54′ 36.4″ N and 07° 10′ 01.4″ E 53

Plate XLI: Photograph showing contact between PBG and GGn at 11° 52′ 22.2″ N and 07° 08′ 40.4″ E 53

Plate XLII: Photograph showing contact between PBG and PGn. The gneiss is older as it is observed to lie above PBG 53

Plate XLIII: Photograph of whale-back outcrop of PBG on parts of Kutcheri hill (PBG) at 11° 49′ 48.7″ N and 07° 02′ 16.4″ E 54

Plate XLIV: Photograph of PBG outcrop with feldspathic veins of varying width at 11° 48′ 17″ N and 07° 06′ 08″ 54

Plate XLV: Photomicrograph of PBG 1 showing pleichroic halo around zircon inclusion in platy, brown coloured biotite 55

Plate XLVI: Photomicrograph of PBG 1 showing different tartan twinning pattern in microcline 55

Plate XLVII: Photomicrograph of PBG 2 with green coloured pyroxene that has high relief and two sets of cleavage intercepting at nearly 90° 55

Plate XLVIII: Photomicrogragh of PBG 2 showing plagioclase feldspar with characteristic narrow multiple albite twinning pattern having ≤15° extinction angle. Pyroxene show pink interference colour 55

Plate XLIX: Low lying whale-back stock of medium to coarse grained biotite granite with quartzofeldspathic veins of varying widths at 11° 58′ 55.8″ N and 07° 14′ 55.2″ E 56

Plate L: Feldspathic vein that trends NS at 11° 56′ 40.8″ N and 07° 13′ 33.8″ E. Note joints in different directions 56

Plate LI: Photomicrograph of M-CBG showing muscovite with perfect basal cleavage. 57

Plate LII: Photomicrograph of M-CBG showing muscovite with pink interference colour 57

Plate LIII: Photograph of low lying fine grained serpentinite outcrop that is dark coloured with quartz crystal in places 57

Plate LIV:	Photograph of hand specimen of serpentinite with light green appearance and small black spots of chromian spinel/magnetite	58
Plate LV:	Photomicrograph of serpentinite showing opaque chromite grains and fibrous amphibole	59
Plate LVI:	Photomicrograph of serpentinite showing chrysotile in vein and unevenly fractured serpentine (olivine pseudomorh)	59
Plate LVII:	Photograph of hard brown laterites around Makera at 11° 12′ 20″ N and 07° 58′ 10″ E	60
Plate LVIII:	Photograph of rail road cut exposure of hard, brown laterites around Kutcheri at 11° 48′ 40″ N and 07° 02′ 30″ E	60
Plate LIX:	Photograph of alluvium deposit along the bed and banks of River Yankuzau at 11° 55′ 30″ N and 07° 03′ 15″ E	61
Plate LX:	Photograph of alluvium deposits on broadland plain enroute Gidan Chido at 11° 52′ 49″ N and 07° 02′ 55″ E	61
Plate LXI:	Photograph of banded gneiss with ptygmatic felsic veins at 11° 47′ 56″ N and 07° 14′ 42″ E.	62
Plate LXII:	Photograph showing foliation pattern in schist interbanded with thin quartzofeldspathic veins (<1cm width) at 11° 45′ 47.2″ N and 07° 06′ 49″ E.	62
Plate LXIII:	Photograph of PBG with non-orthogonal joint pattern enroute Yankara at 11° 47′ 17.4″ N and 07° 04′ 7.9″ E. Human is about 1.7m tall	65
Plate LXIV:	Photograph of exfoliation joints on low lying M-CBG that mainly trend NS (180°) at 11° 57′ 13.5″ N and 07° 14′ 58.8″ E	65
Plate LXV:	Photograph of PBG with rupture joint on in Asaka Ahuta quarry around boundary between Katsina and Zamfara state at 11° 49′ 12.2″ N and 07° 03′ 10.4″ E	65
Plate LXVI:	Photograph of foliation joint and parting on BSch around Dankaya at 11° 55′ 00″ N and 07° 0′3 16″ E	65
Plate LXVII:	Photograph of leucocratic aplite dyke (20 cm width) that trends NNE (204°) in PBG with sinistral displacement by thin quartz vein that trends WNW (284°)	68

Plate LXVIII: Photograph of M-CBG showing quartzofeldspathic veins with dextral and a sinistral strike slip faults at 11°58′55″ N and 07°14′54″E 68

Plate LXIX: Photograph of augen schist showing tight isoclinal fold pattern (hammer is 30 cm long) at 11° 50′ 49″ N and 07° 01′ 31.8 E 68

Plate LXX: Photograph of biotite schist with macroscale crenulation cleavage pattern (GPS 6.5cm width). Note thin quartz vein perpendicular to the foliation but parallel to axial trend at 11° 51′ 15″ N and 07° 01′ 30″ E 68

Plate LXXI: Photograph of augen schist showing disseminated quartz veins (human is about 1.7m tall) at 11° 51′11.9″N and 07°02′2.5″E 69

Plate LXXII: Photograph of biotite schist showing symetrical fold at 11° 52′ 01″ N and 07° 02′ 20″ E 69

Plate LXXIII: Photograph of alluvium cover on biotite schists aroud Gidan Boss at 11° 51′ 42″ N and 07° 01′ 15″ E 93

Plate LXXIV: Symetrical fold on biotite schist at 11° 52′ 01″ N and 07° 02′ 20″ E. Hammer is 30cm long 93

Plate LXXV: Photograph of joint (k) that trends NW-SE on low lying biotite schist outcrop at the bank of stream *Kaya* at 11° 51′ 11.9″ N and 07° 01′ 13.0″ E 94

Plate LXXVI: Photograph of joints that strikes NW-SE on biotite schist at 11° 52′ 00″ N and 07° 02′ 00″ E 94

Plate LXXVII: Photograph of thin quartz vein in brown coloured biotite schist around Gidan Boss at 11° 51′ 52″ N and 07° 01′ 10″ E 94

Plate LXXVIII: Photograph of quartz vein in grey coloured biotite schist near Dutsen Burka at 11° 50′ 48″ N and 07° 01′ 12″ E 94

Plate LXXIX: Photograph of quartz vein in biotite schist host rock of Dutsen Burka at 11° 50′ 53″ BN and 07° 01′ 06″ E 95

Plate LXXX: Photograph of quartz vein in biotite schist host rock near Gidan Boss at 11° 52′ 10″ N and 07° 01′ 40″ E 95

Plate LXXXI: Photograph of PBG with feldspar phenocryst that trend NNE-SSW at 11° 49′ 18″ N and 07° 03′ 49″ E 96

Plate LXXXII: Photograph of quartzofeldspathic pegmatite (50 cm width) in a whale-back PBG outcrop at 11° 49′ 17″ N and 07° 03′ 08″ E 96

Plate LXXXIII: Photograph of artisanal mining activities around Gidan Chido at 11°52′48″N and 07°03′15″E 96

Plate LXXXIV: Photograph of artisanal mining activities around Gidan Boss at 11°51′30″N and 07°02′55″E 96

Plates LXXXV: Photographs of active artisanal mining of placer deposits around Dutsen Burka at 11°51′22″N and 07°02′40″E 97

Plate LXXXVI: Photographs of active artisanal mining of placer deposits around Dutsen Burka at 11°51′22″N and 07°02′40″E 97

Plate LXXXVII: Photograph of pit dug to pan sediments for placer gold around Dutsen Burka at 11° 51′ 16″ N and 07° 01′ 16″ E 97

Plate LXXXVIII: Photograph of mining site under construction showing by Kucheri Mining Co-operative Society at 11° 51′ 50.3″ N and 07° 01′ 49.9″ E 98

Plate LXXXIX: Photograph showing panning by liquefaction 99

Plate XC: Photograph showing concentric groove in panning plate. Observer point to a gold grain 99

Plate XCI: Photograph showing different orientation direction of 6 mm grain with sharp edges 100

Plate XCII: Photograph of grains with (a) sharp edges but flattened and (b) smooth curved edges 100

LIST OF APPENDIX

APPENDIX		PAGE
APPENDIX I:	Point counting with JMicrovision software	118
APPENDIX II:	Trend of foliation in gneisses in degrees (°)	118
APPENDIX III:	Trend of foliation in metasediments (mica schist and phyllite) in degrees (°)	119
APPENDIX IV:	Trend of longer axis of phenocrysts in porphyritic biotite granite in degrees (°)	119
APPENDIX V:	Joints on gneisses in degrees (°)	119
APPENDIX VI:	Joints on schists in degrees (°)	119
APPENDIX VII:	Joints on granites in degrees (°)	120

LIST OF MAPS

MAP		PAGE
1.	Geological map of Funtua Sheet 78, NW at 1:50,000 scale	Back pocket
2.	Geological map of area near Kutcheri at 1:25,000 scale	Back pocket

CHAPTER ONE

GENERAL INTRODUCTION

1.1 THE NIGERIAN BASEMENT COMPLEX

The surface area of Nigeria 923,768 km^2 is covered in nearly equal proportions by crystalline rocks and sedimentary rocks. The crystalline rocks are further divided into three main groups viz: (i) the Basement Complex; (ii) the Younger Granites and (iii) Tertiary – Recent volcanics.

The Nigerian Basement Complex forms a part of the Pan-African mobile belt and lies between the West African and Congo Cratons (Fig. 1.1) and south of the Tuareg Shield (Black, 1980).

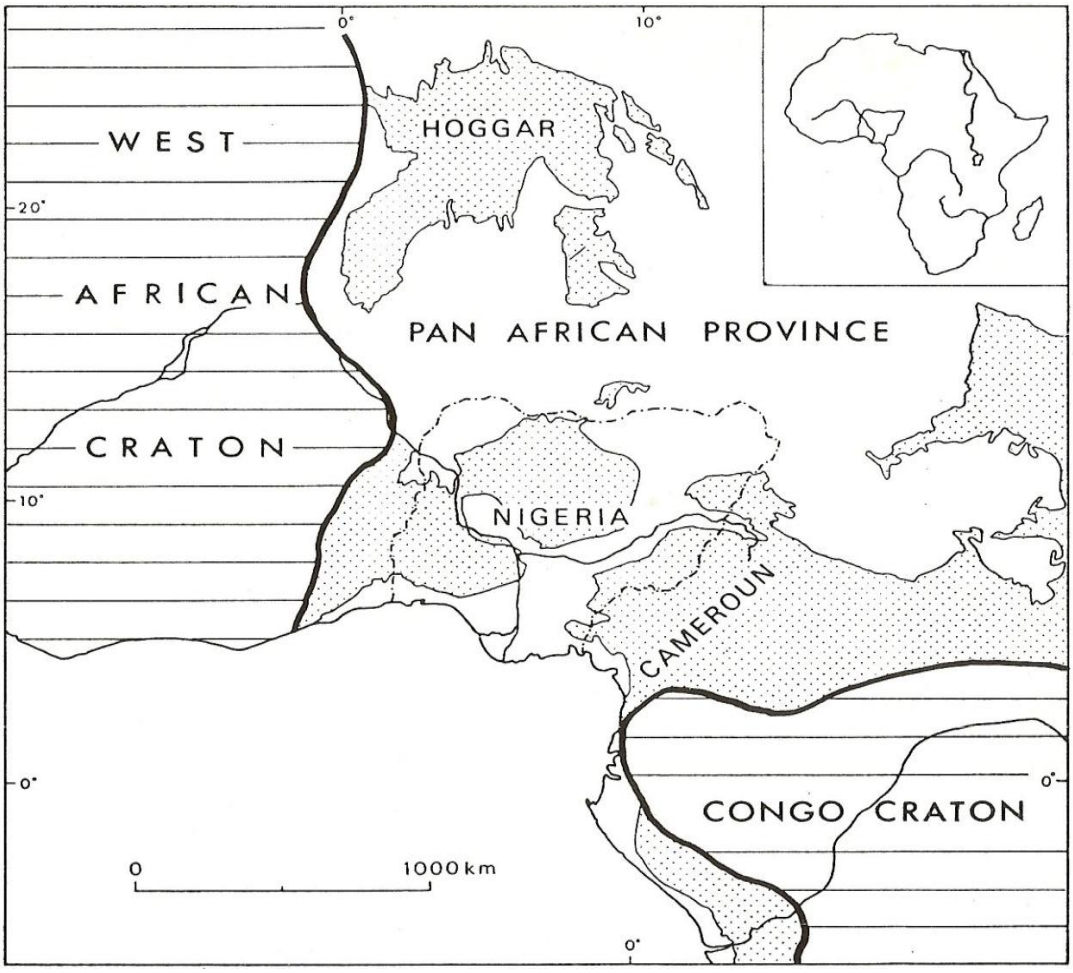


Fig. 1.1: Location of Nigerian sector of the Pan-African Province of West Africa (After Turner, 1983).

The Nigerian basement which occupies the reactivated region that resulted from plate collision between the passive continental margin of the West African Craton and the active Pharusian continental margins affected by Pan-African Orogeny (Burke and Dewey, 1972; Dada, 2006) as illustrated in Fig. 1.2. Condie (1989) observed that the Kibaran and Pan African events affected mostly the Godwana continent and did not seem to have strong counterparts in other continents. Tectonic activities in the interludes between the tectono-thermal events were limited mostly to anorogenic magmatism and rifting.

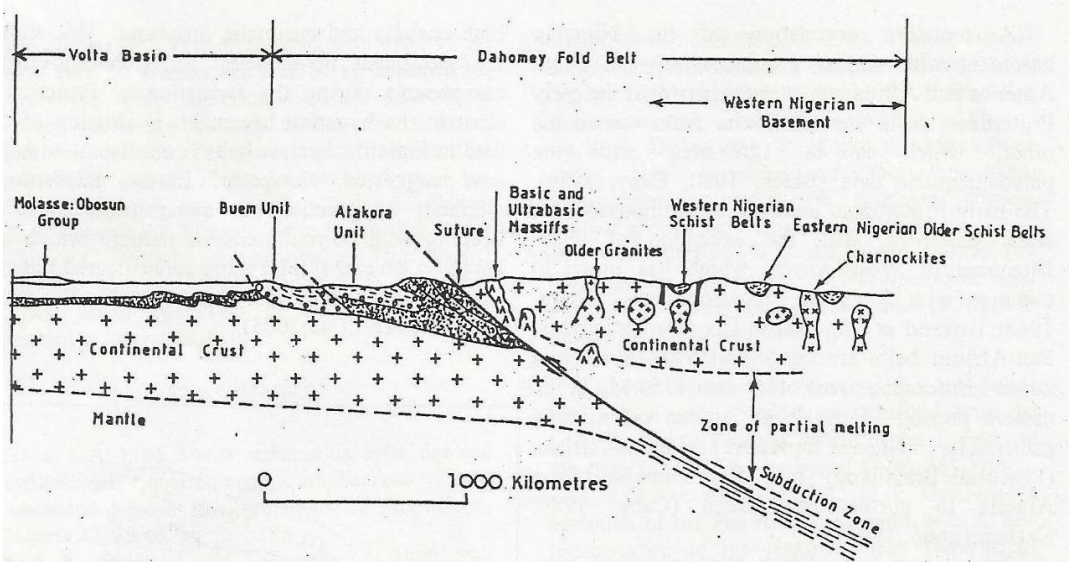


Fig. 1.2: Schematic section across the West African margin showing the effects of Pan-African event in the basement of Western Nigeria (modified from Burke and Dewey, 1972 *in* Danbatta, 2008).

Several researchers have worked on the Precambrian and Upper Paleozoic Basement Complex of Nigeria where they investigated its structural, physical, geochemical, geochronological, metamorphic, petrological and mineralogical aspects.

The present works is aimed at establishing petrogenetic characteristics of the lithological units in Funtua Sheet 78 NW and study some aspects of gold mineralization in Kutcheri, Wonaka Schist Belt, Northwestern Nigeria. The study area is located at the southeastern edge of the belt.

1.2 LOCATION AND ACCESSIBILITY

The study area is located within Tsafe and Faskari Local Government Areas of Zamfara and Katsina States respectively. It lies within the Federal Survey map of Nigeria Sheet 78, Funtua NW. It covers an area of 770 km^2 and is bounded by latitudes 11^{o}45′ and 12^{o}00′ N and longitudes 7^{o}00′ and 7^{o}15′ E (Fig. 1.3).

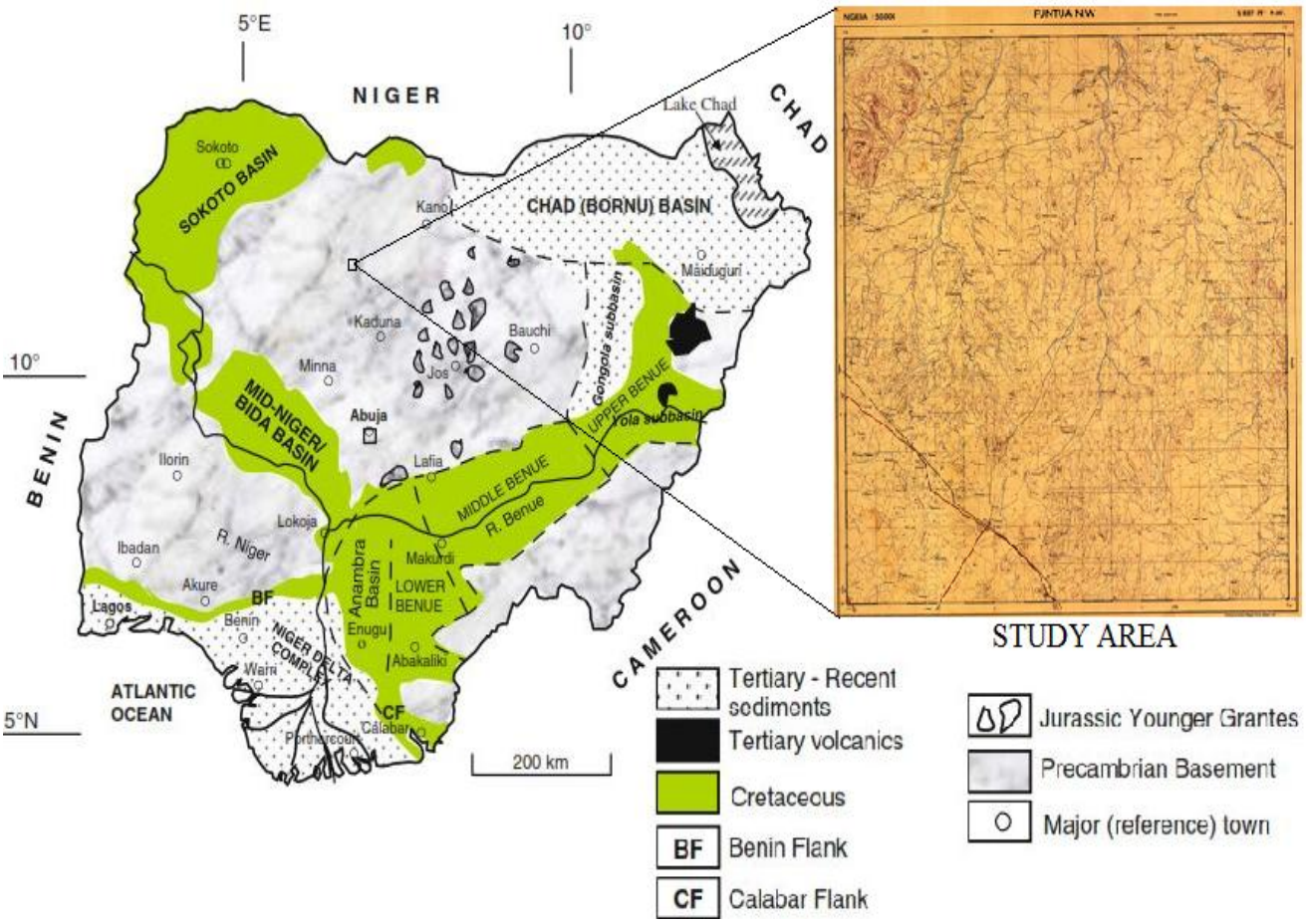


Fig. 1.3: Study area within a Geological sketch map of Nigeria showing the major geological components; Basement, Younger Granites, and Sedimentary Basins (after Obaje, 2009).

Generally, the area is quite accessible during dry season owing to numerous all season and seasonal roads that cris-cross the area. The southwestern part of the study area is traversed by a major tarred road from Zaria through Yankara to Gusau. The southeastern part lies 10 km north of Shemi town with numerous minor roads and foothpaths. A minor road that passes through

Yan Mallamai to Talata and Dan Sabo links the northeastern part of the area. Another minor road that span from Yankara, Yan Mallamai and Talata passed through Yankuzua to Takulawa eased access to the northwestern part.

1.3 RELIEF AND DRAINAGE

The area is generally an undulating plain. The highest peak is the Kuruku Hill at the northwestern edge with elevation of about 820 m above sea level. The other parts are characterised by rugged topography with gently sloping surfaces ranges from 720 m (at the southwestern part) to 740m (at the southeastern part) above sea level. The central and northeastern parts have low relief characterised by valleys and gullies filled with alluvium terraces. This lowland area has elevation of between 460 and 650 m above sea level.

Generally the area has a regional slope from the south to the north and Rivers Geauri, Yankuzau, Gagere and Kamoki drain the area.

1.4 CLIMATE AND VEGETATION

The mapped area lies within the Sudan Savannah Zone. It has a shorter raining season (about five months) than the Guinean type. Annual total rainfall is about 1000 mm, but there are considerable variations from year to year. Both the diurnal and the monthly temperature range are much in the sub-equitorial and Guinean Savannah regions. The relative humidity is low, particularly in the dry season, rising from about 40 % in January to 70 % in July (Udo, 1978). It falls within the Northern Guinea savannah zone (Udo, 1978).

Gallery forests are characteristic feature of the vegetation of this belt. These are areas of greater tree density usually called fringing forests since they are found along water courses where the

soil is usually moist. They are usually low and continuous, covering no more than 12 m (40ft) on each bank (Udo, 1978).

1.5 PREVIOUS WORK

Considerable work has been done on geochronology, petrology, mineralogy, evolution and mineralization potential of the schist belts in northwestern Nigeria.

McCurry (1976) reported that the Paleozoic and Precambrian rocks in northern Nigeria can be divided into four major groups and these are the Basement Complex, Younger Metasediments, Older Granite Series and the Volcanic rocks. Turner (1983) showed that Wonaka belt is distinctive in composition and metamorphism. Also, the metamorphism is of higher temperature and low pressure than in other belts.

Russ (1957) reported that alluvial gold deposits in northwestern Nigeria occur in present river channels and other boulder washed deposits related to older drainage patterns. Garba (2003) reported that gold occurs in quartz veins cutting schists, gneisses, granites and other rock types.

Around Gidan Mesa (formerly called Mallan Tanko or Maimesa) and Shemi areas, several workers (Ogezi, 1977; Onyeagocha, 1979) have investigated ultramafics with chromium, nickel and anthophyllite mineralization. Baer and Glaeser (1981) also reported that chromium occur mainly as drop-like lenticular grains. Shibayan (1985) reported that the Mallam Tanko serpentinites contain chromite pods.

In 1994, some final year students of Ahmadu Bello University, Zaria worked on the geology of areas within southwest and central part of the study area.

McCurry (1976) and Turner (1983) observed that Wonaka belt is distinctive in composition and metamorphism. However, Danbatta (2008) predicted the possibility of the occurrence of BIFs in the Wonaka belt. The lithological and other descriptions of the schist belts revealed close association of the BIFs with the metasediments and metavolcanics (Mucke, 2005).

1.6 PRESENT WORK

1.6.1 Aim and Objectives

The present works is aimed at establishing petrogenetic characteristics of the lithological units in Funtua Sheet 78 NW and study some aspects of gold mineralization in Kutcheri, Wonaka Schist Belt, Northwestern Nigeria.

The objectives include the following:

a. To investigate utilization of Remote sensing technique for lineament, lithological and alteration mapping.
b. To undertake detailed petrographic description of the various rock types.
c. To establish the metamorphic signatures from field studies, petrography and geochemical analysis.
d. To carry out investigation on gold grain morphology and determine indicator elements for gold in the area.

To accomplish the stated aim and objectives, the scope of present work is:

i. To undertake literature review and remote sensing interpretation of the study area.
ii. To produce a detail geological and map of the study area on a scale of 1:50,000.
iii. To produce a detail geological and structural map of area around Kutcheri on a scale of 1:25,000.
iv. To prepare thin section of representative rock samples for petrographic studies.

v. To collect representative samples of rocks for detailed geochemical studies.

vi. To collect sediment samples for panning to recover alluvial/eluvial gold grain in order to determine their morphology.

vii. To collect quartz vein samples randomly in order to determine contents of target and pathfinder elements.

1.7 JUSTIFICATION OF STUDY

A need for large scale mapping of parts of Wonaka schist belt to understand its petrogenesis cannot be overemphasized. Also, most of the schist belts in northwestern Nigeria that have been studied are polymetallic and are known to have mineralization such as gold (Elueze, 1981b; Garba, 2002), BIF (Mucke *et al.*, 1996, Ibrahim, 2008), marble (Wright, 1985), manganese (Mucke, 2005) associated with them. The Wonaka Schist Belt will probably not be an exception; hence the need for its detailed study.

1.8 MATERIALS AND METHODS

1.8.1 Preamble

This covers the methodology adopted in the present research work. The study was carried out in 7 phases. These include: (i) literature review; (ii) remote sensing; (iii) field work (iv) sampling (v) panning (vi) map digitization (vii) laboratory analysis

1.8.2 Remote Sensing Interpretation

Satellite imageries of the study area were acquired and studied. The satellite images were acquired from Landsat 7 Enhanced Thematic Mapper Plus (ETM+). Also, an Advanced Spaceborne Thermal Emission and Reflection (ASTER) Global Digital Elevation Model

(GDEM) draped on topographic map of the study area were used for the interpretation of physiographic features to aid reconnaissance field work. Subsequently, subsets of the ETM+ scene (Path 189/Row 052, acquired on October 19, 1999) were processed using the ENVI 4.5 image processing and analysis software. ArcGIS 9.1 and GCI Geomatica 9.1 software packages are both used in digital processing, spectral enhancement, spectral classification and geospatial analysis of the produced enhanced images for lithological classification and identifying alteration types.

The ENVI 4.5, PCI-Geomatica software was used for digital image processing with methodology shown in Fig. 1.4 below.

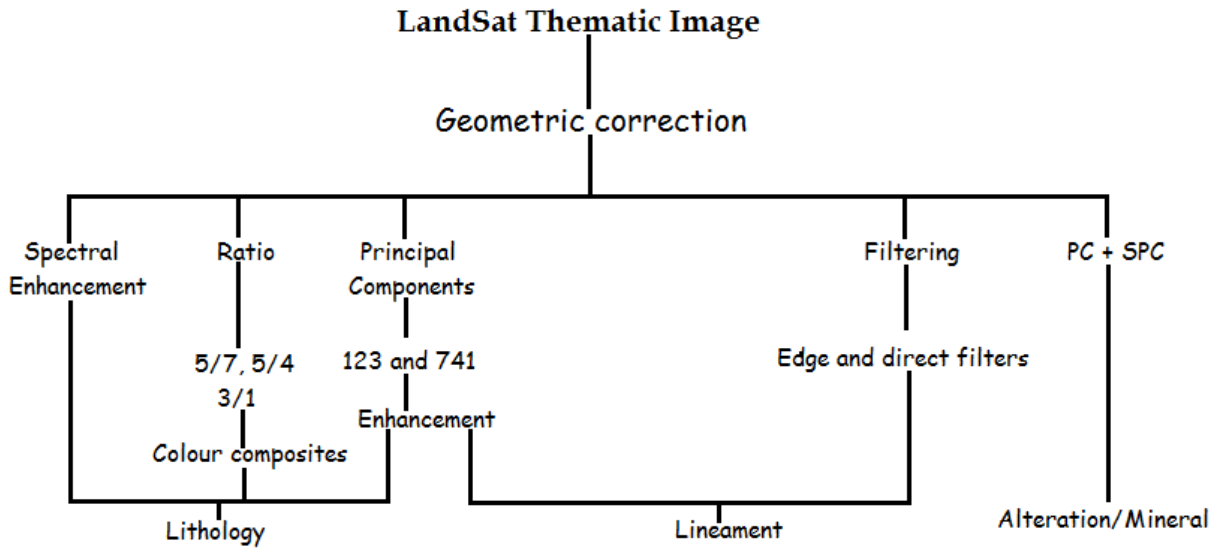


Fig. 1.4: Methodology diagram for processing and enhancement of LandSat Thematic Image (After Amuda *et al.*, 2014).

The color composites with band ratios that are literally known are summarized in the Table 2.2

Table 1.1: Summary of literally known band ratio composites.

RGB display of respective TM band Ratios	Red correspondent	Green correspondent	Blue correspondent	Extra	Reference
5/7 : 3/2 : 4/5	Clay-rich areas	FeO rich areas		Yellow, orange areas both clay and FeO rich	Abrams et al. (1983)
7/4 : 4/3 : 5/7	Minerals containing iron ions	Vegetated zones	OH/ H_2O-, SO_4- or CO-bearing minerals		Kaufmann(1988)
3/4 : 5 : 5/7				FeO as apricot yellow and the background as sky-blue	Jingyuan & Xucman,(1991)
5/7 : 5/4 : 3/1	Clay minerals	Iron minerals	Ferric oxides		Chica-Olmo(2002)
3/1 : 5/7 : 4/5				Highly altered zones dark-blue to violet-blue	Abdelhamid & Rabba(1994)

1.8.3 Fieldwork and Sampling

Three days reconnaissance field work was undertaken in order to establish traverse grids as well as confirm lithologic boundaries deduced from the remote sensing interpretations.

Detailed field mapping using Compass-Global Positioning System (GPS) traversing method was carried out for two weeks from March 15th to 29th, 2012. Compass clinometer was used to measure trend and dips of lithological and structural features on outcrops. All observations at different locations were recorded in field notebook. A shovel was used to sample sediments for panning and sieving. Representative rock samples for petrographic studies and geochemical analysis were collected from outcrops with a sledge hammer. Also, a chisel head hammer was used to randomly sample quartz veins at about 30 m interval. The entire area of sheet 78 NW Funtua was mapped at a scale of 1:50,000, while a small area with gold occurrences were mapped at a scale of 1:25,000.

1.8.4 Panning

Three field sampling pans were used to sample 20 kg each of sediments from pits around banks of River Kaya (Dutsen Burka), Kutcheri Co-operative mining site (Gidan Boss) and Dankaya. Panning of 60 kg sediments was carried out in Sedimentology Laboratory of Department of Geology, Ahmadu Bello University, Zaria.

1.8.5 Map Digitization

Maps of the study area were scanned and uploaded into MapInfo software (MapInfo Professional 11.0). They were digitized at scale of 1:50, 000 and 1: 25,000. The 1:25,000 map for areas of gold mineralization, while the 1:50,000 map covers the whole Funtua 78 NW Sheet.

1.8.6 Laboratory Analysis

Thin section production and Petrographic analysis

Thin sections (30µm thickness) of 16 representative rock samples were prepared, studied under polarised light microscope and photomicrographs were taken with digital camera at the Department of Geology, Ahmadu Bello University, Zaria. JMicroVision software (Appendix I) was used for point counting (modal analysis).

Geochemical Analysis

Samples selected for geochemical analysis were air-dried at room temperature after which they were crushed in a Laboratory Jaw Crusher. The resultant samples were pulverized in a Vibrating Disc Mill. Final size reduction, mixing and homogenization to < 75 µm were done with a Mixer Mill. Eight gram (8.0 g) each of twelve samples inclusing five gneisses, six metasedments and onequartz-tourmaline rock were thereafter shipped to ACME Analytical Laboratories,

Vancouver in Canada for major and trace element geochemistry using Inductively Coupled Mass Spectrophototmeter (ICP-MS) and X-Ray Flourescence (XRF) techniques.

One gram (1.0 g) each of the quartz vein samples was digested with 20 ml of 3:1 mixture of HNO_3-HCl (Aqua Regia) in a 100 ml glass beaker. These were then placed on hot plate and boiled gently at 95° C for 1.5 hours to slowly evaporate to nearly pasty mass and removed from the hot plate to cool. The contents volume was made up to 50 ml with distilled water in a glass stoppered graduated test tube. After filtration, the leached solutions were rinsed with distilled water to 100 ml. The solutions were kept aside, undisturbed overnight and appropriate aliquot of the supernatant solution were taken for analysis of Au, Pb, Hg, Cu, Ag and Zn using Varian AA 240FS Atomic Absorption Spectrophotometer at Multi User Science Research Laboratory, Ahmadu Bello University, Zaria.

1.8.7 Data Interpretation

Geochemical data for petrogenesis were interpreted with geochemical data tool kit (GCDkit) software through the use of various discrimination diagrams. Descriptive statistics and multivariate statistics (t-test, correlation coefficient) were used to establish the distribution, inter-element and inter-sample variability. Also, structural data were plotted with rosette diagram software (Rozeta 2.0).

CHAPTER TWO

REGIONAL GEOLOGY

2.1 PREAMBLE

A review of lithology, evolution, structural framework, geochemistry of the Nigerian Basement Complex and gold mineralization was attempted.

2.2 NIGERIAN BASEMENT COMPLEX

2.2.1 Lithology

The basement is characterised by synclinorial belts of low grade metasediments downfolded into high grade gneisses and migmatites, the whole intruded by batholitic granites. It is characterised by process of several phases of deformation, recrystallization and intrusion, the last of which is the Pan African orogeny (McCurry and Wright, 1977).

Ajibade and Fitches (1988) reported that the basement comprises three major lithological groups (Fig. 2.1):

(i) the migmatite gneiss complex which is widespread throughout the country;

(ii) metasedimentary and metavolcanic rocks which form schist belts and appear to be dominantly restricted to the western half of the country;

(iii) the Older Granites which intrude both the migmatite gneiss complex and the schist belts and have consistently yielded Pan-African ages.

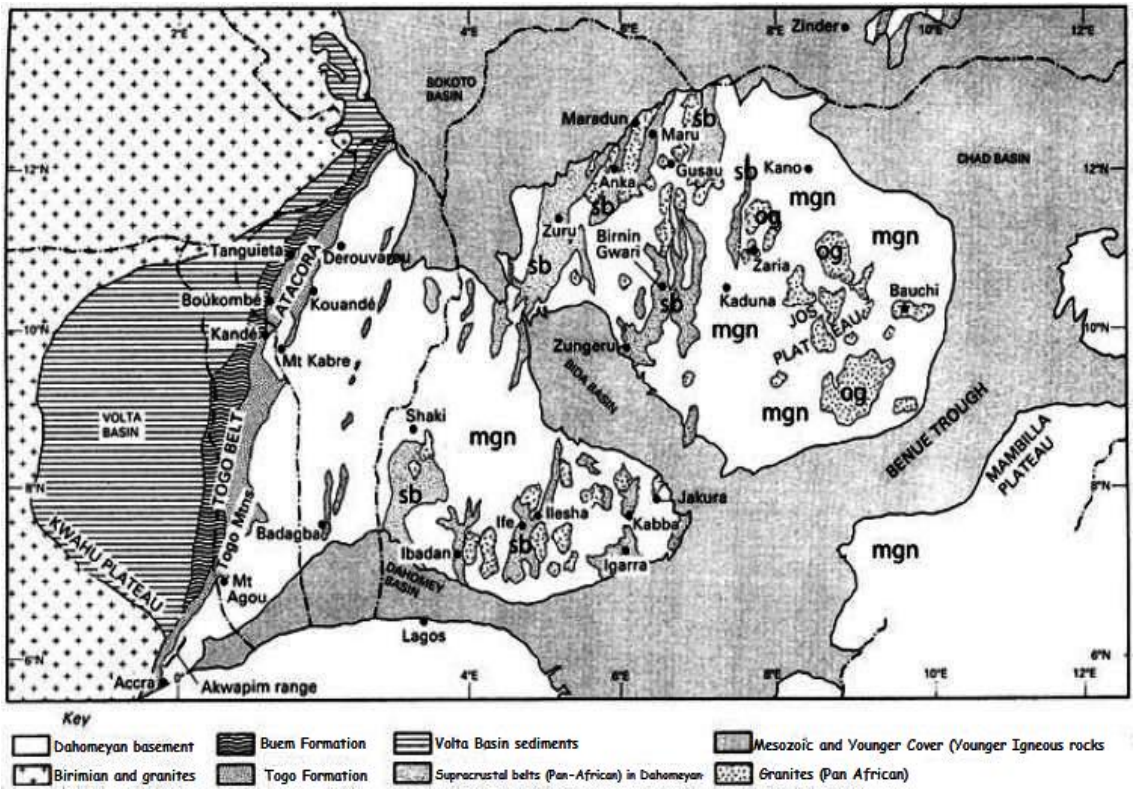


Fig. 2.1: Basement Geology of Nigeria: The Migmatite-Gneiss Complex (mgn), the Schist Belts (sb) and the Older Granites (og). (Wright, 1985).

Migmatite-Gneise Complex

The Migmatite – Gneiss Complex is generally considered as the basement complex *sensu stricto* (Rahaman, 1988; Dada, 2006) and it is the most widespread of the component units in the Nigerian Basement. The migmatite gneiss complex is polycyclic in nature. Russ (1957) considered the gneissic complex to represent the oldest member of Precambrian basement in northwestern Nigeria and that it evolved by successive sedimentation, deformation, metamorphism and igneous intrusion over a vast period of history of the basement.

Three petrologic units characterize the migmatite gneiss complex (Rahaman 1981). These are

i. Grey gneiss or early gneiss: A grey foliated biotite acid/or biotite hornblende quartz feldspathic gneiss of tonalitic to granodioritic composition. It is present in most outcrops.

ii. Mafic to ultramafic component which, where present often outcrops as discontinuous, boudinaged lenses or concordant sheet of amphibolites with minor amount of biotite-rich ultramafics. Except where it constitutes the paleosome to the migmatite, it is present in grossly subordinate amounts to the grey gneiss.

iii. Felsic components which are a varied group of rocks consisting essentially of pegmatites, aplite-quartz-oligoclase veins, fine grained granite gneiss, porphyrytic granites etc.

Metasedimentary and Metavolcanic rocks

Two types of Metasediments are identified; the Older Metasediments which occur predominantly in the southwest (Rahaman, 1976) and the Younger Metasedments (low grade) which occur predominantly in the northwest (McCurry, 1971). The metasedimentary and metavolcanic rocks are considered to be Late Proterozoic cover infolded into the gneiss-migmatite. They outcrop mainly as N-S to NNE-SSW trending belts (Fig. 2.2). They essentially include:

(i). Birnin Gwari Schist Belt: It is underlain by quartzo-feldspathic rocks of Zungeru Formation and together they form a single structural unit named Zungeru-Birnin Gwari Schist Belt. Zungeru Formation outcrops on both flanks of the schist belt. It is largely made up of fine-grained quartzo-feldspathic rocks which are interbedded with amphibolites and some quartzites. The Birnin Gwari Schist belt mainly comprises phyllites, mica schists, interlayered with metagreywacke, pebbly schist and metavolcanics (Ajibade and Wright, 1988).

(ii). Kushaka Schist Belt: This is a metasedimentary succession of schist, phyllites and banded iron formation, intruded by large volume of granitic rocks engulfing the whole formation and fragmenting it into smaller bodies separated by migmatite gneisses. Amphibolites are locally very thick, suggesting large volcanic accumulations (Grant, 1978).

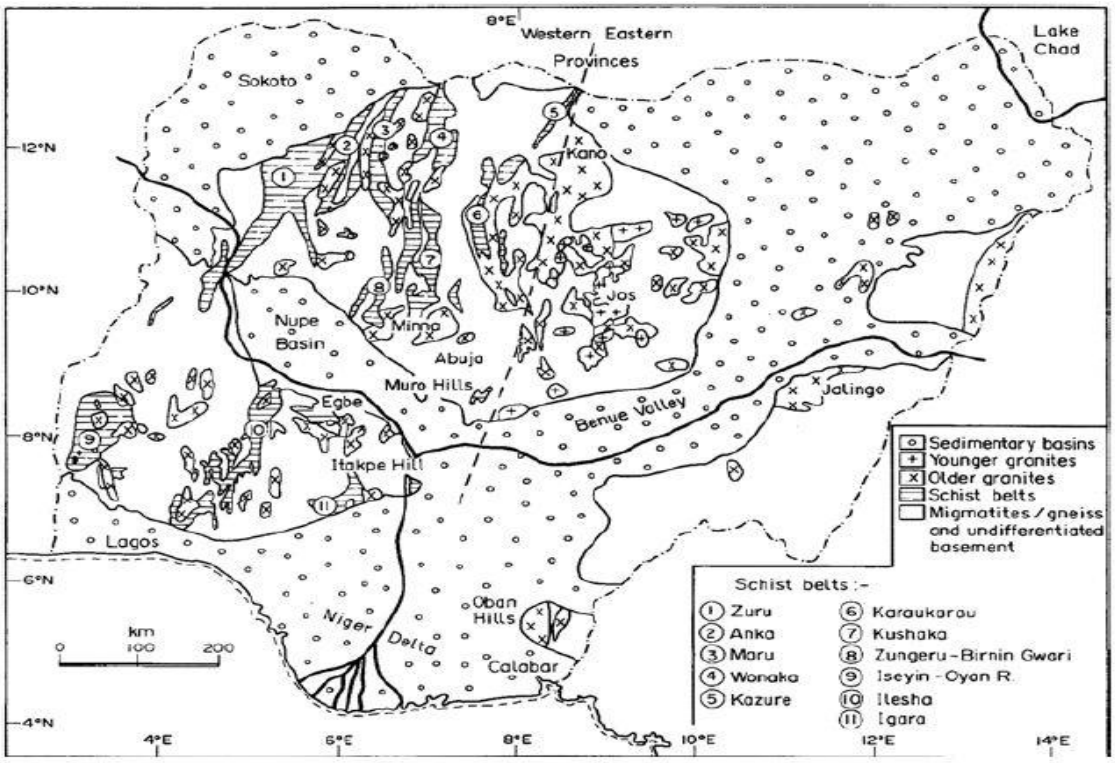


Fig. 2.2: Schist belt localities within the context of the Geology of Nigeria (After Woakes *et al.,* 1987).

(iii). The Ushama Formation**:** This lies west of Zungeru-Birnin Gwari schist belta and is the smallest of all the schist belt of northwestern Nigeria. It was mapped as part of Kushaka Formation by Truswell and Cope (1963). It consists predominantly of mica schists, quartz schists and quartzite with amphibolite layers. Staurolite crystals were collected near the contact with Zungeru mylonites, an indication of amphibolite facies metamorphism. It is not clear if the staurolite was derived from Ushama schist or from the adjacent Zungeru mylonites (Ajibade *et al.,* 1979).

(iv). Maru Schist Belt: This lies 200 km northeast of Kushaka schist belts. Pelitic rocks are dominant occurring mainly as phyllites and slates interlaminated with siltstone. Banded iron formation, containing magnetite and haematite or garnet and grunerite is also present. Mafic volcanic rocks are represented by the amphibolites at several localities and micaceous quartzites

occur near the eastern margin of the belt. Western margin of the belt is characterised by granite intrusion as typified by Maiinchi granodiorite, and at the middle of the belt by Kanoma syenite (Turner, 1983).

(v). Anka Schist Belt: It lies west of Maru schist belt, with both separated by the Pan-African Maiinchi granodiorite, and by a probably older gabbro-granite-pegmatite complex. The rocks include metaconglomerates, sandstones, slates, phyllites and acid volcanic rocks (Holt, 1982).

(vi). Zuru Schist Belt: This is the largest of all the northern schist belts. The metasediments are notably quartzites (massive and schistose varieties), with subordinate amounts of quartz biotite schist (Danbatta, 2008).

(vii). Malumfashi Schist Belt: It lies east of Kushaka schist belt consists mainly of muscovite, muscovite-biotite schists and phyllites interbedded with thin quartzites (McCurry, 1973). The pelitic rocks include minor graphitic and feldspathic schists.

(viii). Kazaure Schist Belt: It lies northeast of Malumfashi belt is an area of low grade metasediments and metavolcanics comprising quartzites, conglomerates, schistose rocks, meta-rhyolites with rare ferruginous quartzites (iron formation). These rocks are bounded by gneisses, older quartzites and intrusive granites (Danbatta, 2002).

(ix). Wonaka Schist Belt: The main rock type in this belt is a fine-grained quartz-biotite rock referred to as hornfelsic schist, in places containing sillimanite, cordierite or garnet, forming a monotonous expanse with constant foliation trend (McCurry, 1973). Metamorphism is of a higher temperature and lower pressure type than in other schist belts. This may be due to the

close association of the belt with large granite batholitic masses of granite and granodiorite which almost engulf the belt (Turner, 1983).

Although they display some lithological contrast, Ajibade and Fitches (1988) conclude that the protolith of all the belts except Zuru in northwestern Nigeria are predominantly pelitic. Kushaka and Maru belts are characterised by quartzites and pillow basic rocks, Birnin Gwari and Anka belts have pre-existing greywackes and conglomeratic horizon before metamorphism Egbuniwe (1982). The Birnin Gwari and Anka on the other hand are characterised the presence of meta-volcanic rocks of calc-alkaline type (Holt, 1982).

Older Granites (Pan-African Granites)

This include a group of discordant, intrusive, late- tectonic to concordant, syntectonic bodies varying from small sub- elliptical plutons to large batholiths (Ogezi, 1988). They constitute about 40-50% of the basement complex outcrop and vary in composition from tonalite through granodiorite, gabbro, charnokites to granite and syenite. Granodioritic composition is the most common (Rahaman, 1976).

Granitic bodies are widespread and range in size from sub-elliptical plutons to masses of batholithic dimensions over 100 km in length. The masses may or may not be foliated and are concordant and elongated to the regional structural trend (McCurry, 1976). Other granitic rocks described according to their petrographic affinities are porphyritic granites, fine to medium grained granite, syenite, quartz syenite and fayalite quartz monzonite (bauchite) as described by Oyawoye (1972).

2.2.2 Evolution of the Nigerian Basement

The Nigerian Basement Complex is a polycyclic assemblage of heterogeneous migmatites and gneisses, metasediments and granites that have undergone a complex evolutionary history spanning through Archaean to Pan-African (Late Proterozoic) times (Ogezi, 1977; Rahaman, 1988). The rocks are believed to be the results of at least four major orogenic cycles of deformation, metamorphism and remobilization corresponding to the Liberian (2,650 ± 150 Ma), the Eburnean (2,000 ± 50 Ma), the Kibaran (1,100 ± 200 Ma), and the Pan-African cycles (600 ±150 Ma). Olade and Elueze (1979), Ogezi (1977) have favoured largely ensialic processes in the evolution of the schist belts whilst Rahaman (1981) and Egbuniwe (1982) have stressed the importance of ensimatic processes in the formation of the schist belts.

Danbatta (2008) observed that the lithostratigraphy and close association of the Nigerian schist belts with either Anka-Yauri-Iseyin (AYI) or Kalangai-Zungeru-Ifewara (KZI) fault is sufficiently known to allow the erection of a new model of evolution for the whole schist belts. The model considers the evolution of some of the schist belt to correspond to the initial stages of rifting, back-arc extension, formation of epicratonic basins; and deposition of rocks of the schist belts in Birrimian time. This was followed by the first tectono-metamorphic event during Eburnean time, culminating in a second tectono-metamorphic Pan-African event. He concluded that Nigerian schist belts with Algoma type BIF's are ensialic and Eburnean in age, while those without BIF's are ensimatic and Pan-African in age.

2.2.3 Structures

The basement terrain is highly deformed as a result of various tectonic events with differing intensities. The resultant structure includes foliation (alternation of silicic-mafic minerals), minor folds, joints, fractures and faults.

Each of the thermotectonic events produced characteristic imprints on the basement rocks. However, the Pan-African event was so pervasive that it nearly obliterated most of the structures of the earlier events, leaving behind mostly their traces (McCurry, 1976; Rahaman, 1976; Grant, 1978). Two major regional (transcurrent) fault systems (Anka-Yauri-Iseyin-AYI and Kalangai-Zungeru-Ifewara-KZI fault systems) trending NE-SW occur in Nigeria and these had probably developed during the late Pan-African orogeny (Garba, 2000). These fault systems are dextral wrench faults with displacements in the order of tens of kilometers and have associated locally developed conjugate sinistral faults (Danbatta, 2003).

The most prominent structural trends are the N-S planar structures but relicts of E-W, NW-SE and NE-SW structures are preserved (Oluyide, 1988). Oluyide and Udoh (1989). The basement is also characterised by several sets of fractures with the north easterly and north westerly conjugate sets predominating (Oluyide, 1988).

Zungeru-Birnin Gwari Schist belt is a simple N-S syncline, 150 km long, with the northern part displaced dextrally by a NE-SW transcurrent fault. The Birnin Gwari Schist Belt occupies the synclinal axis of the belt and is characterized by conspicuous NNE-SSW trending ridges (Ajibade, 1980). Kazaure schist belt is structurally simple, free from central granite intrusion and mafic igneous rock.

The Pan-African granites are usually elongated in a northernly direction an observation that shows that the Pan-African granite plutonism most probably exploited existing structures in the Older Basement (Oluyide, 1988). Maru belt is a straight NNE-trending belt with a steeply dipping foliation (Ogezi, 1977). Zuru schist belt can be described in terms of three phases of regional deformation D1, D2 and D3. D2, being the main cleavage-producing deformation phase that intensely folded the rocks into isoclinals N-S trending upright folds (Danbatta, 2002).

2.2.4 Geochemistry

The main types of geochemical works undertaken on the basement rocks of Nigeria include major, trace, and rare earth element (REE).

Rahaman (1988) concluded that a significant geochemical step forward in the study of the schist belts of Nigerian basement is the realization that most of the amphibolites are of igneous rather than sedimentary origin. Amphibolites are largely tholeitic in nature and of oceanic floor and island arc affinities (Ogezi, 1977; Ajibade, 1980; Olade and Elueze 1979).

Geochemical studies by Olanrewaju, (1981) and Olanrewaju and Rahaman, (1982) have shown that although the Older Granites in the basement contain significant amount of alkalies they are slightly paraluminous with corundum appearing in the norm.

Okunlola and Okoroafor (2009) noted that variation plots involving Na_2O_3, Al_2O_3, and K_2O on one hand and TiO_2 and SiO_2 on the other hand reveal arkosic sedimentary progenitors for the rocks in Okemesi fold belt. In addition, La/ Th and Th/U ratio suggest that the rocks especially biotite schist is associated with post Archean recycled Upper Crustal sources while Chondrite normalized rare earth element signatures of samples further indicate low grade post Archean terrigenous sedimentation of rocks derived from possible mixture of granite- tonalities.

Also from trace element geochemistry of Ile-Ife Schist belt, Rahaman *et al.*, (1988) noted that the varieties of amphibolites (massive melanocratic and foliated leucocratic) were derived from two non-comagmatic igneous precursors. Relatively high abundances of incompatible trace elements and light rare earth elements (LREE) in the gneisses are thought to be due to contamination with crustal sources.

Rahman *et al.*, (1987) worked on the geochemistry of granitic rocks of western part of Oban Massif and noted that the granitic rocks are peraluminous and exhibit an apparent trend of decreasing normative diopside and increasing normative corundum with increasing SiO_2. Major and trace element compositions of the rocks show a typical calc-alkaline differentiation trend.

Chemical data show that the lit-par-lit gneiss in southeastern Nigeria is granodioritic in composition (Ekwueme, 1992). The trace elements characteristics of the migmatitic gneisses, charnockitic gneisses and meta-peridotite in the area of southwest Obudu Plateau indicate that the area exhibits a high degree of geochemical variability (Ukwang *et al.* 2003).

Onyeagocha (1986) worked on geochemistry of basement granitic rocks from northcentral Nigeria. He noted that the granites and granite gneisses has similar major element composition. Chondrite normalized rare earth pattern show normal magmatic abundance and point to derivation by partial melting of country rocks (schists and gneisses). High Th content of 15.1-31.3 ppm suggests a crustal origin for these granitic rocks.

On geochemistry and origin of ensialic alpine-type serpentinite association from Mallam Tanko (Shemi) and Ribah (Wasagu) northwestern Nigeria, Ogezi (1988) noted that the metasediments and granites are similar to depleted alpine-type peridotite. Also, absence of typical mafic

components of layered complexes suggests that they are tectonic intrusions of depleted upper mantle rocks emplaced along basement lineaments during the deformation of the basement.

Danbatta and Ike (2001) concluded from major and trace element geochemistry of metasediments (mica schists and quartzites) in Kazuare Schist Belt that the protolith include shale-greywacke and clay sediments. Moreover, Danbatta and Garba (2007) noted that major and trace element data reveal that the amphibolites in Zuru Schist Belt have extremely low K_2O; high Al_2O_3 and low TiO_2, Nb, Zr, Y, Ni and Cr contents, which are typical of island-arc or back arc settings.

2.2.5 Sediment maturity and Source area weathering of metasediments

The weathering effect on metasediment can be estimated by the Chemical Index of Alteration; CIA = $100[Al_2O_3/(Al_2O_3 + CaO^* + Na_2O + K_2O)]$ in molecular proportions, where CaO* is CaO in silicates only (Nesbitt and Young, 1982). Nesbitt and Young (1982) also proposed Correction for CaO (CaO*) = CaO – $(10/3 \times P_2O_5)$. If the corrected CaO* was less than the amount of Na_2O, this corrected CaO* value was adopted. If the CaO* value is greater than the amount of Na_2O, it was assumed that the concentration of CaO equals that of Na_2O.

Furthermore, the Index of Compositional Variability, ICV = $(Fe_2O_3 + K_2O + Na_2O + CaO + MgO + TiO_2)/Al_2O_3$ of Cox *et al.,* (1995) measures the abundance of alumina relative to the other major cations in a rock or mineral and generally reflects the degree of maturity of rocks delivered to a sedimentary basin.

The Chemical Index of Alteration (CIA) and Index of Compositional Variability (ICV) are useful geochemical parameters for the study of provenance, paleoclimate conditions, maturity and intensity of weathering (Cox *et al.,* 1995; Nesbitt and Young, 1982). Variable degrees of

weathering in the source area lead to relative depletion of alkali and alkali earth elements and enrichment in Al_2O_3 and TiO_2 in the resulting terrigenous sedimentary rocks (Nesbitt *et al.,* 1980).

The Index of Compositional Variability (ICV) value is more than 1 in immature sedimentary rocks with a high content of non-clayey silicate minerals, which tends to be found in tectonically active settings (van de Kamp and Leake, 1985). Mature pelitic rocks enriched in clay minerals are characterized by lower ICV values (Cox *et al*., 1995), which characterize tectonically quiescent or cratonic environments (Weaver, 1989) where recycling and concomitant weathering are active.

Okunlola and Okoroafor (2009) reported Chemical Index of Alteration (CIA) of schistose rocks in the Okemesi fold belt, southwestern Nigeria reveal average values of 69.7 %, 85.9 % and 91.2 % for the quartz schist, mica schist and quartzite respectively. These values point to relatively intense chemical weathering of the source rocks. The quartz schist, biotite-muscovite schist and the quartzite have average ICV values of 0.68, 0.85 and 0.83 respectively. Also, Okunlola *et al.,* (2009) reported average CIA values for quartz schist (57%) and amphibolite schist (42%) in Ibadan area. In comparison, quartz schists from Igarra area have an average CIA value of 53.9% (Okeke and Meju, 1985) which is less than those of Jakura area (Elueze and Okunlola, 2003) with an average value of 62.1%.

2.2.6 Gold Mineralization

Gold occurrences in Nigeria

The Nigerian Pan-African is perceived to be less endowed with gold when compared with similar, but older terrains known in Early Proterozoic West African Craton (Garba, 1990).

There are several areas of gold occurrences in Nigeria, mostly concentrated in the western half of the country and associated with the supracrustal (schist belts). The first report of gold occurrences in Nigeria was by Dustan (1911). Gold mineralization is present in alluvial and elluvial placers and primary veins from several parts of supracrustal (schist) belts in the northwest and southwest of Nigeria. The most important occurrences are found in Anka, Zuru, Maru and Kushaka schist belts in the northwest and Egbe – Isanlu and Ilesha schist belts in the southwest (Garba, 2003) as shown in Fig. 2.6.

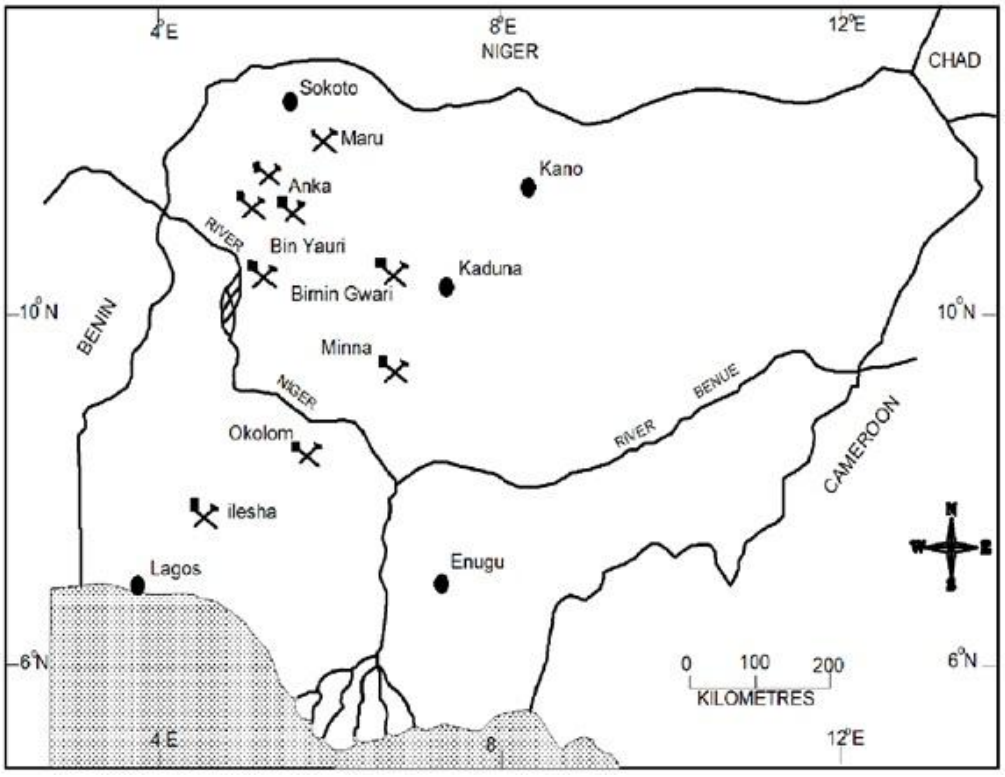


Fig. 2.3: Areas of Gold mineralization in Nigeria (after Garba, 2000).

About twenty five percent of the total 12 tonnes of the recorded (1932 – 1945) gold production was derived from Ife-Ilesha-Egbe goldfields (Fig. 2.8), while others came from the Minna-Birnin Gwari and Sokoto gold fields (Ajayi, 2003).

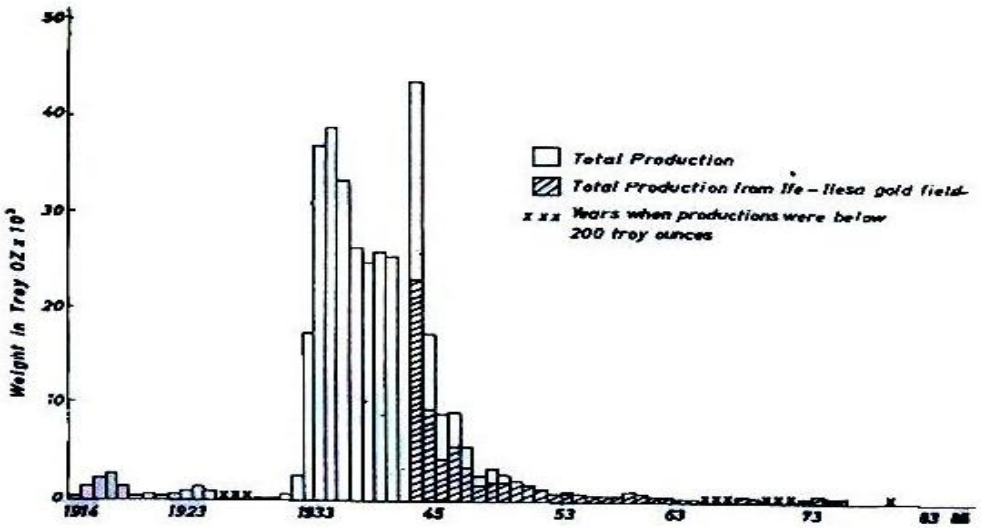


Fig. 2.4: Gold production potential in Nigeria (Ajayi, 2003)

Earlier workers (Russ, 1957; Akande *et al*., 1988; Garba, 2003; Talaat and Mohammed, 2010) have been able to outline four goldfields within the western province of the basement rocks of Nigeria. The four goldfields are:-

i. Okeogun, Ife – Ilesha and Isanlu – Egbe goldfields
ii. Minna – Birnin Gwari goldfields
iii. Zamfara (Anka, Sado and Maru) goldfields
iv Yelwa (Bin Yauri) and Okolom goldfields

Structural controls of gold mineralization and metamorphism

In Nigeria, gold mineralization and hydrothermal alteration appear to have accompanied the brittle faulting. CO_2–rich metamorphic (hydrothermal) fluids of crustal origin have been implicated for the genesis of the mineralization. The gold mineralizing fluids were channelled to

depositional sites via a NW – SE trending subsidiary brittle fault that was linked to the transcurrent Anka fault (Garba, 2000; 2003). The mineralized veins vary from 0.5 cm to 0.5 m along a strike length of over 2 km (Akande and Kinnaird, 1990).

The NE–SW and NNE–SSW regional fractures controlling the mineralization are deep seated. The similarity of the possible fluid source in the entire gold mineralization site studied in the Nigerian Basement may be an indication of gold ore-fluids active on a regional scale. Structural settings also suggest the emplacement of gold mineralization to be late Pan-African, subsequent to peak regional metamorphism and granitoid intrusion (Garba, 2003).

The workings in the old gold mines in the Anka area consist of elongate open pits aligned generally in a N-S direction, indicating that the mined auriferous quartz veins were also aligned in a N-S direction conformable with the surrounding host rocks (Danbatta, 2006). Also, Akande *et al.*, (1988) observed that vein contacts are strongly sheared and the contact zones consist of quartz, sulfide, stockworks and stringers.

Some of the Nigerian goldfields lie in the amphibolite facies biotite granite gneiss of the Proterozoic age. The gold mineralization occurs in quartz-carbonate veins extending about 1km along a second–order fault/shear zone trending NNE parallel to the Ifewara transcurrent fault, which is 4 km to the west (Garba, 2000). Gold emplacement here was inferred to be late Pan-African on the basis of structural relationships, and the main control of mineralization being subsidiary fault zone which is parallel to the Ifewara transcurrent fault (Garba, 2000; 2003). Gold-quartz-carbonate veins, for example at Bin Yauri, are located by a brittle fault zone cutting hornfels in a contact zone of Pan-African granodiorite batholith intruding phyllites and tourmalinites of the Zuru schist belt (Garba and Akande, 1992).

CHAPTER THREE

REMOTE SENSING AND SPECTRAL ANALYSIS

3.1 PREAMBLE

In this study ASTER-GDEM was draped on tapographic map to have a 3-D view of the study area. Also, image processing techniques including band ratioing and false colour composition on Landsat TM bands aided lithologic, structural and alteration mapping.

3.2 DIGITAL ELEVATION MODEL

Digital cartographic dataset of elevations in xyz coordinates of the study area was draped on topographic map to have a 3-D perspective view of physiographic features. Atlas shader displayed topographic variations with color (Fig. 3.1).

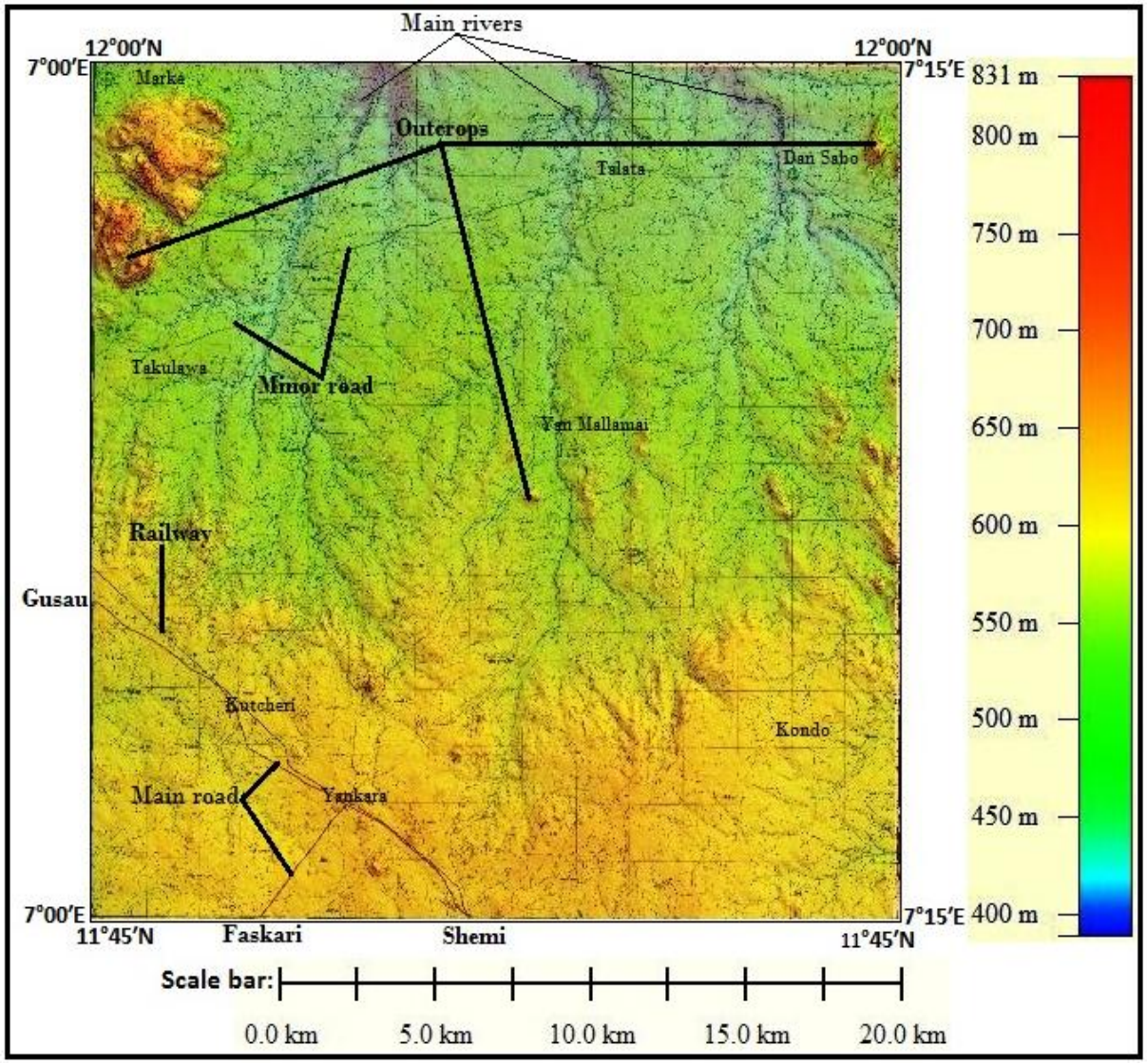


Fig. 3.1: ASTER GDEM draped on topographic map of the study area.

The highest outcrop (Kuruku Hill) lies at the northwestern edge of the study area. Other smaller outcrops and features like the major rivers and their tributaries, access roads (main and minor) are seen.

3.3 BAND RATIOING

Band ratios were prepared by dividing the digital number (DN) values of each pixel in one band by the corresponding DN values of another band (Drury, 1993). Band ratio technique enhances the objects based on the differences in reflectivity between the numerator and denominator spectral bands (Frei and Jutz, 1990).

Several researchers dealt with the lithological mapping using band ratio images which was applied on Thematic Mapper images (e.g., Kaufmann, 1988; Sultan *et al.*, 1987; Kusky and Ramadan, 2002; Gad & Kusky, 2006; Frei & Jutz, 1990). In the current contribution, the band ratios (5/7) and (3/1) were applied on the ETM+ subset covering the study area.

The band ratio 5/7 image (Fig. 3.2) clearly discriminates the granite and gneisses (bright tone) and the metasediments (dark tone). A similar image tone was also noted for granitods in the South Eastern Desert, Egypt (Zoheir and Enam, 2012).

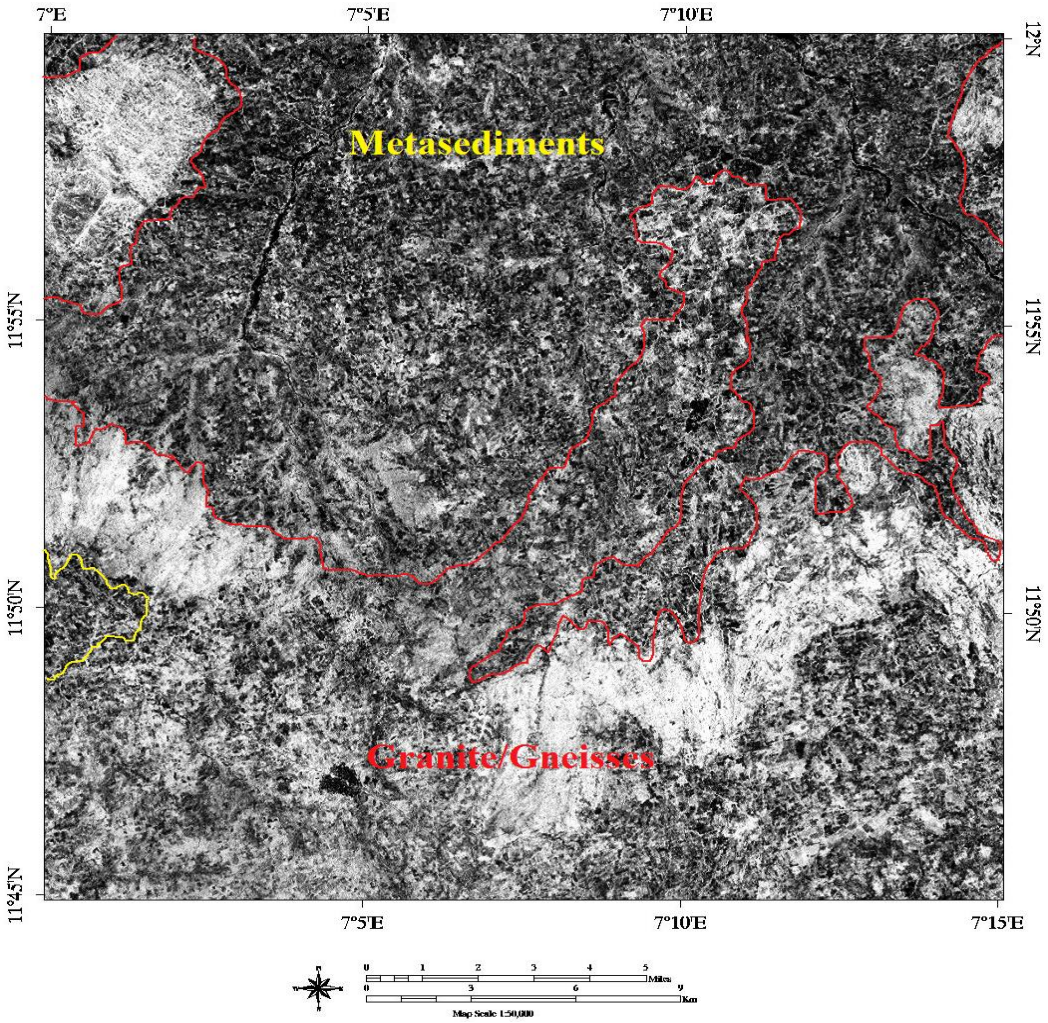


Fig. 3.2: ETM+ band ratio 5/7 of the study area showing granite and gneisses with high tone white to mist grey.

Reverse of band ratio 5/7 was observed for granitoid rocks on the ETM+ band ratio 3/1 as they mainly displayed dark grey tone. Alluvium on terrace around stream channels had bright white tone (Fig. 3.3). Yousif and Shedid (1999) reported similar pattern for granitoids in central eastern desert of Egypt. Shalaby *et al.*, (2009) also used the ratio to discriminate between mafic/ultramafic rocks (bright tone) from granitoids (dark tone) in granitic plutons in eastern Egypt.

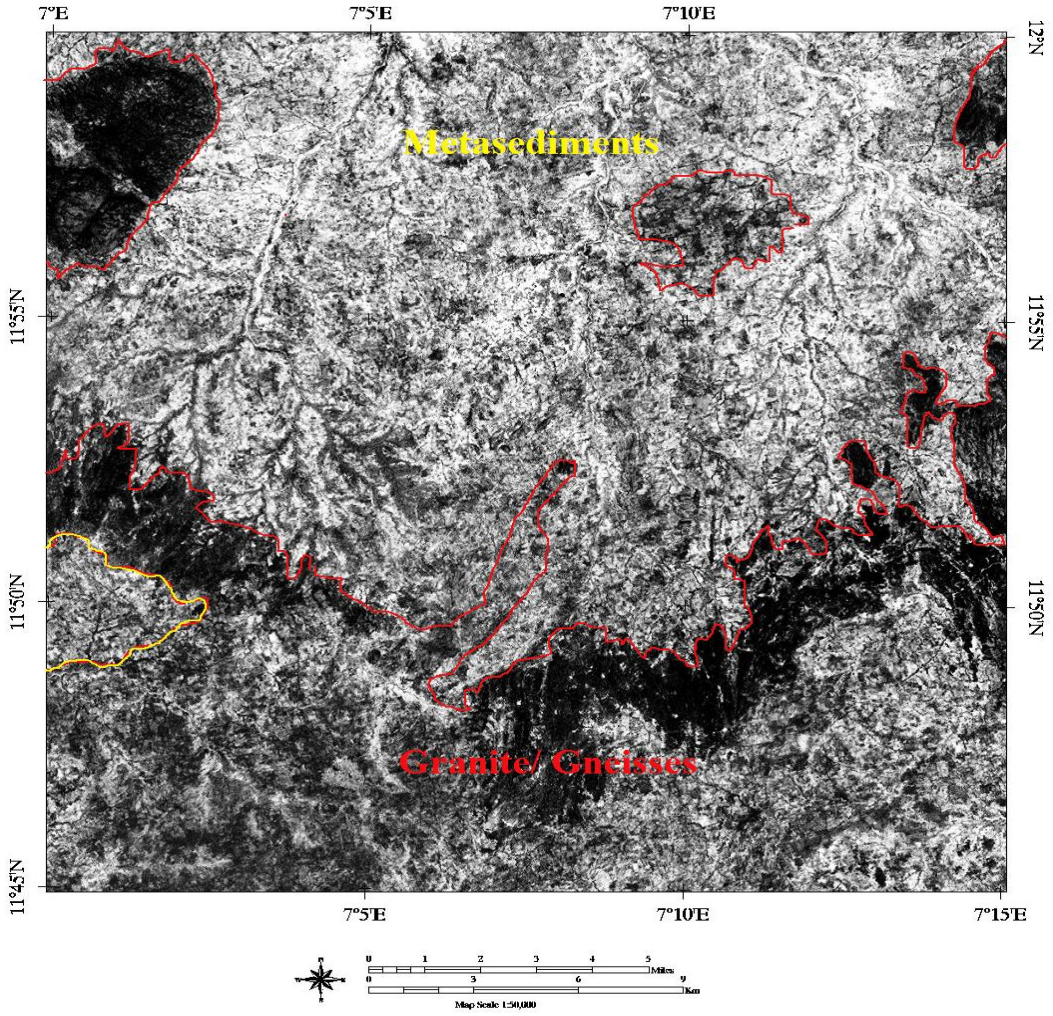


Fig. 3.3: ETM+ band ratio 3/1 of the study area showing granite and gneisses show dark grey tone.

3.4 COLOUR COMPOSITES

3.4.1 Chica-Olmo ratio

In 2002, Chica-Olmo developed a ratio (Chica-Olmo ratio) which include the combination of ETM+ band ratios 5/7 (Red), 5/4 (Green) and 3/1 (Blue) sequence as images for the detection of hydrous minerals and iron-rich zones. This ratio was adopted in the study area. Red correspondences are for clay minerals (alteration from feldspars) while iron minerals and ferric oxides are green and blue respectively (Chica-Olmo, 2002). The quartzofeldspathic granites displayed red tone while the metasediments with iron and ferric oxides are green. Clear green

signature indicating presence of iron minerals are also observed on some parts of Kuruku hill in the northwestern part of the study area (Fig. 3.4).

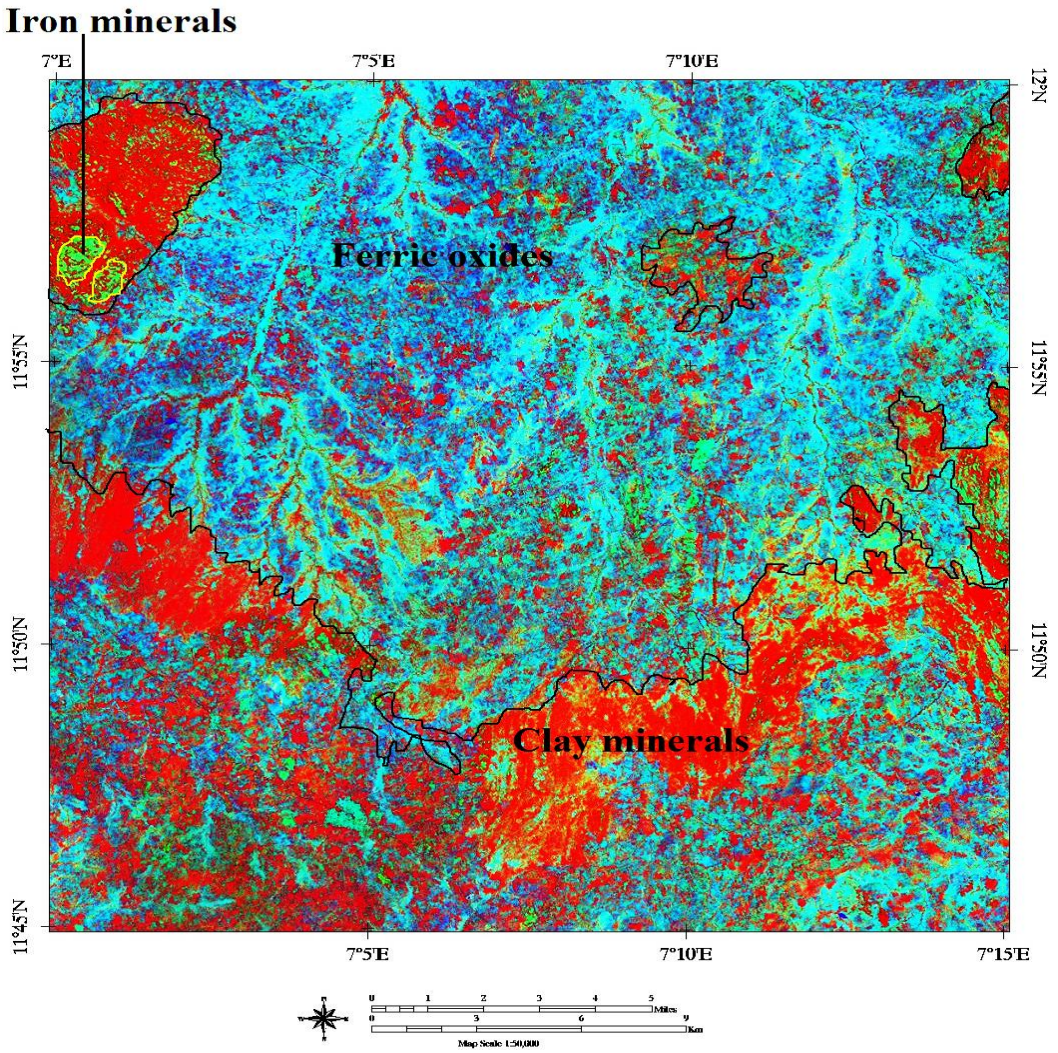


Fig. 3.4: Colour composite (Chica-Olmo ratio) which include the combination of ETM+ band ratios 5/7 (R) for clay minerals, 5/4 (G) for iron minerals and 3/1 (B) for ferric oxides.

3.4.2 Kaufmann ratio

Also, the color composite created by band ratio 7/4, 4/3 and 5/7 displayed as RGB respectively of (Kaufmann, 1988) was adapted. Consequently red color represents the minerals containing iron ions; green represents the vegetated zones and blue represents OH/ H_2O-, SO_4- or CO bearing minerals (rocks and soils). Minerals containing iron ion (red) and vegetated zone largely

occur within the undifferentiated metasediments. Also, the OH/ H_2O-, SO_4- or CO bearing minerals mainly occur within the quartzofeldspathic granite and gneisses (Fig. 3.5).

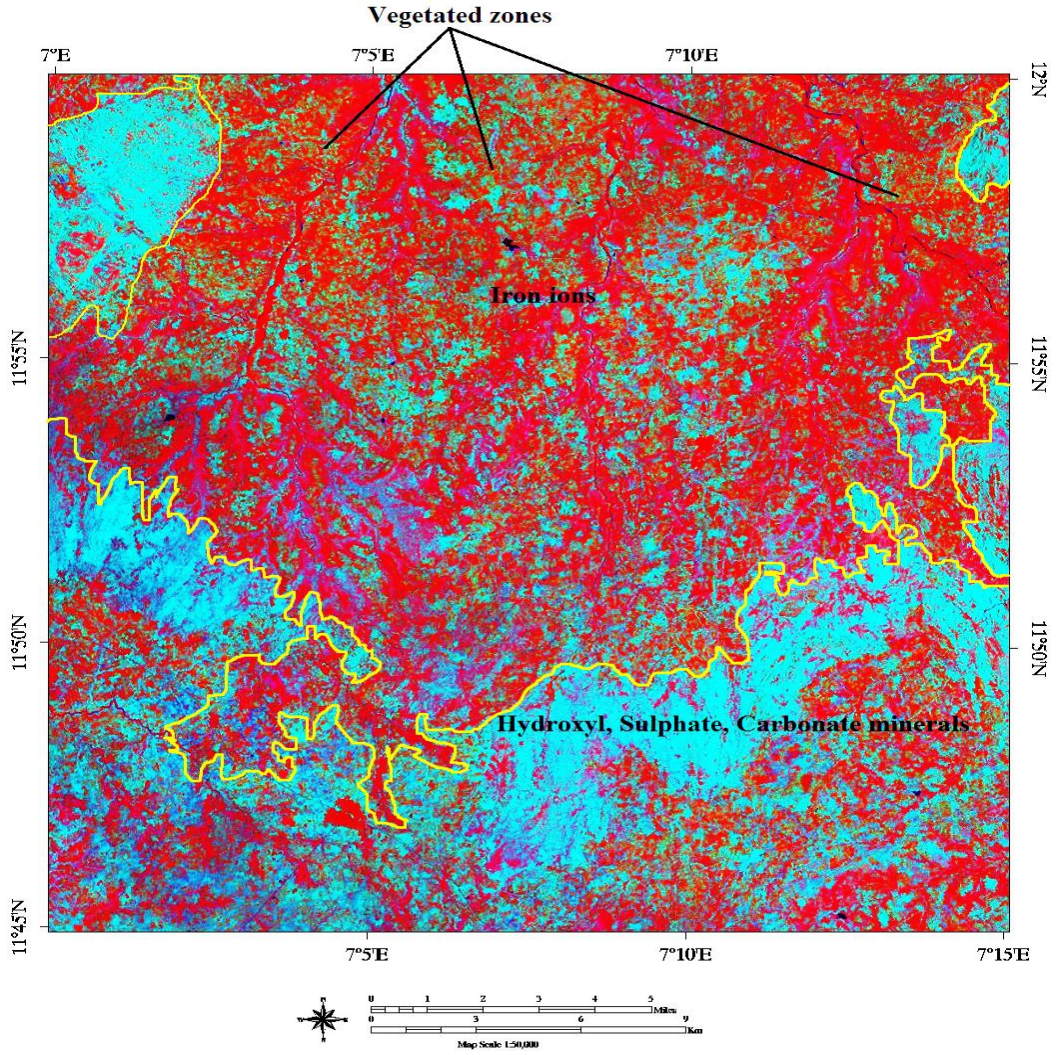


Fig. 3.5: Colour composite (Kaufmann ratio) which include the combination of ETM+ band ratios 7/4, 4/3 and 5/7 displayed as RGB showing areas of mineral alteration.

3.5 AUTOMATIC LINEAMENTS EXTRACTION

The surface expression of geological structures such as, fractures, faults, joints, shear zones and foliations are shown in the form of lineaments on airborne and orbital remote sensing data (Koch and Mather, 1997). Automatic lineament extraction from remote sensing data is an important approach for regional structural and mineralization studies (Rowan and Bowers, 1995).

The lineaments analysis was undertaken in order to understand the relationship between the lineament trends (faults) as the main structural element affecting the rock units exposed at the study area. Landsat panchromatic image was prepared to conduct this test under the default parameters of LINE module of PCI software (Table 3.1).

Table 3.1: Default parameters for LINE module for lineament extraction.

Parameter	**Default**
Filter radius (pixel)	10
Edge gradient threshold	40
Curve length threshold (pixel)	30
Line fitting error threshold(pixel)	3
Angular differece threshold(degree)	30
Linking distance threshold (pixel)	20

Automatic lineaments extraction from Landsat panchromatic image was run with three major steps: 1) edge detection, 2) threshold and 3) lineaments extraction. Fig. 3.6 shows the main lineament trends automatically extracted in the study area.

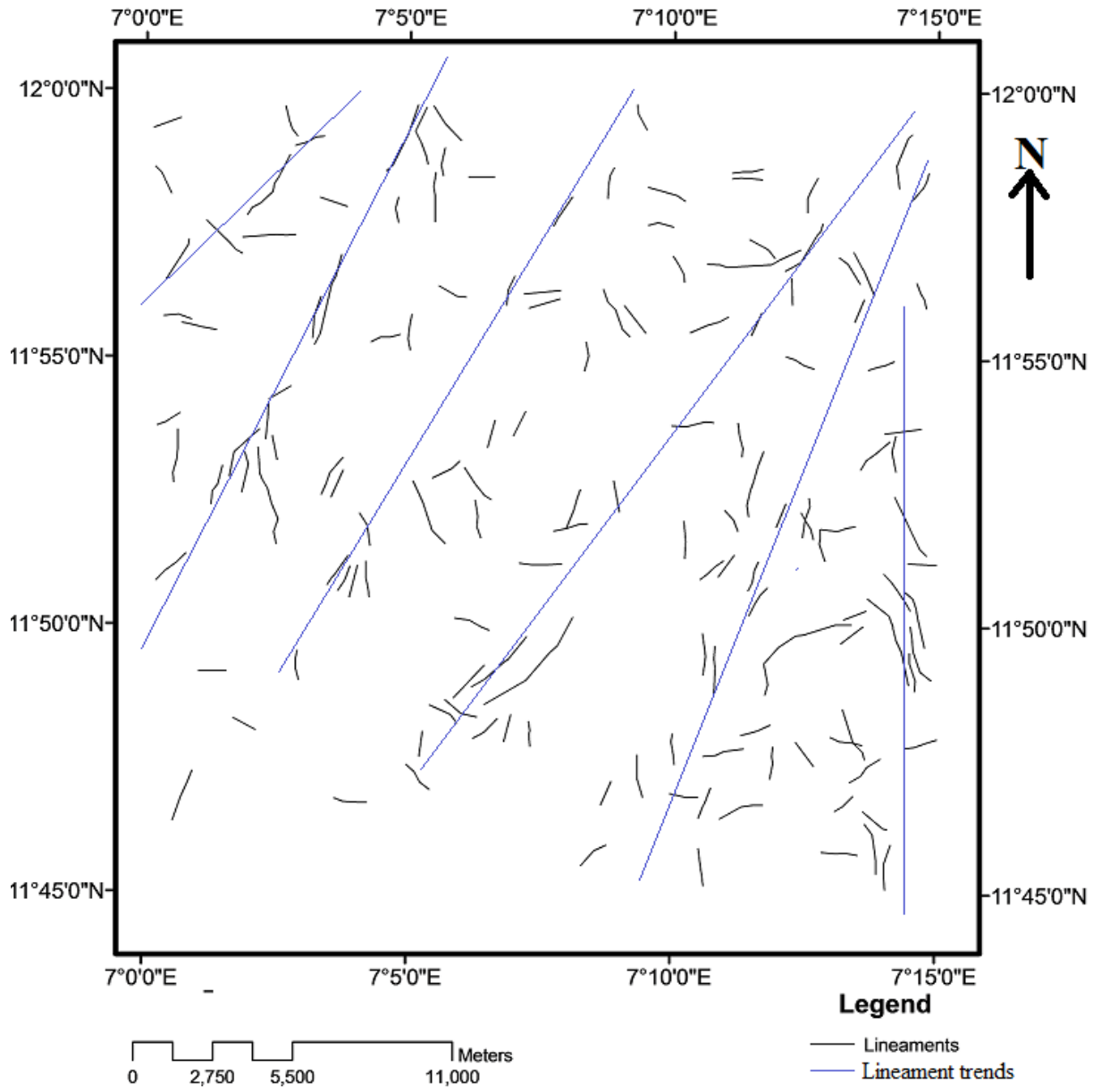


Fig. 3.6: Automatic extracted lineament trends (default setting) of structures in the study area.

The lineament frequency/rose diagram reveals that the most prominent strike direction is NNE-SSW, NE-SW, NNW-SSE. Nearly E-W trend and others are subordinate direction (Fig. 3.7).

There is good relationship between the lineaments and drainage pattern system distribution especially with respect to first and second order rivers. Lineaments in other parts of the area

display a typical pattern of the fault system in the area. These were confirmed in rose plot from ground truthing.

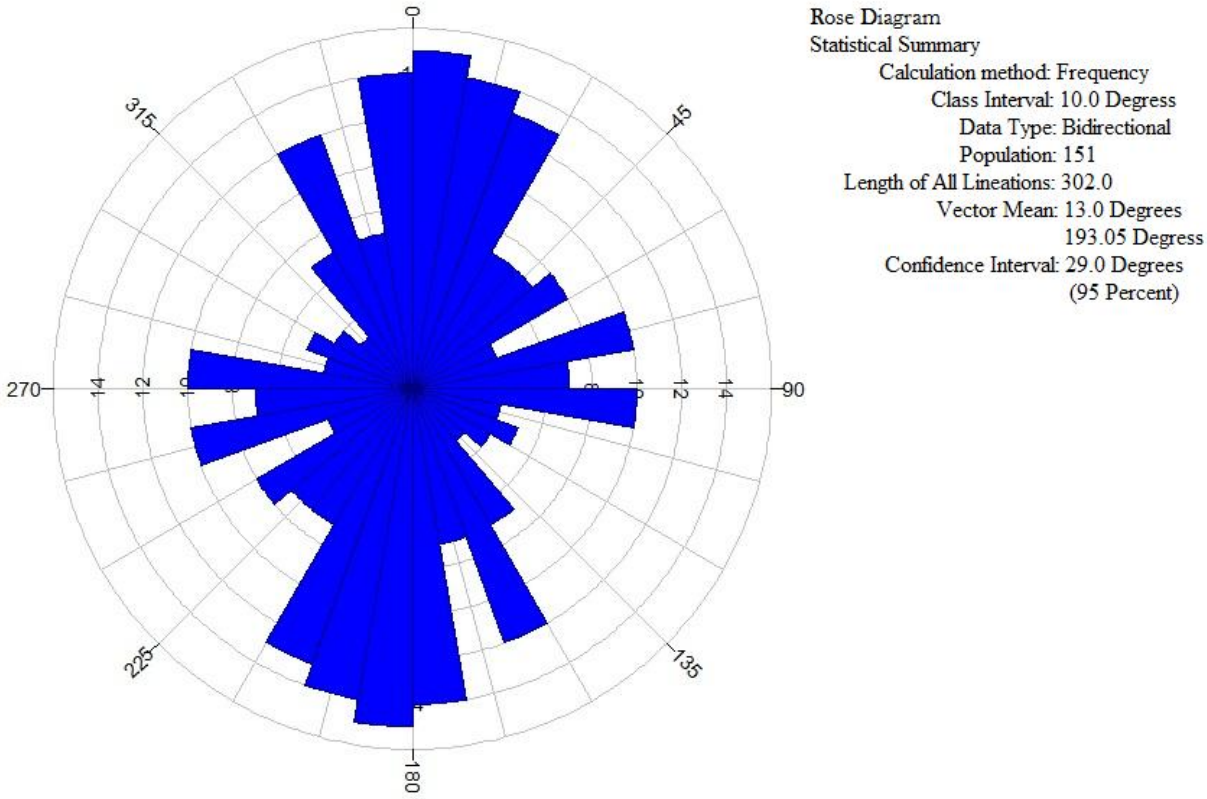


Fig. 3.7: Rose (azimuth-frequency) diagram of lineaments orientations

Result of lineament analysis is in agreement to a large extent with the results of rose plot from manually documented readings on field work (see Appendices III – VII).

CHAPTER FOUR

FIELD GEOLOGY, PETROGRAPHY AND STRUCTURES

4.1 PREAMBLE

The major rock types in the study area comprise of gneisses (porphyroblastic, granitic and banded gneisses), metasediments (schists and phyllites), biotite granites (porphyritic and medium to coarse grained varieties) and serpentinite (Map in back cover). The minor rocks types are schist xenolith, quartz veins, quartzofeldspathic pegmatites and quartz-tourmaline rock. Alluvium, laterite (iron stone) and soil occur as superficial deposit. Structurally, both ductile (foliation, fold) and brittle structures (joints, faults) were mapped in the study area.

The mode by volume for each mineral in the major rock types are presented in Tables 4.1.

Table 4.1: Modal composition of minerals in major rock types in the study area

	Percentage composition (by volume)											
Rock	Quartz	Orthoclase	Plagioclase	Microcline	Perthite	Sericite	Biotite	Muscuvite	Chlorite	Pyroxene	Olivine	Opaque
PBG 1	30.8	-	10.4	34.1	-	-	24.9	-	-	-	-	-
PBG 2	48.2	-	28.8	-	-	-	17.1	-	-	3.9	-	1.0
MBCG	40.5	-	9.4	19.5	10.0	-	15.6	5.0	-	-	-	-
BSch 1	50.5	-	-	-	-	-	46.2	-	-	-	-	3.3
BSch 2	39.2	-	-	-	-	-	45.8	-	4.2	-	-	5.8
BSch 3	49.9	-	-	--	-	-	41.1	9.2	-	-	-	5.8
BSch 4	40.2	-	4.5	-	-	-	53.1	-	-	-	-	2.2
BSch 5	45.3	-		-	-	-	34.7	-	6.2	-	-	8.8
BSch 6	56.3	-	5.2	-	-	-	31.7	-	-	-	-	6.8
Phy 1	51.8	-	-	-	-	-	49.2	-	-	-	-	-
Phy 2	55.0	-	-	-	-	-	45.0	-	-	-	-	-
BGn 1	44.2	-	15.0	-	-	-	32.8	-	5.8	-	-	2.2
BGn 2	30.2	19.8	10.5	18.1	-	-	19.5	-	-	-	-	2.9
GGn	40.2	-	8.2	11.6	9.8	5.0	16.4	-	2.8	-	-	6.2
PGn	35.2	-	5.5	24.0	-	2.4	20.8	-	-	9.9	-	-
Serpt	-	-	-	-	-	-	-	-	-	25	65	10

Where:

PBG = Porphyritic Biotite Granite
MBCG = Medium to Coarse grained Biotite Granite
BSch = Biotite Schist
Phy = Phyllite
BGn = Banded Gneiss
PGn = Porphyroblastic Gneiss
GGn = Granite Gneiss
Serpt = Serpentinite

4.2 PORPHYROBLASTIC GNEISS AND GRANITE GNEISS

4.2.1 Field relationships

Porphyroblastic gneiss occur as low lying outcrop that are light to dark grey in colour (Plate I). It is also light brown in other places (Plate II). The porphyroblastic gneiss (PGn) has gradational to sharp contact with porphyritic biotite granite east of Kura Mota in the central part of the study area. It also has sharp contact with schist around Danyaro. It constitutes about 12% of the rocks in the study area. The outcrops have quartzofeldspatic vein mainly perpendicular to the gneissose texture (Plate II). The veins are parallel in places.

The porphyroblastic gneiss (PGn) has a gradational contact with granite gneiss around Kura Mota. The granite gneiss is grey in colour and is not mappable at the scale of the map.



I



II

Plate I: Photograph of PGn with white coloured porphyroblasts at 11° 50′ 22.4″ N and 7° 11′ 14.0″ E.
Plate II: Photograph of feldspathic porphyroblasts in PGn and boudins of feldpathic veins (4 cm width) perpendicular to the NE-SW (040°) trend of host rock at 11° 50′ 2.4″ N, 07° 09′ 12.2″ E.

4.2.2 Petrography of Porphyroblastic Gneiss

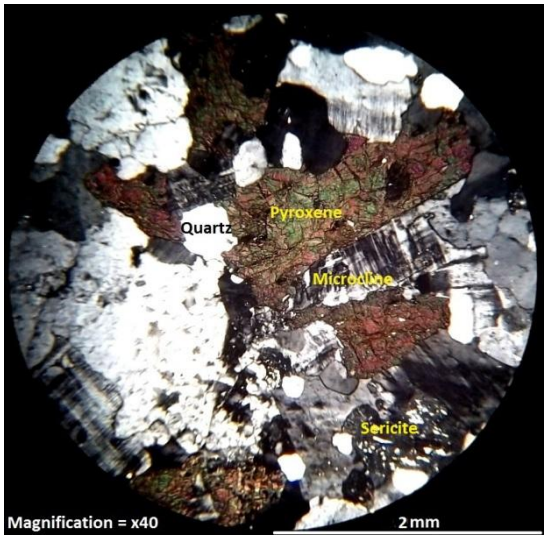
In hand specimen, it is composed of creamy-white feldspar and quartz, together with dark minerals. The dark minerals are arranged in a streaky banding, giving the rock a gneissic texture. Mineralogically, it is composed of quartz, feldspars and biotite with foliation defined by biotite.

In thin section, it is inequigranular with biotite, pyroxene, quartz and feldspar. The quartz is colourless and anhedral. The pyroxene grains are brown coloured with high relief and two direction cleavages intersecting at nearly 90° (Plate III). Biotite and pyroxene had moderate double refraction. Feldspars are colourless but cloudy (Plate III) in plane polarised light (PPL) while quartz is also colourless with low relief (Plate III).

In crossed polarised light (XPL), pyroxene displayed red to green interference colours and oblique extinction while biotite displayed light brown interference colour with straight extinction. The microcline displayed tartan twinning pattern (Plate IV) with myrmekitic intergrowth texture (Plate V). It is also altered in places into sericite (Plate IV). Deformation of quartz grains is evidently revealed by cracks and wavy extinction in places (Plate IV and V).

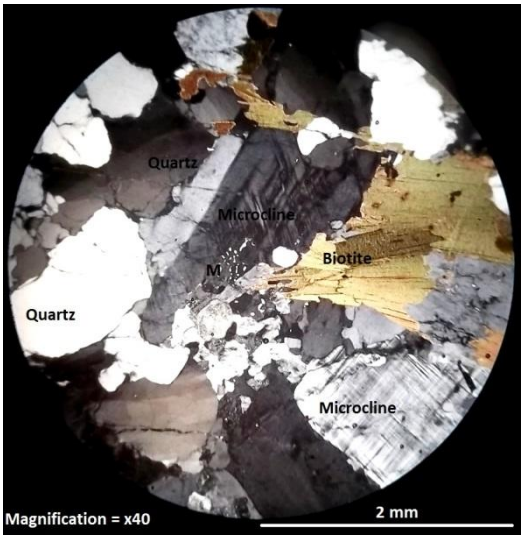


III (PPL)

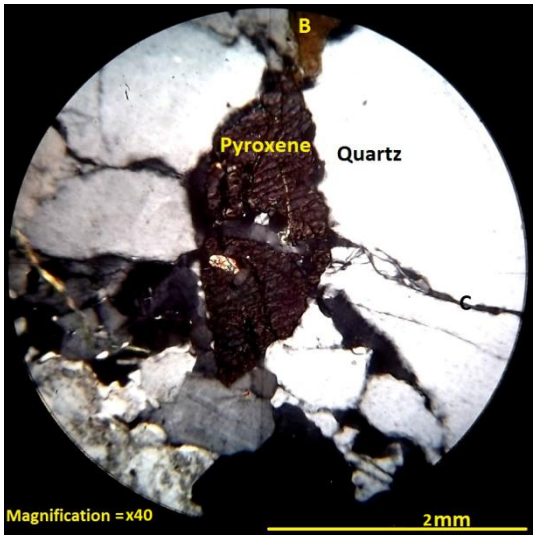


IV (XPL)

Plate III: Photomicrograph of PGn showing brown pyroxene with cleavages in two directions.
Plate IV: Photomicrograph of PGn with red to green interference colours in pyroxene.



V (XPL)



VI (XPL)

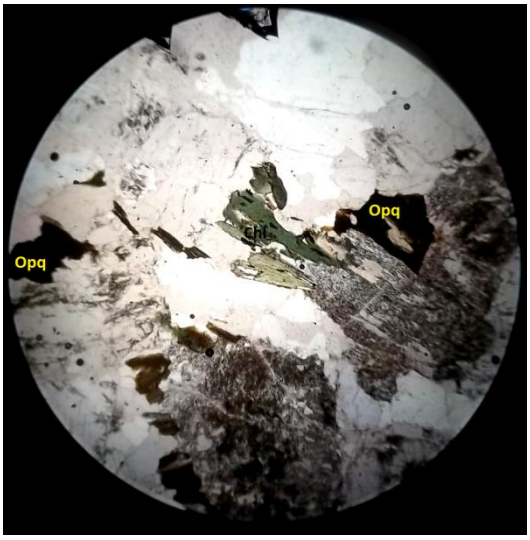
Plate V: Photomicrograph of PGn with myremekitic intergrowth texture (M) in microcline.
Plate VI: Photomicrograph of PGn showing pyroxene with deep pink interference colour.

The porphyroblastic gneiss is composed of quartz, microcline, biotite, pyroxene, plagioclase and sericite (Table 4.1)

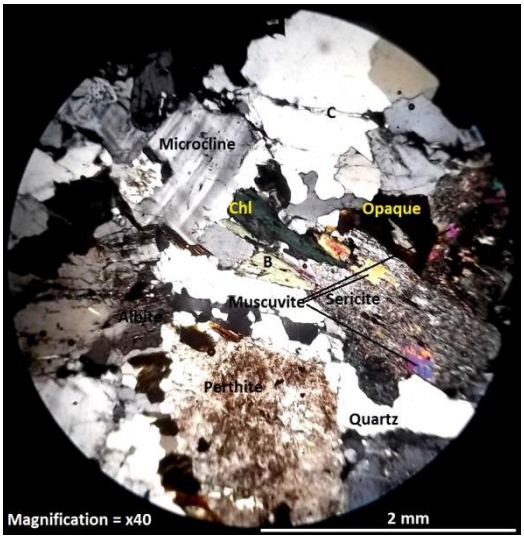
In PPL, the granite gneiss (GGn) also has cracks in the quartz with significant alteration of albite into sericite and biotite to chlorite (Plate VII). The opaque mineral is probably magnetite or ilmenite. All the feldspars are colourless but cloudy except microcline. This confirms that microcline is the most stable of the feldspars.

In XPL, the microcline had 1st order grey interference colour and one set of twin lamellae predominates (Plate VIII). There is Poikilitic inclusion of muscovite in sericite (alteration product of albite) and opaque mineral. The microcline had low relief. The feldspars show inclined extinction at an angle of 18° while biotite shows straight extinction at an angle of 92°.

The granite gneiss is composed of quartz, biotite, microcline, micro perthite, plagioclase, sericite, opaque mineral(s) and chlorite (Table 4.1).



VII (PPL)



VIII (XPL)

Plate VII: Photomicrograph of GGn with light green chlorite (Chl) and opaque minerals (Opq).
Plate VIII: Photomicrograph of GGn (Slide AA14) with cracks (C) in quartz and grey microcline.

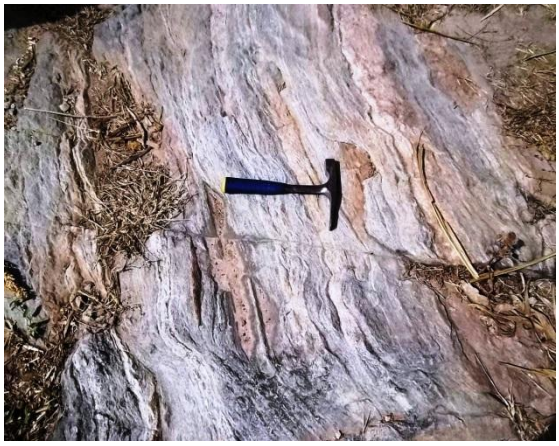
4.3 BANDED GNEISS

4.3.1 Field relationships

Banded gneiss (BGn) occurs in most of the southern part (around Angwan Shawo and Tanimu) towards Gidan Mesa in southeastern part of the study area. It constitutes about 10% of the rocks in the area and mainly occurs as weathered low lying unit, though the degree of weathering varies. It is generally dark to grey (when fresh) and light brown when weathered (Plate IX and X). Texturally, it is medium to coarse grained. Under hand lens observation, the rock contains feldspar and quartz as the light coloured minerals and flakes of biotite dominates the dark ferromagnesian minerals. Both the light and dark coloured minerals are aligned (foliated) in NNE – SSW direction.



IX



X

Plate IX: Photograph of BGn with joints mainly trending parallel to the direction of the bands with few perpendicular to it at 11° 45′ 33″ N and 07° 08′ 25″ E.
Plate X: Photograph of BGn with alternating light and dark coloured bands that are slightly folded in places around Tanimu at 11° 49′ 10″ N and 7° 14′ 22″ E.

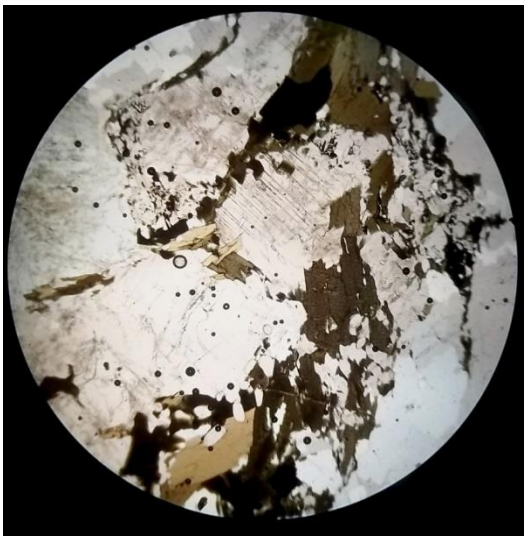
4.3.2 Petrography of banded gneiss

In hand specimen the banded gneiss displays distinct banding of grey and white coloured minerals. The white bands are coarser grained and very poor in mafic minerals. The dark brown to grey bands contains mafic minerals, principally biotite. The flakes of biotite are also aligned with their long dimensions parallel to the mineral banding. The banding reveals that the rock has undergone some episode of deformation.

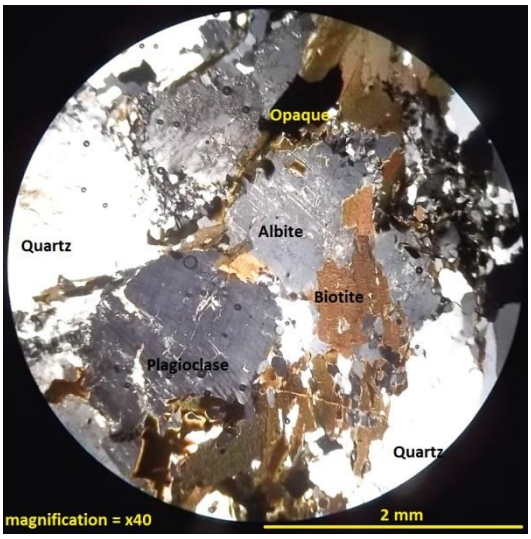
In PPL, felsic band predominates in the BGn 1. The leucocratic band is composed mainly of quartz and plagioclase feldspar while the mesocratic band consists predominantly of foliated biotite (Plate XI). The quartz is colourless with low relief and anhedral. The plagioclase is colourless but cloudy. Biotite has moderate relief and shows strong pleichroism from light to dark brown. Traces of alteration of biotite to chlorite are noted along the grain boundaries and cleavage planes in BGn 1 (Plate XIII) and BGn 2 (Plate XVII). In BGn 2, symetrical

microfolding of foliated brown to light green biotite minerals were observed (Plate XV and XVII).

In XPL, the feldspar displays light grey (BGn 1), low 1st order interference colour with albite twinning (Plate XII). The microcline display tartan twinning (Plate XIV). Also, plagioclase feldspar in BGn 2 has myremekitic intergrowth texture (Plate XX).

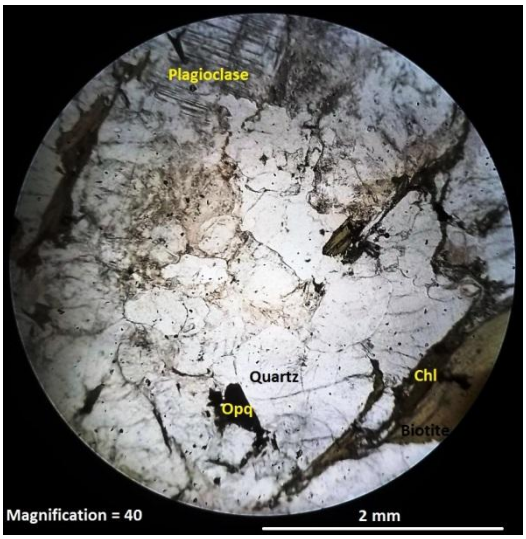


XI (PPL)

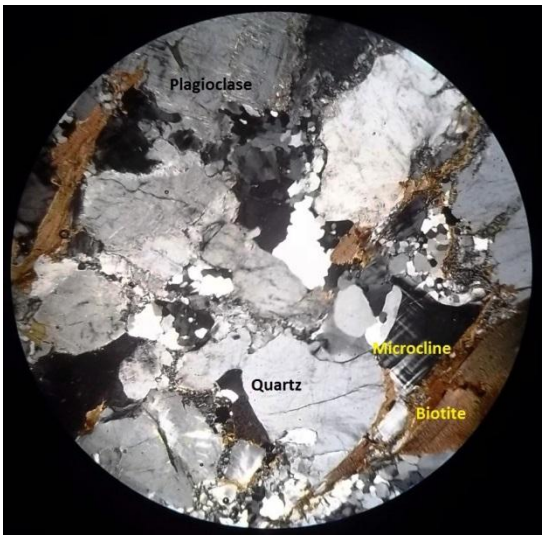


XII (XPL)

Plate XI: Photomicrograph of BGn 1 showing foliated brown coloured biotite.
Plate XII: Photomicrograph of BGn 1 showing plagioclase feldspar dominates the feldspar.

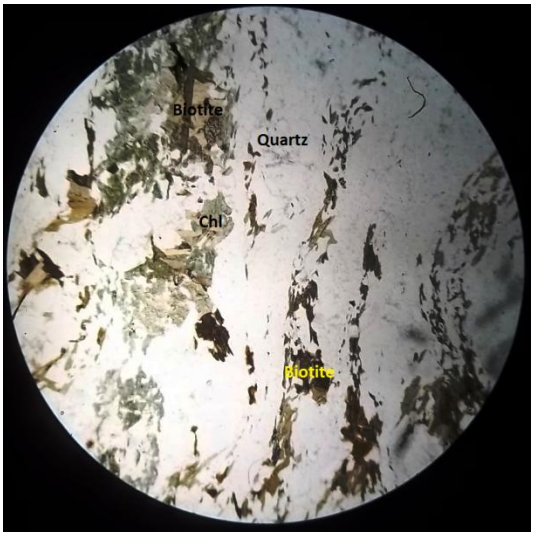


XIII (PPL)

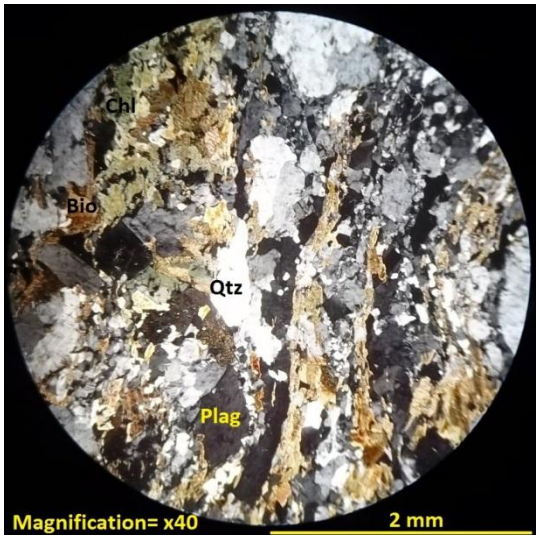


XIV (PPL)

Plate XIII: Photomicrograph of BGn 1 with colourless quartz with low relief.
Plate XIV: Photomicrograph of BGn 1 with small scaled tartan twinning in microcline.

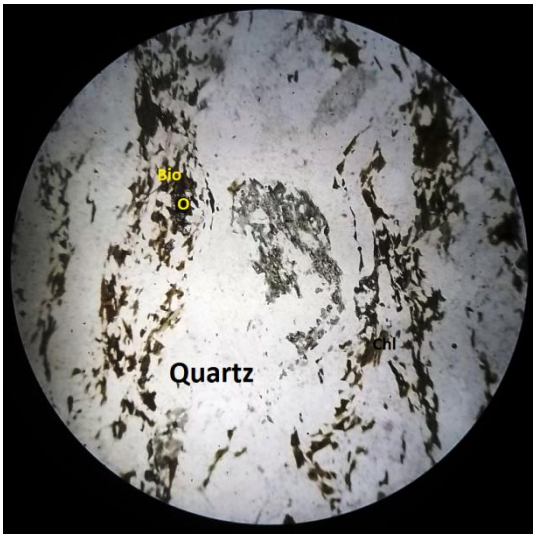


XV (PPL)

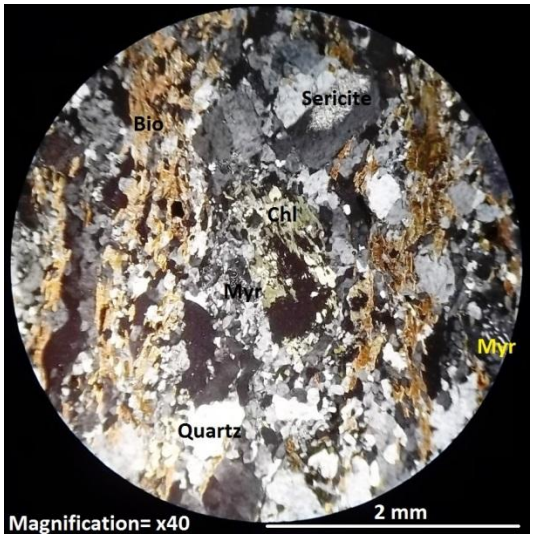


XVI (XPL)

Plate XV: Photomicrograph of BGn 2 with lineated and folded brown biotite.
Plate XVI: Photomicrograph of BGn 2 showing grey coloured plagioclase feldspar.



XVII (PPL)



XVIII (XPL)

Plate XVII: Photomicrograph of BGn 2 with foliated dark brown biotite and light green coloured chlorite.
Plate XVIII: Photomicrograph of BGn 2 with myrmekitic intergrowth texture (Myr) in plagioclase and its alteration to sericite in places.

The banded gneiss is composed of quartz, biotite, orthoclase feldspar, microcline, plagioclase feldspar, chlorite and opaque mineral (Table 4.1).

4.4 BIOTITE SCHIST

4.4.1 Field relationships

The biotite schists occur as low lying outcrops (subdued relief), road cuts and river bank exposures. It constitutes about 37% of the rocks in the study area. It predominates the northeastern part (around Dan Sabo, Takeri and Talata) but exclusively with inferred boundaries with medium to coarse grained granites. The BSch underlies areas around Danwari in the northwestern part through Yankuzau to Takulawa. It also has sharp contact with medium to coarse grained biotite granite in Mai Anita area. Also, the rock has interlocking lithologic boundaries with banded gneiss in the southeastern part around Gidan Mesa and Tanimu.

Quartzofeldspathic veins are parallel to trend direction of the schists though some are perpendicular (Plate XIX and XX).



XIX



XX

Plate XIX: Photograph of parallel and perpendicular leucocratic quartzofeldpspathic vein in biotite schist at 11° 57′ 46″ N and 07° 13′ 21″ E.
Plate XX: Photograph of biotite schist in a river channel with parallel quartzofeldspatic veins at 11° 57′ 30″ N and 7° 6′ 50″ E (hammer is 30 cm long).

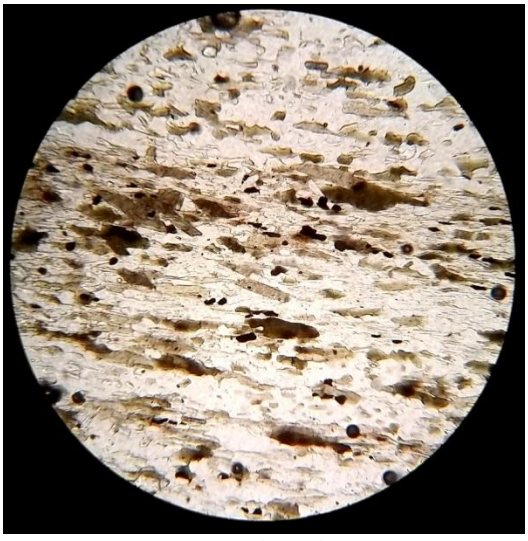
4.4.2 Petrography of biotite schist

In hand specimens, the schist is mostly dark grey (BSch 2, BSch 3, BSch 4 and BSch 5) to light brown (BSch 1 and BSch 6). It is generally medium grained. Biotite flakes are foliated and

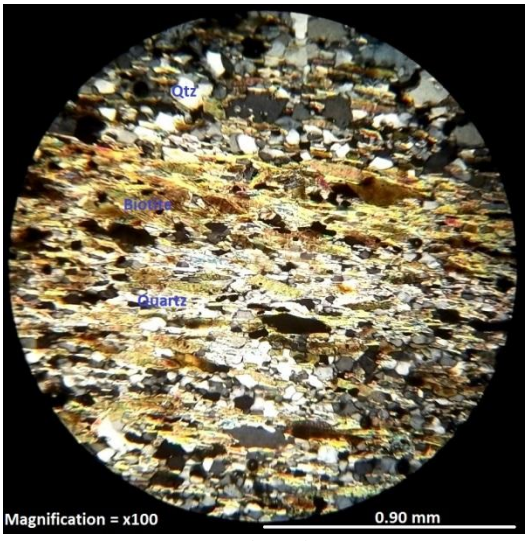
separated by light-coloured material, which are mostly millimetre-centimetre sized quartz/feldspar crystals with schistose texture.

Six thin sections (Samples BSch 1, BSch 2, BSch 3, BSch 4, BSch 5 and BSch 6) were analysed. The schists are equigranular and foliated (Plates XXI, XXIII, XXV, XXVII, XX1X and XXXI). In PPL, the quartz is colourless with low relief. The biotite displayed pleichroism from light to dark. Also, biotite grains show perfect basal cleavage (Plates XXIII, XXV, XXVII and XXIX) except few that are cut parallel to the crystallographic axis (Plate XXI). Alteration of biotite to chlorite was observed along cleavage planes and grain boundary (Plate XXIII). Also, colourless muscuvite with perfect basal cleavage occur in BSch 3 (Plate XXV).

In XPL, biotite mainly has brown interference colour (Plate XXII, XXVI, XXVIII and XXXII) while others have yellow, green and pink false colour (Plate XXIV and XXX). Muscuvite has blue polarization colour (Plate XXVI).

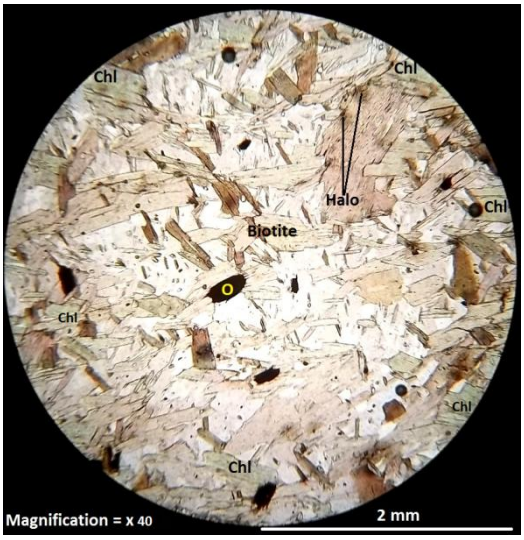


XXI (XPL)

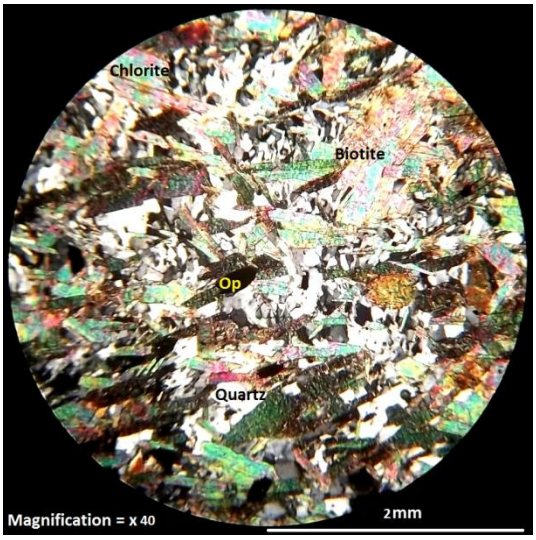


XXII (PPL)

Plate XXI: Photomicrograph of BSch 1 showing lineated brown coloured biotite with weak pleichroism
Plate XXII: Photomicrograph of BSch 1 showing yellow to brown interference colour in biotite.



XXIII (PPL)



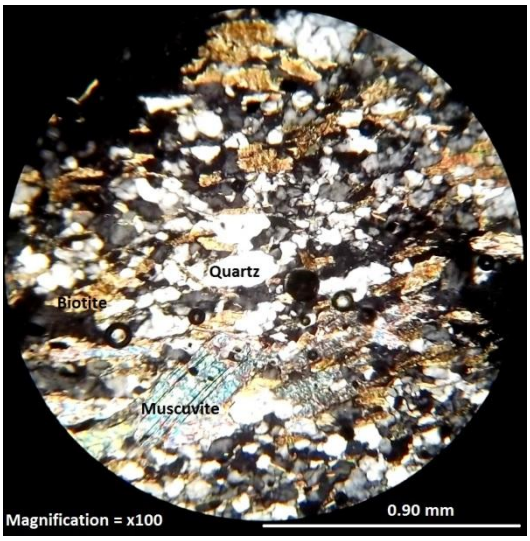
XXIV (XPL)

Plate XXIII: Photomicrograph of BSch 2 with brown coloured biotite with pleichroic halo in places. It has moderate relief.

Plate XXIV: Photomicrograph of BSch 2 showing biotite with different interference colours (green, yellow, brown and pink).



XXV (XPL)



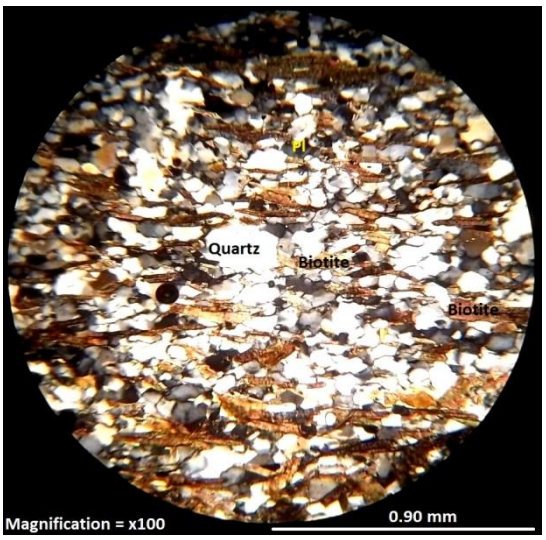
XXVI (PPL)

Plate XXV: Photomicrograph of BSch 3 with colourless muscovite and brown biotite that have moderate relief and perfect cleavage.

Plate XXVI: Photomicrograph of BSch 3 with mica (biotite and muscovite). The micas display different interference colour.



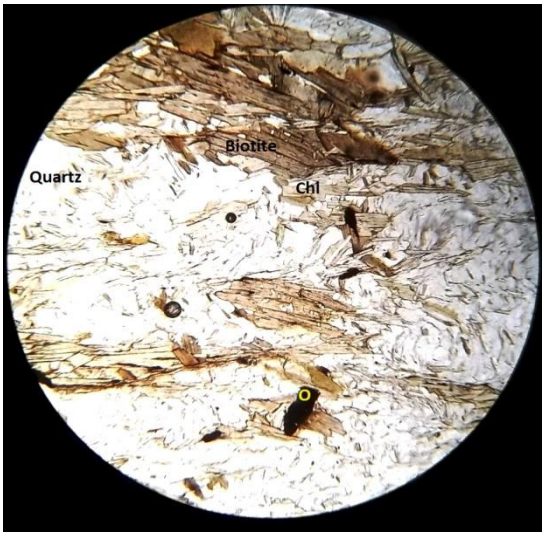
XXVII (XPL)



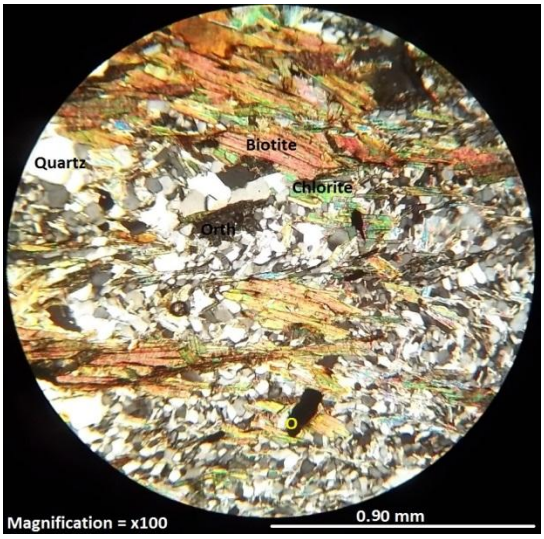
XXVIII (PPL)

Plate XXVII: Photomicrograph of BSch 4 with lepidoblastic foliation pattern and colourless equigranular quartz with low relief.

Plate XXVIII: Photomicrograph of BSch 4 with plagioclase feldspar (Pl) and biotite with grey and brown interference colour respectively.



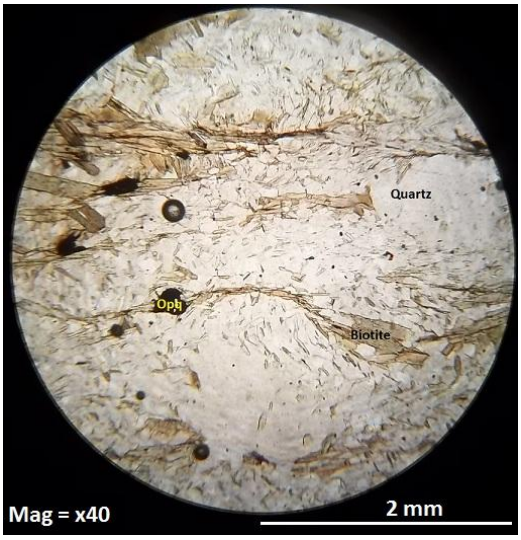
XXIX (PPL)



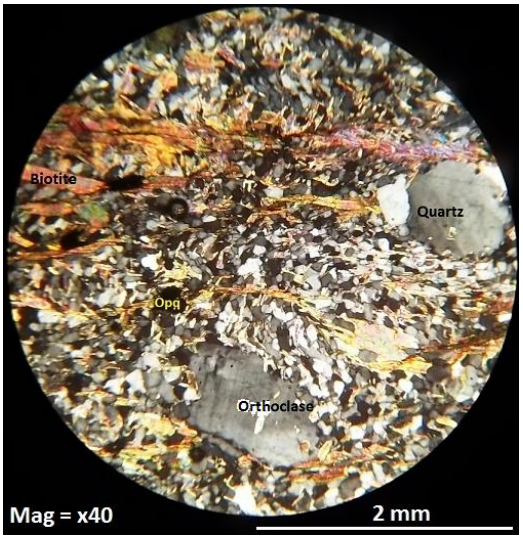
XXX (XPL)

Plate XXIX: Photomicrograph of BSch 5 with foliation of subidioblastic biotite with moderate relief, alteration to chlorite and inclusion of opaque minerals in places.

Plate XXX: Photomicrograph of BSch 5 showing xenoblastic quartz with wavy extinction on some grains.



XXXI (PPL)



XXXII (XPL)

Plate XXXI: Photomicrograph of Bsch 6 showing brown coloured granoblastic biotite with opaque inclusions.

Plate XXXII: Photomicrograph of Bsch 6 showing porphyroblastic quartz and orthoclase feldspar in fine grained groundmass.

The biotite schists are composed of quartz, biotite, plagioclase feldspar, muscovite, chlorite and opaque minerals (Table 4.1).

4.5 PHYLLITE

4.5.1 Field relationships

The phyllite (Phy) occur as low lying outcrops mainly along river banks and are light brown coloured, medium grained with cleavage produced by alignment of biotite (Plate XXXIII and XXXIV). It constitutes about 6% of varying lithologies in the study area. It occurs at the northwestern part underlying area around Gimba. The boundaries with adjoining biotite schist are inferred as alluvium cover prevented determination of sharp or gradational contact.



XXXIII



XXXIV

Plate XXXIII: Photograph of light grey coloured phyllite around Yankuzua at 11° 57′ 41.9″ N and 07° 05′ 39.8″ E.

Plate XXXIV: Photograph of phyllite with tarnished and brown appearance trend at the banks of an ephemeral stream channel at 11° 58′ 00″ N and 07° 06′ 23.5″ E.

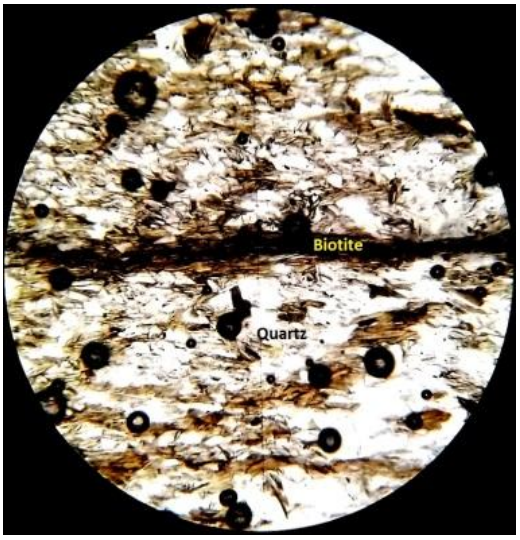
4.5.2 Petrography of phyllite

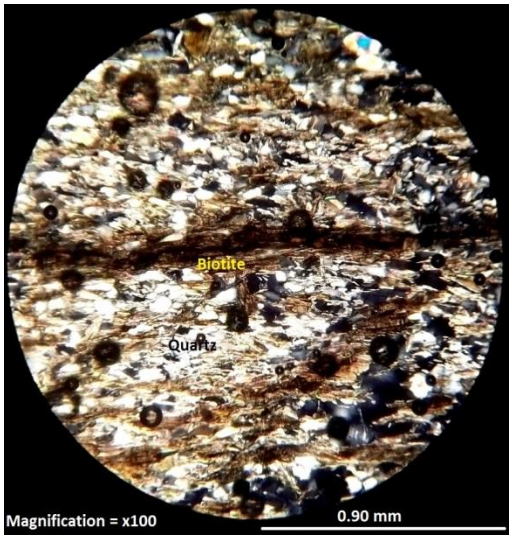
The phyllite hand specimen appears flattened with tiny platy minerals line up in the same direction, giving the rock a cleavage. It readily split into thin sheets along the cleavage. Most of the phyllite has a bright appearance on the cleavage surfaces. It reflects the light and gives a bright sheen. Others are tarnished and brown.

In PPL, equigranular colourless quartz with low relief, weak birefringence was observed. It also shows brown to faint yellow biotite that is needle like with wavy phyllitic texture, moderate relief and strong pleichroism from light to dark brown (Plate XXXV).

In XPL, The biotite show 2nd order light to dark brown interference colour. It displays straight extinction parallel to the cleavage planes (XXXVI).

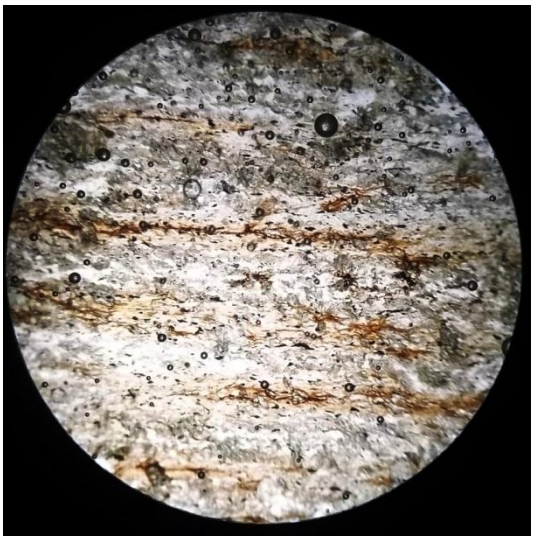
The phyllite is mainly composed of quartz and biotite (Table 4.1).

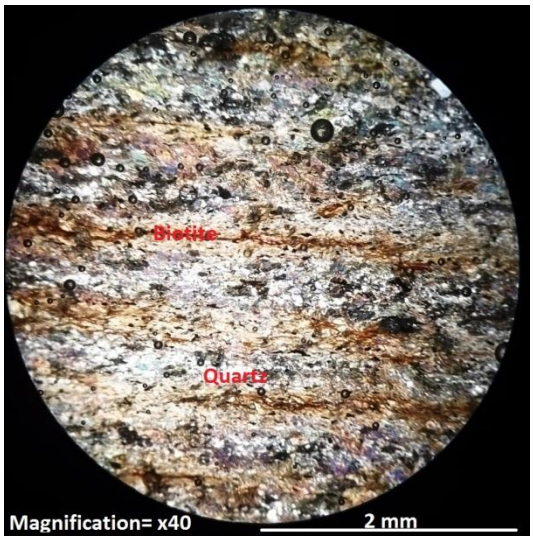




XXXV (PPL) XXXVI (XPL)

Plate XXXV: Photomicrograph of Phy 1 showing brown to biotite with wavy slaty texture and pleichroic.
Plate XXXVI: Photomicrograph of Phy 1 with light to dark brown interference colour.





XXXVII (PPL) XXXVIII (XPL)

Plate XXXVII: Photomicrograph of Phy 2 with slaty foliation pattern in biotite and quartz.
Plate XXXVIII: Photomicrograph of Phy 2 showing light brown polarization colour in biotite.

4.6 PORPHYRITIC BIOTITE GRANITE

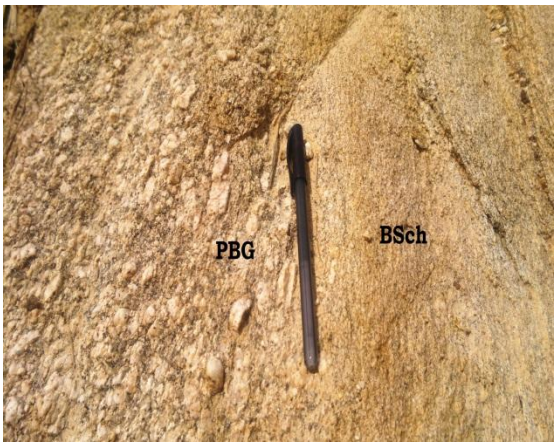
4.6.1 Field relationships

Porphyritic biotite granite (PBG) is light grey in colour and covers about 26% of the entire study area. They are characterised in most places by low lying whale-back outcrops nearly covering all

southwestern part (near Kucheri, Yankara and Danyaro), the central part (near Yan Mallamai) and the northwestern part near Marke. The rock obliterate the older biotite schists in Yan Mallamai into relic rafts (Plates XXXIX and XL). Its sharp contact with porphyroblastic gneiss was also observed near Kura Mota (Plates XLI and XLII). Dimension of the phenocrysts range from 2.4 to 5.0cm by 1.0 to 2.4cm.

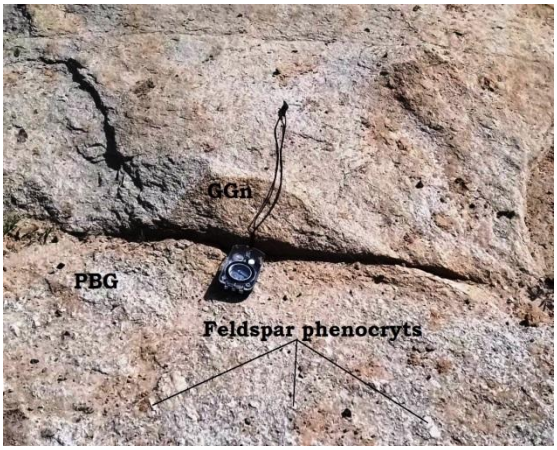


XXXIX

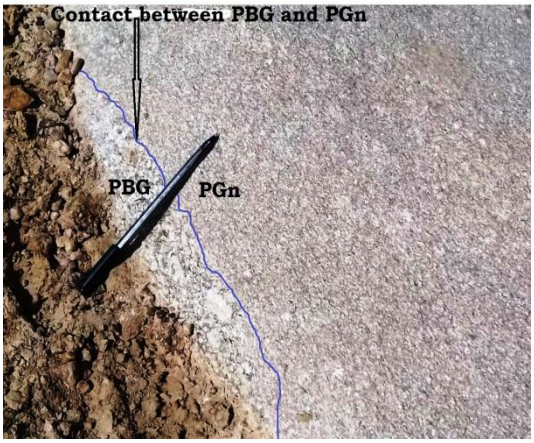


XL

Plate XXXIX: Photograph showing relic raft brown coloured BSch in contact with PBG. Observer (1.7m tall is at the foot of PBG hill at 11° 55′ 05″ N and 07° 10′ 02″ E.
Plate XL: Photograph of a closer view to the sharp intrusive contact between PBG and BSch at the foot of PBG stock at 11° 54′ 36.4″ N and 07° 10′ 01.4″ E. Pen is 15cm long.



XLI



XLII

Plate XLI: Photograph showing contact between PBG and GGn at 11° 52′ 22.2″ N and 07° 08′ 40.4″ E. Also showing feldspar phenocrysts in PBG.
Plate XLII: Photograph showing contact between PBG and PGn. The gneiss is older as it is observed to lie above PBG at 11° 52′ 20.2″ N and 07° 08′ 40″ E.



XLIII



XLIV

Plate XLIII: Photograph of whale-back outcrop of PBG on parts of Kutcheri hill (PBG) at 11° 49′ 48.7″ N and 07° 02′ 16.4″ E. Note joints are mainly parallel to the trend.
Plate XLIV: Photograph of PBG outcrop with feldspathic veins of varying width at 11° 48′ 17″ N and 07° 06′ 08″.

4.6.2 Petrography of porphyritic biotite granite

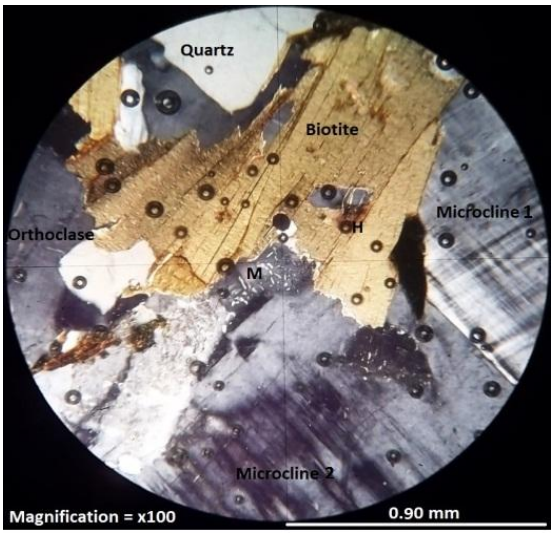
The hand specimen PBG 1 is light grey with foliated phenocryst of feldspars. The feldspar phenocrysts show regular blocky shapes. Sample from other places (e.g PBG 2) are relatively leucocratic (light brown) with pink coloured feldspar phenocrysts that lack clearly defined trend. Quartz is glassy and transparent. Biotite occurs as black specks. The most striking feature of its texture is the large well-formed pink angular feldspar (phenocryst) in finer matrix.

In PPL, quartz is colourless, with low relief, low double refraction and has anhedral form. Microcline phenocryst is also colourless and not cloudy (Plate XLV). The microcline was distinguished from the quartz with becke line movement. The biotite is brown coloured with subhedral form and moderate relief. It shows pleichroic halo around zircon inclusion in places.

In XPL, microcline has grey interference colour with tartan twinning pattern. The biotite had brown intereference colour in all PBG (Plate XLVI and XLVIII). The phenocryst in PBG 2 (Plate XLVIII) is plagioclase feldspar.



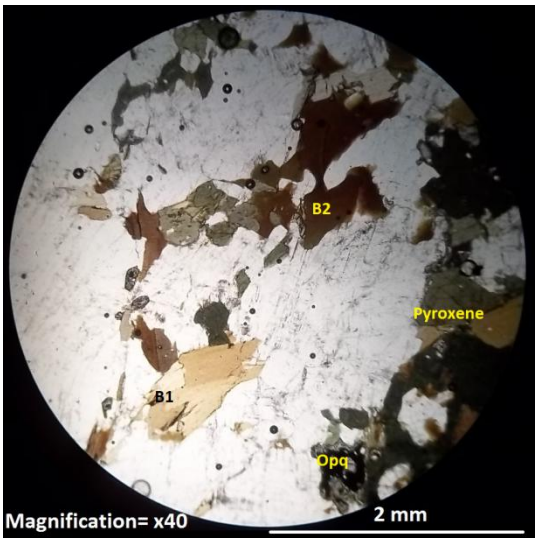
XLV (PPL)



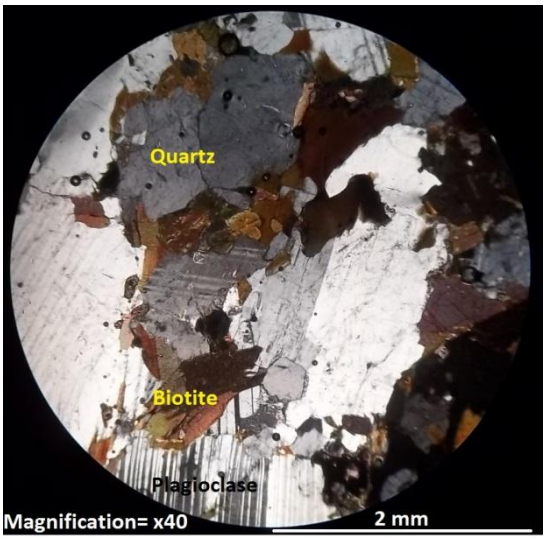
XLVI (XPL)

Plate XLV: Photomicrograph of PBG 1 showing pleichroic halo around zircon inclusion in platy, brown coloured biotite. Biotite (B1) shows perfect cleavage cut normal to the crystallographic-axis (B1). Sections parallel to it lack cleavage (B2).

Plate XLVI: Photomicrograph of PBG 1 showing different tartan twinning pattern in microcline. Myremekitic texture (M) in plagioclase feldspar.



XLVII (PPL)



XLVIII (XPL)

Plate XLVII: Photomicrograph of PBG 2 with green coloured pyroxene that has high relief and two sets of cleavage intercepting at nearly 90°.

Plate XLVIII: Photomicragh of PBG 2 showing plagioclase feldspar with characteristic narrow multiple albite twinning pattern having ≤15° extinction angle. Pyroxene show pink interference colour.

The PBG is composed of quartz, biotite, microcline, plagioclase feldspar and pyroxene (Table 4.1)

4.7 MEDIUM-COARSE GRAINED BIOTITE GRANITE

4.7.1 Field relationship

Outcrops of medium to coarse grained biotite granites (M-CBG) are observed north of Danwari and about 2 km to east of Dan Sabo. It constitutes about 6 % of varying lithologies in the area. The contacts with metasediments are largely inferred as they are covered by secondary alluvium and laterites. They are mainly low-lying with quartzofeldspathic veins of varying widths (Plate XLIX and L).



XLIX



L

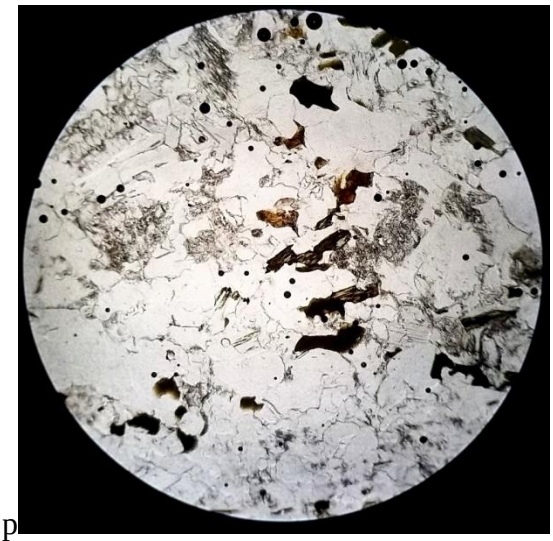
Plate LIII: Low lying whale-back stock of M-BCG with quartzofeldspathic veins of varying widths at 11° 58′ 55.8″ N and 07° 14′ 55.2″ E. Human is 1.7m tall.
Plate LIV: Feldspathic vein that trends NS (hammer is 30 cm long) at 11° 56′ 40.8″ N and 07° 13′ 33.8″ E

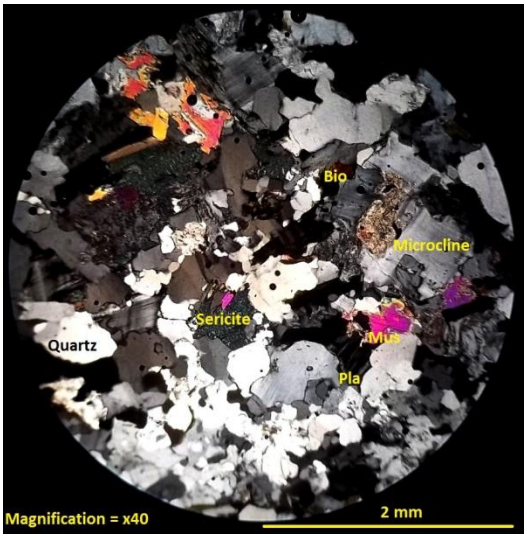
4.7.2 Petrography of medium-coarse grained biotite granite

In hand specimens, the rocks are light grey. Specks of mica are visible with the aid of hand lens.

In PPl, mica (muscovite and biotite) is subhedral in form and had perfect basal cleavage with moderate relief. Biotite is brown and pleichroic from light to dark brown while the muscovite is colourless and not pleichroic (Plate LI).

In XPL, the muscovite displayed pink colour while biotite dispayed brown interference colour. Alteration of feldspars to sericite is also visible (LII).

p



LI (XPL) LII (PPL)

Plate LI: Photomicrogrph of M-CBG showing muscovite with perfect basal cleavage.
Plate LII: Photomicrograph of M-CBG showing muscovite with pink interference colour. Alteration of feldspars to sericite is also visible.

4.8 SERPENTINITE

4.8.1 Field relationships

Outcrops of serpentinite are generally fine to medium grained and massive (LIII). It occurs as discontinuous bodies with approximately linear trend in N-S direction. The contacts with adjacent lithologies are inferred.

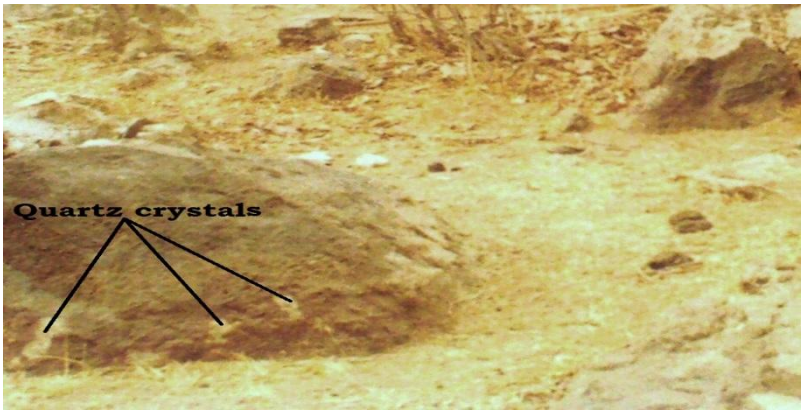


Plate LIII: Photograph of low lying fine grained serpentinite outcrop that is dark coloured with quartz crystal in places at 11° 47′ 42″ N and 07° 10′ 35″ E.

4.8.2 Petrography of serpentinite

The hand specimen of serpentinite is black with traces of light green colour. Spots of black (opaque) chromian spinel occur as tiny grains in places (Plate LIV).

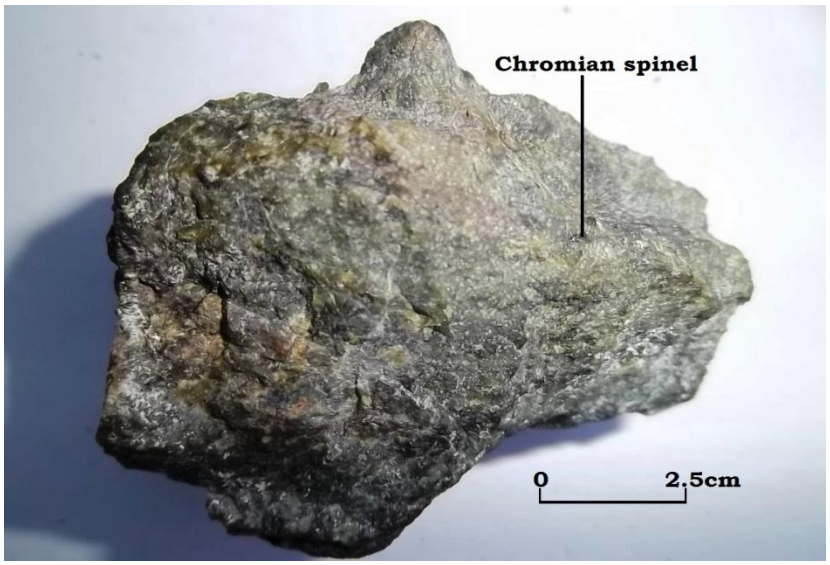
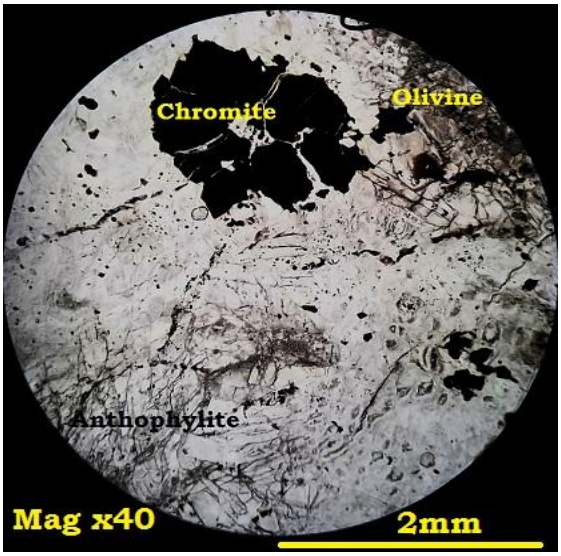


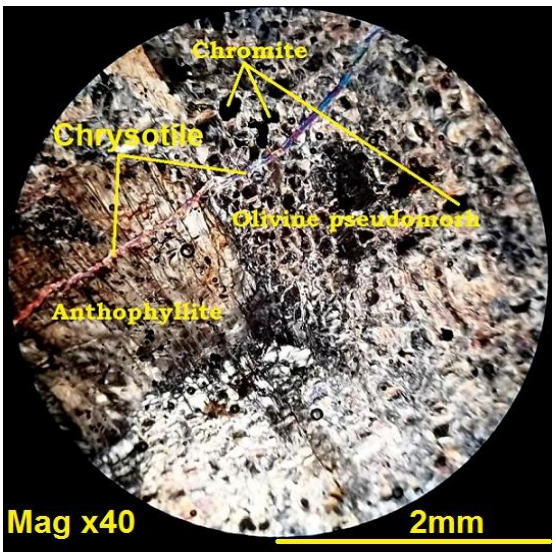
Plate LIV: Photograph of hand specimen of serpentinite with light green appearance and small black spots of chromian spinel/magnetite.

In PPL, the fine to medium grained olivine pseudomorph and anthophyllite (amphibole) are colourless to pale green.The fibrous amphibole (anthophyllite) is slightly pleicroic, has 2 sets of cleavage intersecting at 90° with high indices of refraction (relief) and birefringence. Opaque and subhedral chromite grains with transparent thin edges in places (Plate LV).

In XPL, the anthophylite displays light brown interference colour with oblique extinction. Chrysotile with pink and blue interference colours occur in a micro vein that crosscuts serpentine (LVI).



LV (PPL)



LVI (XPL)

Plate LV: Photomicrograph of serpentinite showing opaque chromite grains and fibrous pyroxene.
Plate LVI: Photomicrograph of serpentinite showing chrysotile in vein and unevenly fractured serpentine (olivine pseudomorh).

The serpentinite is mainly composed of olivine, pyroxene and opaque chromite grains (Table 4.1).

4.9 MINOR LITHOLOGIES

4.9.1 Field relationships

The minor lithologies constitute about 4% of rocks in the study area. These include schist and gneiss xenolith, quartz-tourmaline rock, aplite dyke, quartz vein and quartzofeldpathic vein. The schist and gneiss xenoliths mainly occur with different dimension in granites in different parts of the study area. The quartz-tourmaline rock mainly occurs as veins within schists around Takulawa and Takeri. Leucocratic aplite dyke was observed in porphyritic biotite granite in Yankara. Quartz vein with glassy texture and quartzofeldpathic veins that are white and pink coloured of varying width are emplaced in all the major lithogies in the area.

Independent field occurences of all minor lithologies are not mappable at the scale of the map

Results from petrographic studies confirm the view of Turner (1983), that the main rock type is quartz-biotite rock with constant foliation trend. Harper *et al.*, 1973 also confirmed the main rock in Wonaka schist belt is hornfelsic biotite schist. Lack of characteristic index minerals in the metamorphic rocks in the area is presumed to be due to fact that metamorphism in the belt are of higher temperature and lower pressure type than in other schist belts (Turner, 1983). This may be due to large batholitic masses which almost engulf the study area. The absence of staurolite and kyanite in the metasediments may either be an indication the low grade of metamorphism or the low alumina content of the original sediments (Odeyemi, 1977).

4.10 SUPERFICIAL DEPOSITS

4.10.1 Laterites

These are the low level laterites which occur extensively in the mapped area especially around Makeri and Angwan Shawo in the northeastern and southeastern part (Plate LVII). Rail ruoad cut exposures are observed near Kutcheri in the southwestern part of the study area (Plate LVIII).



LVII



LVIII

Plate LVII: Photograph of hard brown laterites around Makera at 11° 12′ 20″ N and 07° 58′ 10″ E
Plate LVIII: Photograph of rail road cut exposure of hard, brown laterites around Kutcheri at 11° 48′ 40″ N and 07° 02′ 30″ E.

Their occurrence is thought to be due to the fact that the area is generally flat and falls within the zone of seasonal fluctuation of the water table (i.e. savanna zone). They are brownish and hard, and up to 1m thick in places. They are termed the "Younger laterites" by McCurry and Wright, (1973).

4.10.2 Alluvium deposit

These are deposits derived from weathering and erosion of the surrounding rocks and which have been transported and deposited along many stream and river channels (especially the broad ones) in the mapped area (Plate LIX). They form low lying loose, unconsolidated soil or sediments at side of hills and broadland (Plate LX).

These deposits consist mainly of sands, but silt and clays also occur. When they reach a thickness of between 1- 2 m, they are called older alluvium (McCurry, 1971).



LIX



LX

Plate LIX: Photograph of alluvium deposit along the bed and banks of River Yankuzau at 11° 55′ 30″ N and 07° 03′ 15″ E.

Plate LX: Photograph of alluvium deposits on broadland plain enroute Gidan Chido at 11° 52′ 49″ N and 07° 02′ 55″ E.

4.11 STRUCTURES

4.11.1 Foliation

Foliation represents the most conspicuous structural feature in the gneisses and metasediments in the study area. In the gneisses, it is defined by parallel alignment of mafic and felsic minerals (Plates LXI) having a major trend in a NNE-SSW direction (Fig. 4.1). In the metasediments (biotite schist and phyllite), it is defined by the alignment of platy minerals (biotite) and quartzofeldpathic veining (Plate LXII) having trend in NE-SW with few NW-SE (Fig. 4.2). Longer axis of feldspar phenocrysts (NNE-SSW) are used to determine foliation in granites (Fig. 4.3).



LXI



LXII

Plate LXI: Photograph of banded gneiss with ptygmatic felsic veins at 11° 47′ 56″ N and 07° 14′ 42″ E.
Plate LXII: Photograph showing foliation pattern in schist interbanded with thin quartzofeldspathic veins (<1cm width) at 11° 45′ 47.2″ N and 07° 06′ 49″ E.

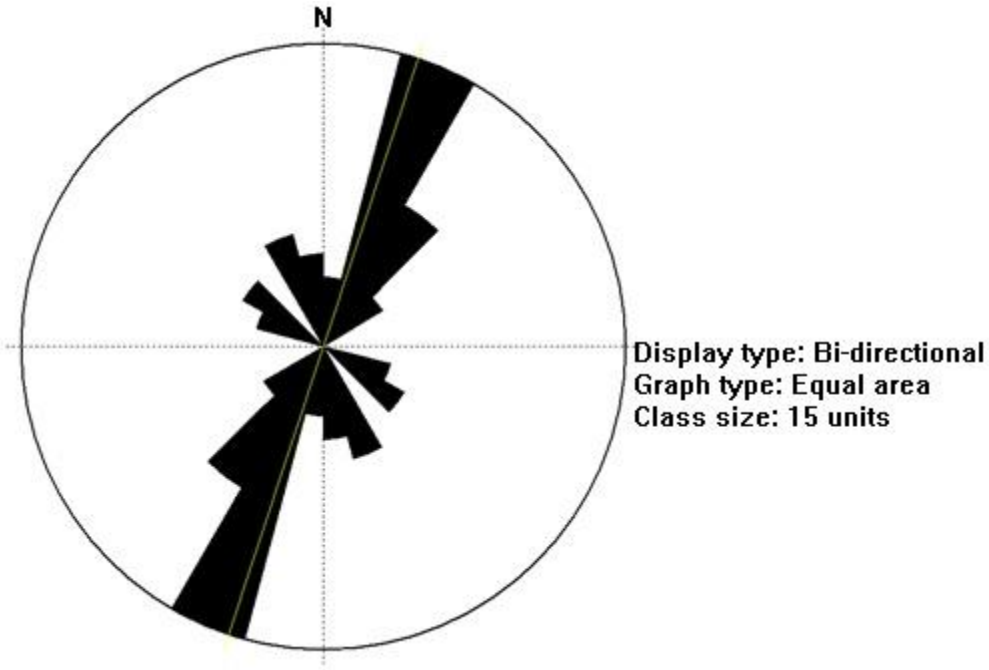


Fig. 4.1: Rose diagram of foliation trends in gneisses

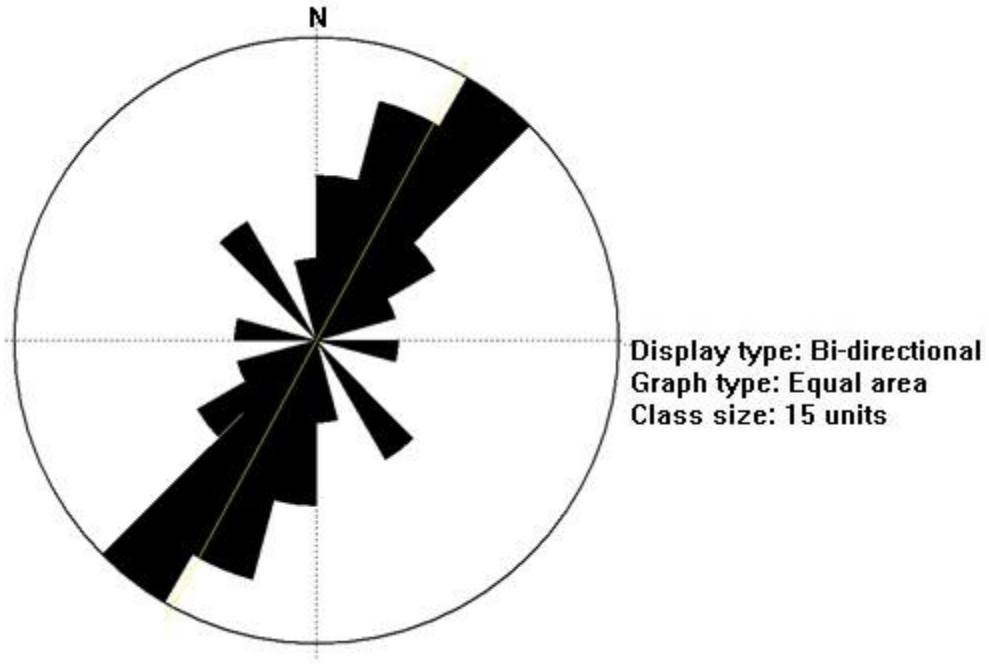


Fig. 4.2: Rose diagram of foliation trends in metasediments (biotite schist and phyllite)

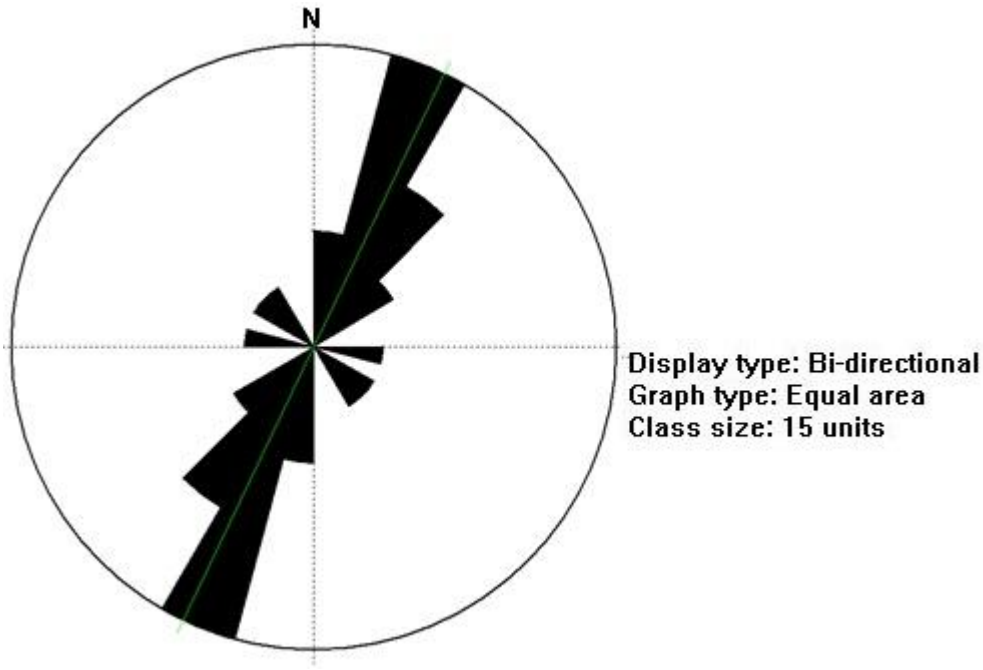


Fig. 4.3: Rose diagram of longer axis trends of phenocrysts in porphyritic biotite granite

Generally, the dominant strike of the foliation is mostly NNE-SSW direction with variation between, NE-SW and rare NW-SE direction. The dominant strike of foliation in Nigerian basement is N-S with variations between NW-SE and NE-SW (Oluyide 1988).

4.11.2 Joints

Discontinuity plane of natural origin along which there is no visible displacement are seen in nearly all lithologies in different directions within the study area. According to McCurry, (1971) and Danbatta, (1999) the joints often result from contraction on cooling and are believed to be associated with a single episode of cooling and fracturing during epirogenic uplift.

Non-orthogonal joint sets are mainly observed on the porphyritic biotite granite (Plate LXIII) and porphyroblastic gneiss. Exfoliation joints also occurred on granite in places (Plate LXIV). Some man made joints (rupture) are observed in quarry sites (Plate LXV). Discontinuities along

foliation planes are observed in the metasediments (foliation joints and partings) (Plate LXVI). It is also observed that some of the joints are filled with felsic (quartz) veins.

Joint direction readings (appendixes IV, V, VI) and rose plots were drawn (Fig. 4.4, 4.5 and 4.6).



LXIII



LXIV

Plate LXIII: Photograph of PBG with non-orthogonal joint pattern enroute Yankara at 11° 47′ 17.4″ N and 07° 04′ 7.9″ E. Human is about 1.7m tall.
Plate LXIV: Photograph of exfoliation joints on low lying M-CBG that mainly trend NS (180°) at 11° 57′ 13.5″ N and 07° 14′ 58.8″ E.



LXV



LXVI

Plate LXV: Photograph of PBG with rupture joint on in Asaka Ahuta quarry around boundary between Katsina and Zamfara state at 11° 49′ 12.2″ N and 07° 03′ 10.4″ E.
Plate LXVI: Photograph of foliation joint and parting on BSch around Dankaya at 11° 55′ 00″ N and 07° 0′3 16″ E.

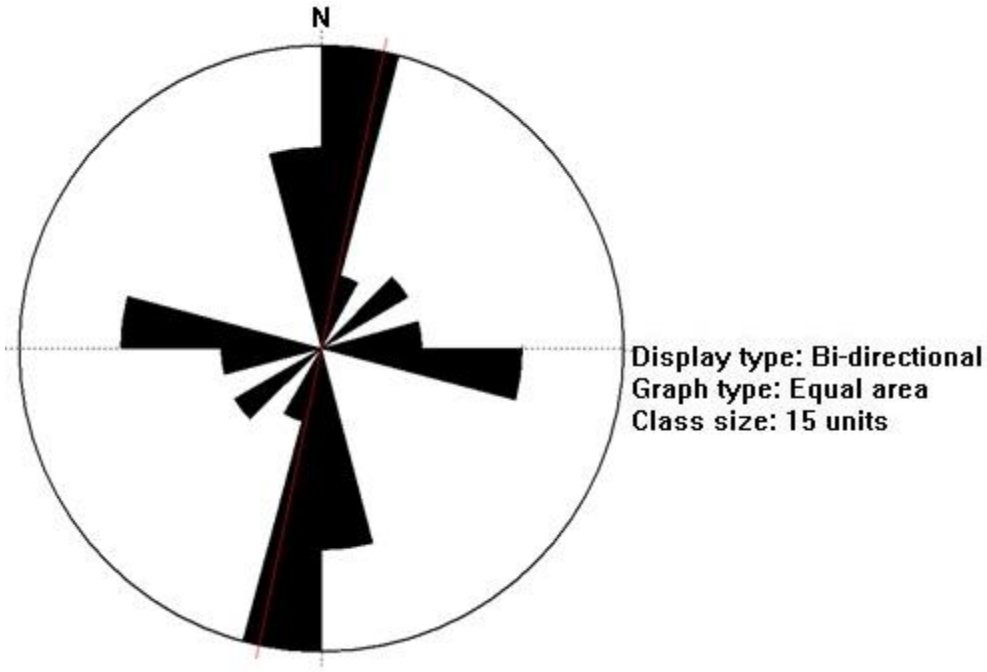


Fig. 4.4: Rose diagram of joint trends in gneisses within of the study area.

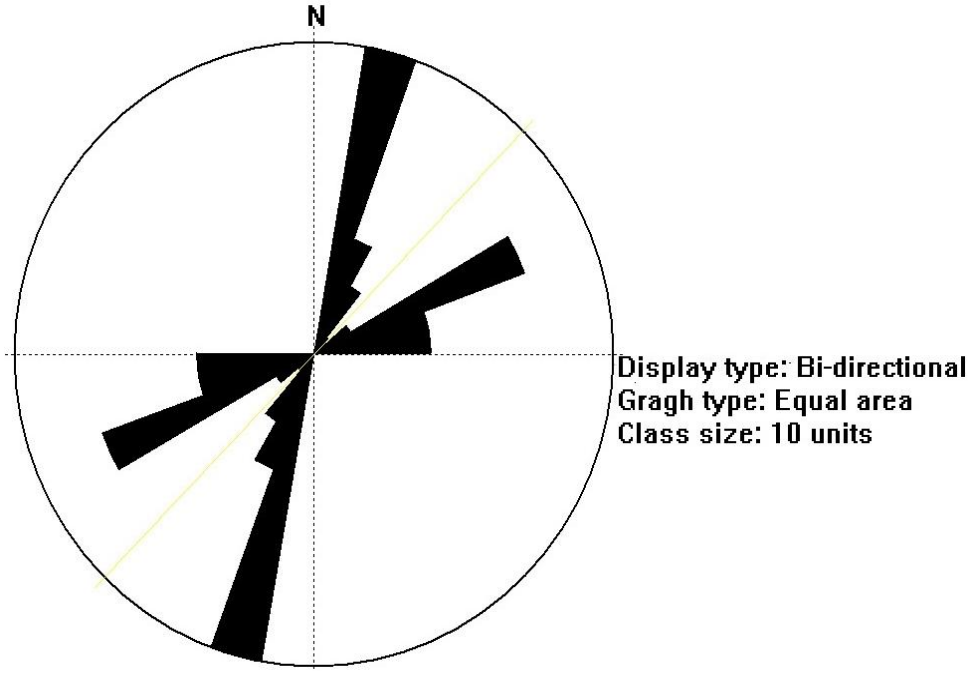


Fig 4.5: Rose diagram of joint trends in metasedimants within the study area

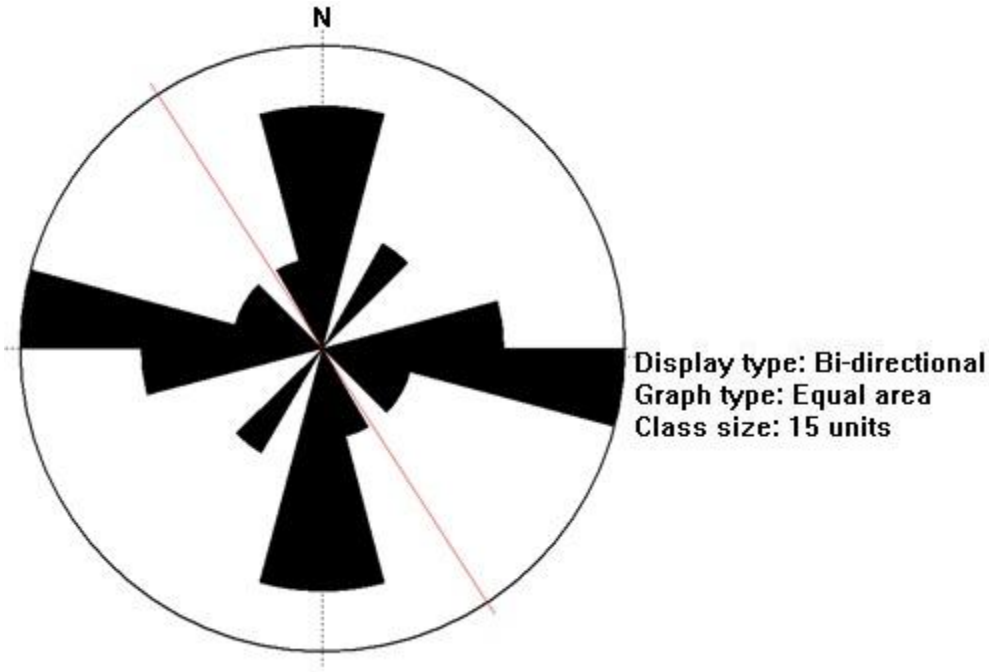


Fig. 4.6: Rose diagram showing trends of joints in granite within the study area

Tectonic joints are the most common type in gneisses and metasediments in the area. They are characterised by a general strike direction NNE-SSW with variations NNW-SSE and ENE-WSW indicating their formational stress direction to be dominantly E-W. This follows the major stress direction of Pan African Orogeny. Also, prominent E-W and N-S joint directions are noted on the gneisses. These are probably pre- Pan African and Pan African respectively.

4.11.3 Faults

The faults observed in the area are marked by displacement of felsic veins and microgranite dykes (aplite dyke). Both dextral (Plate LXVII) and sinistral (Plate LXVIII) strike slip faults are observed on the granite, tourmaline-quartz rock and gneisses. Generally the faults mostly trend between 90° to 110°, conforming to the E-W trending joint sets.



LXVII



LXVIII

Plate LXVII: Photograph of leucocratic aplite dyke (20 cm width) that trends NNE (204°) in PBG with sinistral displacement by thin quartz vein that trends WNW (284°).
Plate LXVIII: Photograph of M-CBG showing quartzofeldspathic veins with dextral that trends 110° and a sinistral strike slip faults that trends 98° at 11°58′55″ N and 07°14′54″E. Hammer is 30 cm long.

4.11.4 Folds

Simple disharmonic ptygmatic folding was seen on the gneisses in places within the mapped area. Isoclinal folding was seen in biotite schist within the southwestern part (Plate LXIX) while macroscale crenulation cleavage pattern (Plate LXX), disseminated quartz vein (Plate LXXI), and open folding (Plate LXXII) are observed on biotite schist in places. All folds mainly had NNE-SSW axial trends.



LXIX



LXX

Plate LXIX: Photograph of BSch showing tight isoclinal fold pattern at 11° 50′ 49″ N and 07° 01′ 31.8 E.
Plate LXX: Photograph of BSch with macroscale crenulation cleavage pattern (GPS 6.5cm width). Note lines traces the cleavages at 11° 51′ 15″ N and 07° 01′ 30″ E.



LXXI



LXXII

Plate LXXI: Photograph of BSch showing disseminated quartz veins (human is about 1.7m tall) at 11° 51′11.9″N and 07°02′2.5″E.
Plate LXXII: Photograph of BSch showing symetrical fold at 11° 52′ 01″ N and 07° 02′ 20″ E

Axis of folds in the study area are mainly trending in NNE-SSW confirms the conclusion of Olade (1978) that axis of fold in Nigerian Basement terrain generally trends in NNE-SSW direction. Also, the crenulation cleavage is indicative of multiply deformed rocks (Johnson *et al.*, 2006).

CHAPTER FIVE

GEOCHEMISTRY

5.1 MAJOR ELEMENTS DISTRIBUTION IN THE GNEISSES AND METASEDIMENTS

On the basis of major rock types, the data have been subdivided into two main groups which include the gneisses (banded gneiss, porphyroblastic/granite gneiss) and metasediments (biotite schist and phyllite). Major element composition of these rocks is presented in Table 5.1.

The metasediments have high Al_2O_3 to K_2O, Na_2O ratios, low MgO and CaO contents with MgO exceeding CaO. Contents of K_2O are generally greater than those of Na_2O except in few cases. Rahaman (1976) noted same trend for pelitic rocks in the Nigerian Basement Complex and these correspond closely to the average composition of pelitic rocks. They were argillaceous sediments prior to metamorphism. The greater abundance of Na_2O over K_2O in some samples may be due to association of some greywackes with shales (Rahaman, 1976; Elueze, 1981a).

Table 5.1: Showing major element content of gneisses and metasediments

	Biotite schist				Phyllite	Banded gneiss		Augen gneiss	Porphyroblastic/Granite gneiss	
Element	BSch 1	BSch 2	BSch 3	BSch 4	Phy 1	BGn 1	BGn 2	AGn	PGn	GGn
SiO_2	67.2	67.9	58.8	65.3	68.5	67.1	71.0	72.2	64.2	64.7
TiO	0.92	0.82	0.94	0.61	0.82	0.58	0.33	0.34	0.98	0.49
Al_2O_3	13.8	13.9	17.7	15.68	13.4	15.4	15.2	19.9	14.7	14.5
Fe_2O_3	6.73	5.77	8.86	6.55	5.85	4.45	2.74	2.14	6.31	4.85
MnO	0.12	0.09	0.14	0.12	0.10	0.03	0.04	0.04	0.08	0.09
MgO	2.47	2.41	4.19	2.30	2.44	0.91	0.63	0.34	1.14	2.97
CaO	1.74	1.68	2.09	1.07	1.95	1.86	2.76	1.14	2.86	3.71
Na_2O	2.85	2.46	2.11	1.07	3.35	3.70	5.18	3.44	3.39	3.91
K_2O	2.38	3.22	3.41	0.04	1.98	4.75	1.42	5.32	4.54	2.79
P_2O_5	0.16	0.2	0.22	0.78	0.16	0.20	0.12	0.09	0.38	0.27
Cr_2O_3	0.02	0.01	0.02	0.02	0.02	0.01	0.00	0.01	0.00	0.01
LOI	1.32	0.89	1.54	1.25	0.85	0.49	0.44	0.42	0.56	1.26
Total	99.8	99.5	100	94.8	99.3	99.8	99.8	99.9	99.5	99.5

5.2 TRACE ELEMENT DISTRIBUTION IN GNEISSES AND METASEDIMENTS

This essentially include Transition metals (Cr, Co, Ni, Cu, V and Zn), alkali and alkali earths (Rb, Be, Ba, Cs and Sr), High field strength elements (Ti, Hf, Nb, Ta, Mo, W and Zr), Actinides and heavy metals (Tl, Pb, Bi, Th and U) Siderophile and chalcophile (Ag, Cd, Pd, In, Sn, Sb, Au, Hg) and others (Table 5.2).

Trace element content obtained in this study were compared with estimates of different workers including values from Condie (1993), Taylor and McLennan (1995) and Rudnick and Gao (2003) for the upper continental crust (UCC) and bulk continental crust (BCC).

Generally, estimates of trace element of the metasediments are close to estimate values for UCC than gneisses to BCC. Contents of alkalis and alkaline earths Rb (58.9-130.1 ppm) and Ba (419-715 ppm) in metasediments scatter around UCC values Rb (84 ppm) and Ba (624 ppm) of Rudnick and Gao (2003). It span nearly an order of magnitude each in the gneisses Rb (67.6-336.9 ppm) and Ba (215-1415 ppm) and are generally higher than the estimates for BCC Rb (49 ppm) and Ba (456 ppm) of Rudnick and Gao (2003). The contents of Ga (13.3-22.0 ppm) in metasediments and gneisses Ga (17.2-26.3 ppm) are mainly around UCC (17.5 ppm) and BCC (16.0 ppm) values of Rudnick and Gao (2003).

Table 5.2: Showing trace element content of gneisses and metasediments

	Biotite schist				Phyllite	Banded gneiss		Augen gneiss	Porphyroblastic/Granite gneiss	
Element	BSch 1	BSch 2	BSch 3	BSch 4	Phy 1	BGn 1	BGn 2	AGn	PGn	GGn
Ba	652	715	582	419	115	1390	215	492	1415	830
Be	6	2	2	<1	5	<1	3	3	2	3
Co	18.4	16.7	26.7	15.1	35.4	7.9	5.8	2.9	11.4	6.2
Cs	4.9	5.6	6.2	4.8	9.5	3.4	1.6	11.6	3.4	1.8
Ga	16.6	16.3	22	13.3	22.3	26.3	17.7	20.3	22.1	17.2
Hf	5.1	5.8	4.6	4.4	5.3	14.8	3.1	6.7	14.8	4.1
Nb	13.8	14.5	10.6	8	10.9	27.4	11.4	24.1	36.8	8.8
Rb	87.1	130.1	98	58.9	170.4	211.5	67.6	336.9	169.6	87
Sn	2	3	4	2	5	6	3	16	4	3
Sr	213.1	145.5	166.7	194.7	60	251.8	326.9	103.1	287.3	574
Ta	0.9	1	0.6	0.5	0.7	0.5	0.5	1.8	1.6	0.6
Th	8.1	10	6.9	5	8.3	127.5	3.6	40.8	18.7	121.8
U	2.4	2.3	2.5	1.7	1.8	4.4	0.6	3.7	1.7	1.2
V	118	107	193	120	197	31	22	33	54	16
W	1.4	1.5	2.2	0.6	4.1	<0.5	0.6	1.3	0.5	4.2
Zr	193.2	205.6	186.2	178.3	174.9	572	110.6	236.7	613.7	150
Mo	0.4	0.1	0.6	0.5	0.2	0.6	0.6	0.4	1.9	0.6
Cu	33	3.9	87	39.6	38.5	4.5	12.8	4.2	23.1	6.5
Pb	3.1	1.8	2.2	1.7	3	5.9	2.6	5.9	5.6	5.7
Zn	79	97	106	61	134	74	60	52	105	75
Ag	0.1	<0.1	<0.1	<0.1	<0.1	<0.1	<0.1	<0.1	<0.1	<0.1
Ni	41.3	40.4	80.9	45.7	89.4	7.5	5.9	4.5	11.1	72
As	<0.5	0.7	<0.5	0.7	1	<0.5	<0.5	0.7	0.7	<0.5
Au(pp)	2.9	2.2	3.6	0.7	10	2.4	0.9	<0.5	<0.5	2.2
Cd	<0.1	<0.1	0.3	0.1	<0.1	<0.1	<0.1	<0.1	<0.1	<0.1
Sb	<0.1	<0.1	<0.1	<0.1	<0.1	<0.1	<0.1	<0.1	<0.1	<0.1
Bi	<0.1	0.1	0.1	0.2	0.6	<0.1	<0.1	0.1	<0.1	<0.1
Hg	0.02	<0.01	0.03	<0.01	<0.01	<0.01	<0.01	<0.01	<0.01	<0.01
Tl	0.4	0.8	0.6	0.3	0.8	0.9	0.4	0.9	0.9	0.9
Se	<0.5	<0.5	<0.5	<0.5	<0.5	<0.5	<0.5	<0.5	<0.5	<0.5

Mean contents of High Field Strength elements in gneisses Hf (8.7 ppm), Nb (21.7 ppm), Ta (1.0 ppm), Mo (0.8 ppm), W (1.7 ppm) and Zr (336.6) are higher than in metasediments Hf (5.0 ppm), Nb (11.6 ppm), Ta (0.7 ppm), Mo (0.4 ppm) and Zr (187.6 ppm) except for W (2.0 ppm). Also, mean contents of actinides are also higher in gneisses Tl (0.8 ppm), Pb (5.1 ppm), Th (62.5 ppm), U (2.3 ppm) than in the metasediments Tl (0.6 ppm), Pb (2.4 ppm), Th (7.7 ppm), U (2.1 ppm). The reverse occur in transition elements as its mean is higher in the metasediments Co (22.5 ppm), Cu (40.4 ppm), Ni (59.5 ppm), Zn (95 ppm) than in gneiss Co (6.8 ppm), Cu (10.2 ppm), Ni (20.8 ppm), Zn (73 ppm). Siderophile and chalcophile elements are mainly below detection limit in the gneisses and low in the metasediments.

5.3 RARE EARTH ELEMENTS DISTRIBUTION IN GNEISSES AND METASEDIMENTS

The rocks display a great range of rare earth element (REE) concentrations. This resulted from variations between and within the rocks. These essentially include the 15 lanthanide elements and yttrium and are presented in Table 5.3 below:

Table 5.3: Showing rare earth element content of gneisses and metasediments

	Biotite schist				Phyllite	Banded gneiss		Augen gneiss	Porphyroblastic/Granite gneiss	
Element	BSch 1	BSch 2	BSch 3	BSch 4	Phy 1	BGn 1	BGn 2	AGn	PGn	GGn
Y	24.4	27.2	32.3	23.4	29.6	31	11.2	31.8	52.9	30.1
La	29	26.4	26.8	20.2	28.5	392.3	14.2	83.5	102.4	345
Ce	59.8	54.5	55.2	41.8	60.3	690.5	29	167.9	202.3	112.8
Pr	7.45	7.17	7.27	5.89	7.92	76.81	3.95	21.18	26.79	20.61
Nd	28.1	30.4	29.2	25.2	34.5	260.1	15.8	72.4	107.9	47.4
Sm	5.92	5.71	6	5.37	6.81	34.7	3.15	12.52	17.54	7.94
Eu	1.2	1.17	1.31	1.08	1.15	2.44	0.87	0.74	2.55	1.73
Gd	4.64	5.36	5.86	4.38	5.74	18.23	2.44	8.32	12.81	5.41
Tb	0.78	0.86	0.97	0.71	0.91	1.99	0.38	1.17	1.91	2.1
Dy	4.28	4.85	5.19	4.14	5.02	8.36	1.94	5.65	10.14	3.91
Ho	0.96	1.05	1.27	0.84	1.14	1.17	0.42	1.09	2.06	1.23
Er	2.77	3.38	3.23	2.69	3.55	2.67	1.2	3.06	5.36	1.92
Tm	0.41	0.46	0.49	0.35	0.49	0.3	0.16	0.39	0.76	0.34
Yb	2.57	2.94	3.21	2.53	3.39	1.7	1.1	2.62	5.07	1.64
Lu	0.36	0.44	0.5	0.36	0.49	0.19	0.15	0.42	0.72	0.23

5.4 GEOCHEMICAL CHARACTERIZATION

5.4.1 Harker Diagram

In the gneisses, strong negative correlation is noted in plot of SiO_2 against TiO_2, MgO, CaO, P_2O_5, Fe_2O_3t, and MnO. Na_2O show low positive correlation, whereas K_2O did not correlate with SiO_2 (Fig. 5.1).

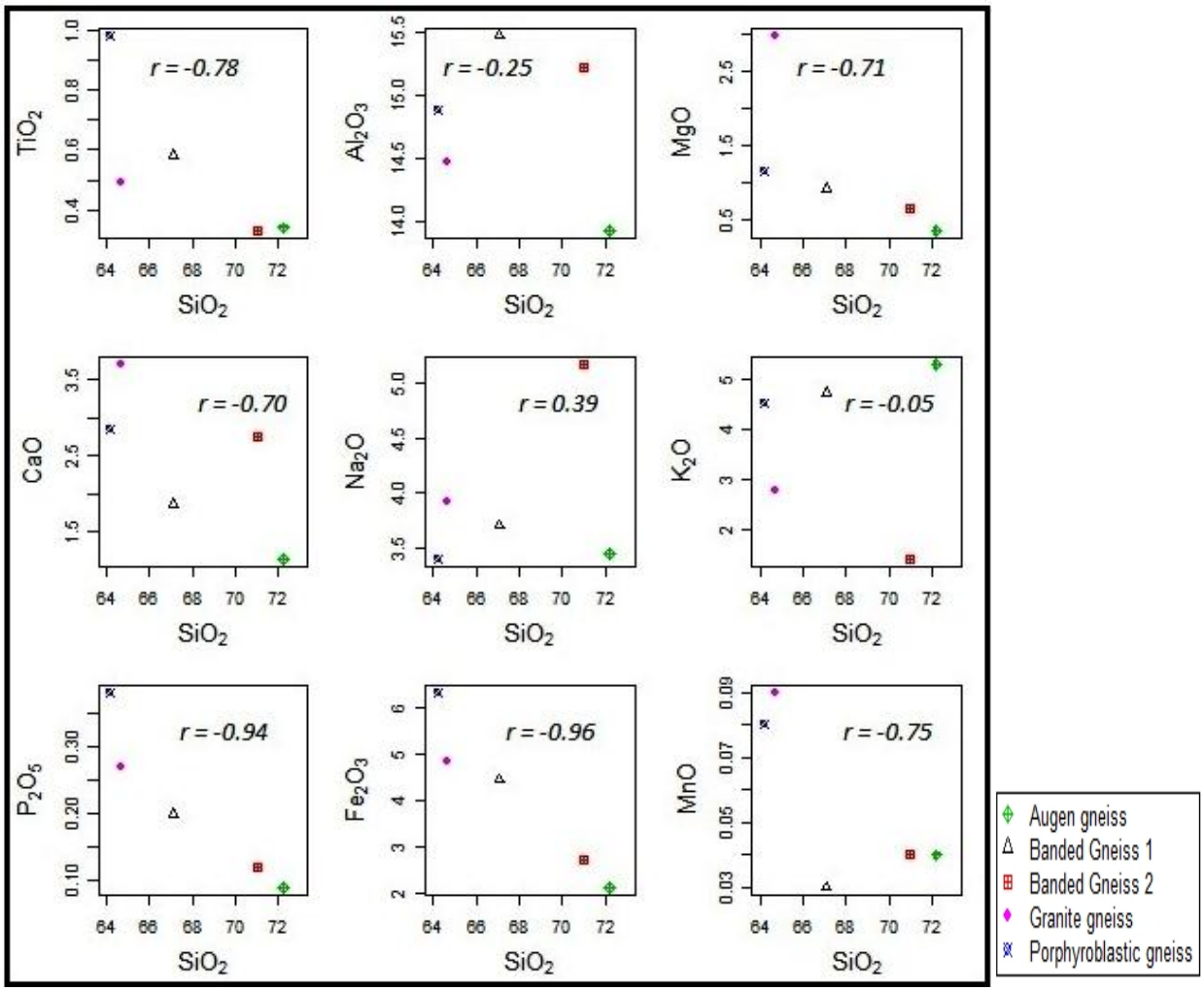


Fig. 5.1: Binary variation plots of SiO_2 with the other major oxides in gneisses.

Correlation coefficient values from Harker diagram shows strong negative correlation (inverse relationship) between SiO_2 and most of other major oxides in the metasediments. There is moderate positive correlation with Na_2O (Fig. 5.2).

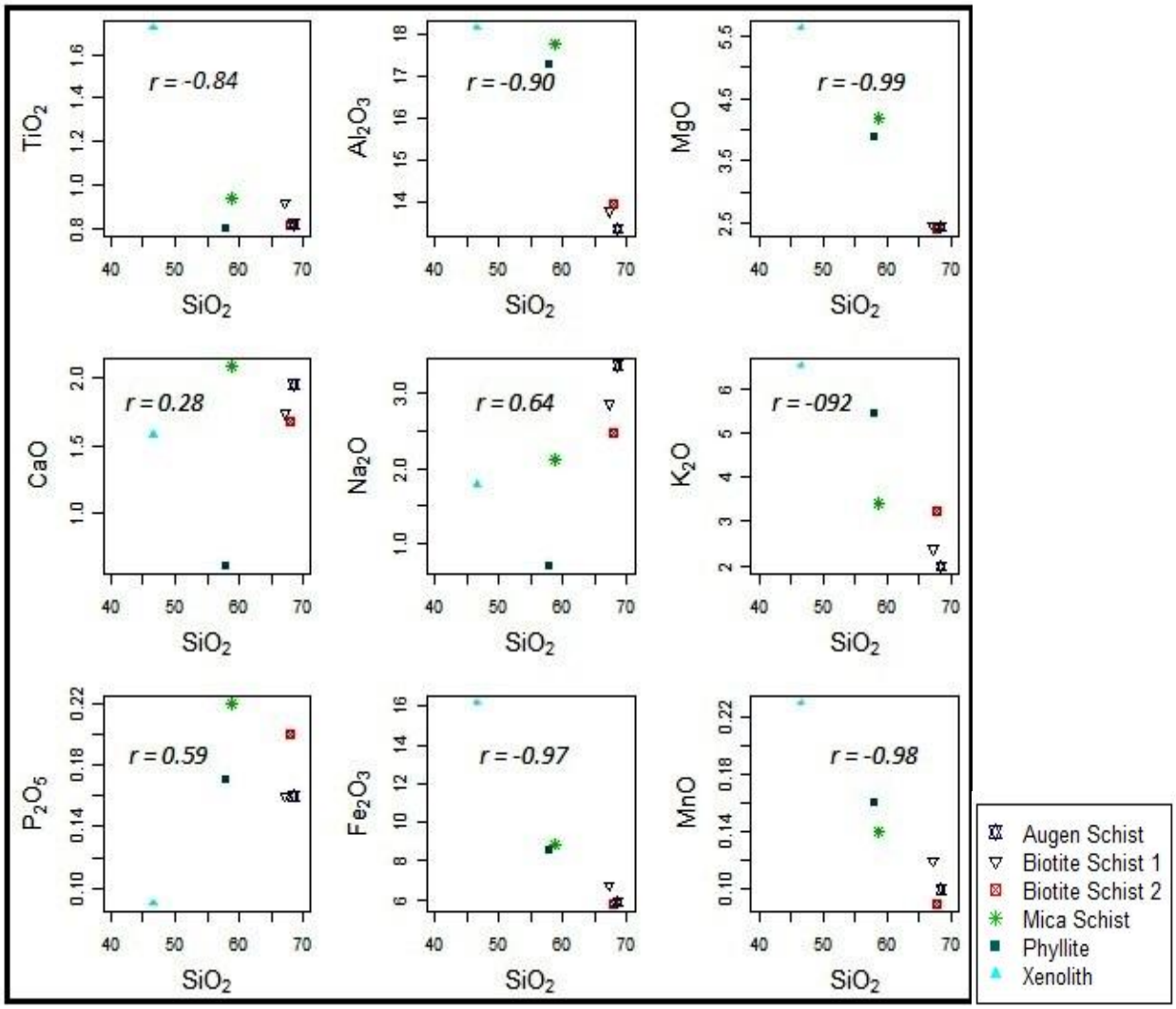


Fig. 5.2: Binary variation plots of SiO_2 with the other major oxides in metasediments

The strong negative correlation between SiO_2 and Fe_2O_3, SiO_2 and MgO and SiO_2 and MnO in the gneisses suggests pyroxene and hornblende fractionation in protolith (Okonkwo and Folorunsho, 2013).

The alkali metals (Na and K) are often highly mobile elements during metamorphism, hydrothermal alteration and weathering (Middelburg *et al.*, 1988). There is lack of correlation to low positive correlation for SiO_2 against K_2O and Na_2O in the gneisses (Fig. 5.1). Also, the metasediments exhibit limited data scatter with moderate positive correlation with Na_2O and

strong negative correlation with K_2O (Fig. 5.2). This indicates that these major elements probably undergo varying mobility during metamorphism confirming low grade metamorphism for the metasediments (greenschist facies) and low to medium grade for the gneisses (greenschist to lower amphibolite facies).

5.4.2 Alumina variation for gneisses

The $Al_2O_3/(Na_2O+K_2O)$ versus $Al_2O_3/(CaO+Na_2O+K_2O)$ binary diagram has been used to discriminate peraluminous, metaluminous and peralkaline magma series (Shand 1943). This diagram was adapted and it reveals that the samples are peraluminous (Fig 5.3).

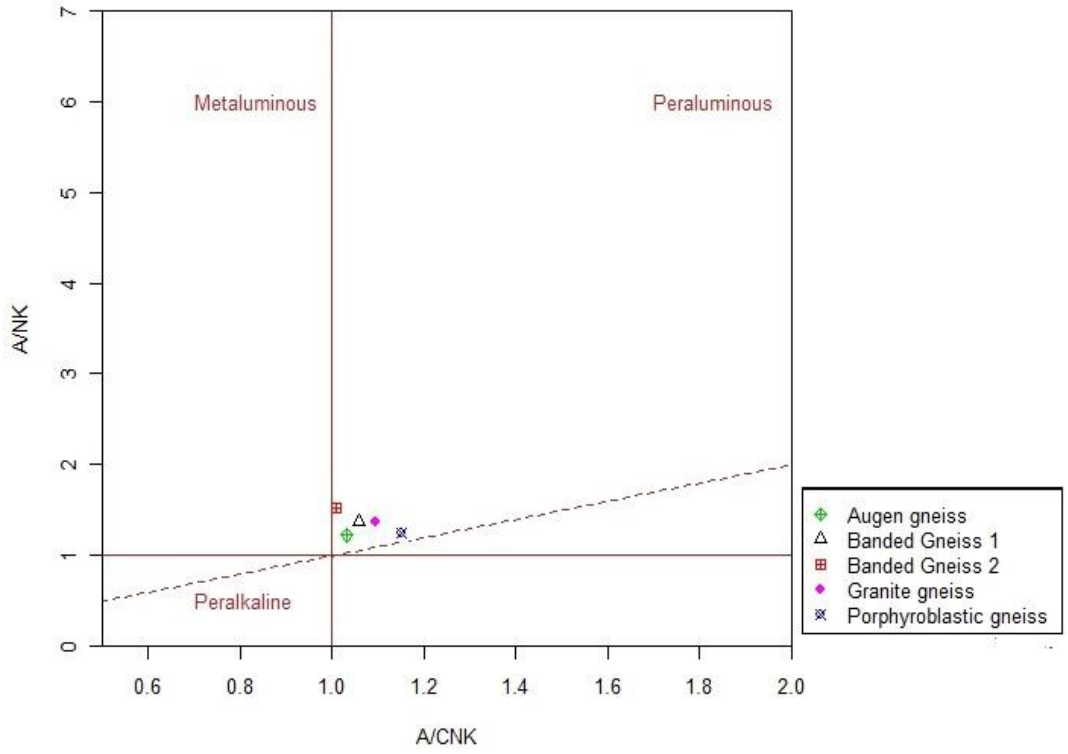


Fig. 5.3: Binary plot of molecular ratio of alumina to alkalis [$Al_2O_3/(Na_2O+K_2O)$] versus alumina to lime and alkalis $Al_2O_3/(CaO+Na_2O+K_2O)$] of Shand (1943) showing chemical classification of the gneisses.

Being paraluminous, the gneisses probably contain muscovite, garnet and is corundum-normative (Brown *et al.*, 1995b). This pattern is also noted for Older Granites in northern and southwestern Nigeria basement as they contain significant amount of alkalies and are

paraluminius with corundum appearing in the norm (Odeyemi, 1977; Olanrewaju and Rahaman, 1982). Also, granitic gneiss around Jebba peraluminous in Jebba area (SW Nigeria) that are paraluminous (Okonkwo and Ganev, 2012).

Rahman *et al.,* (1987) also noted that granitic rocks around Oban Massif, southeastern Nigeria are peraluminous. The foliated granitic gneisses of Aderan area are calc-alkaline and peraluminous granites emplaced during the Pan-African orogeny (Okonkwo and Folorunsho, 2013). They are different from granitic rocks in Igbeti (SW Nigeria) (Rahaman *et al.,* 1988), Ityowanye and Katsina-Ala areas (SE Nigeria) (Obiora, 2012) that are metaluminous.

5.4.3 Evolution Indices (Discriminant Function) of gneisses

It is possible to determine the protolith of quartzofelpdspathic rock samples with discriminant function (DF) if the MgO < 6% and SiO2 < 90% (Shaw, 1972). In general positive and negative DF values have been attributed to igneous and sedimentary parentage respectively by Shaw (1972).

$DF= 10.44 - 0.21\ SIO_2 - 0.32\ Fe_2O_{3T} - 0.98\ MgO + 0.55\ CaO + 1.46\ Na_2O + 0.54\ K_2O$

The DF of the gneisses including banded gneiss 1 are (3.0), banded gneiss 2 (3.9) Augen gneiss (2.8), porphyroblastic gneiss (2.8) and granite gneiss (1.5) are positive. Essentially, this suggests igneous precursors for all the gneisses.

5.4.4 Crustal discrimination for gneisses

On a ternary plot of K_2O-TiO_2-P_2O_5 (after Pearce *et al.,* 1975), gneisses are relatively enriched in K_2O than P_2O_5 and TiO_2. All rock samples essentially plot within the continental crust (Fig 5.4).

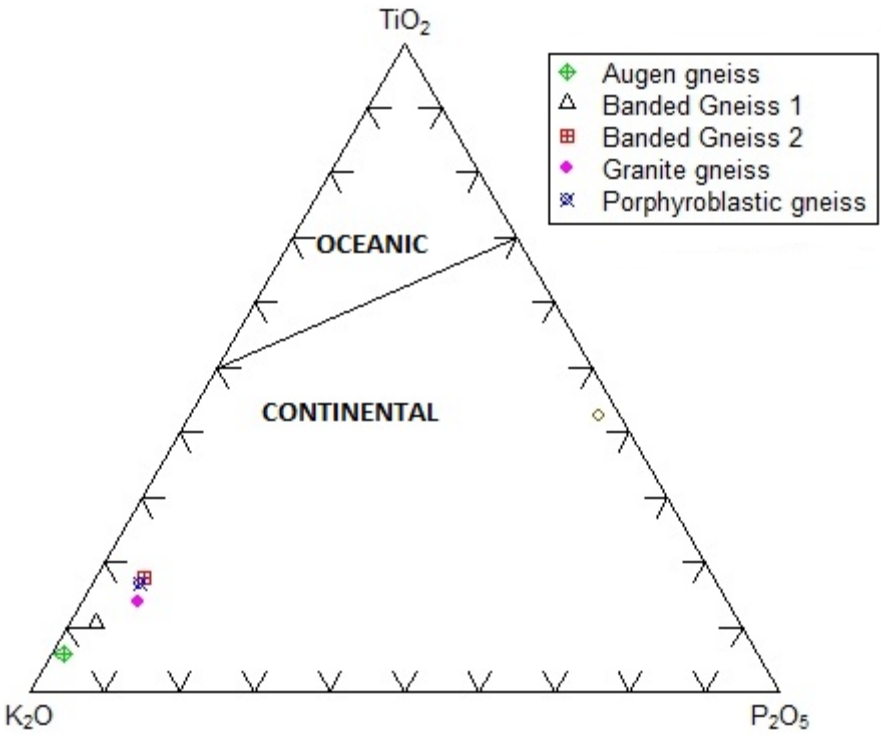


Fig. 5.4: Ternary Plot of K_2O-TiO-P_2O_5 of Pearce *et al.*, 1975 showing crustal discrimination of gneisses and quartz-tourmaline rock in the study area.

5.4.5 ACF diagram for the gneisses and metasediments

The ACF (A=Al_2O_3-K_2O, C=CaO+Na_2O+3.33*P_2O_5, F=Fe_2O_3t+MnO+MgO-TiO) content of the rock was plotted in a ternary diagram (Fig. 5.5).

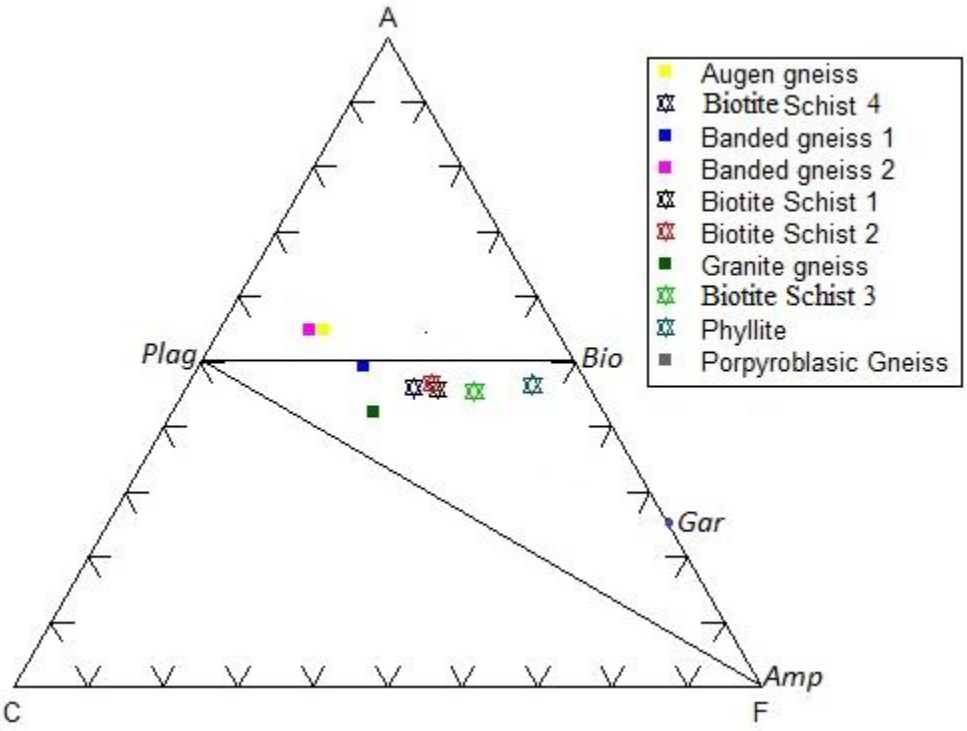


Fig. 5.5: Ternary ACF plot of James *et al.*, 1978 showing compositional variation in the gneisses, quartz-tourmaline rock and metasediments.

The metasediments and gneisses reflects variation in plagioclase end members (anorthite to albite) relative to biotite content and form a relatively convergent array parallel to the plagioclase-biotite joints (mid AC and AF apex). The phyllite plot close to the A-F sideline reflecting very low CaO content (and near absence of plagioclase).

5.4.6 Protolith precursor diagrams

Gneisses

The Al_2O_3 versus MgO diagram (Fig. 5.6), after Marc (1992), shows that most of the gneisses are orthogneiss except the granite gneiss that falls in paragneiss field.

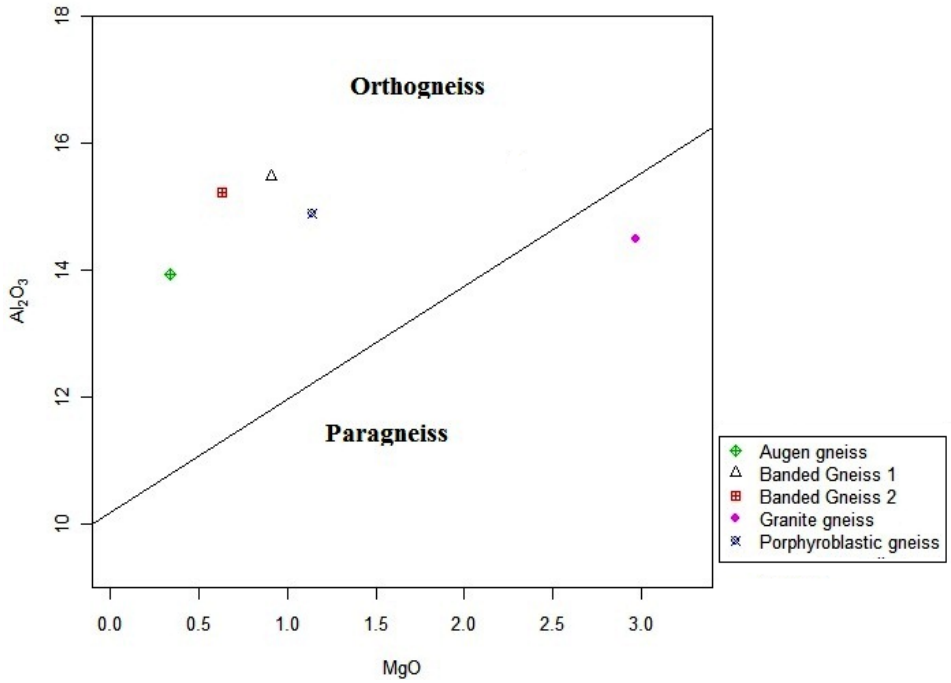


Fig. 5.6: Bivariate (Al_2O_3 versus MgO) discrimination diagrams of Marc, 1992 with line that seperate paragneiss from orthogneiss for gneisses in the study area.

The chemical classification and nomenclature of volcanic rocks using the total alkali (Na_2O+K_2O) versus SiO_2 (TAS) diagram of Cox *et al.* (1979), adapted by Wilson (1989) for plutonic rocks, was adapted for the chemical classification and nomenclature of gneisses (Fig. 5.7).

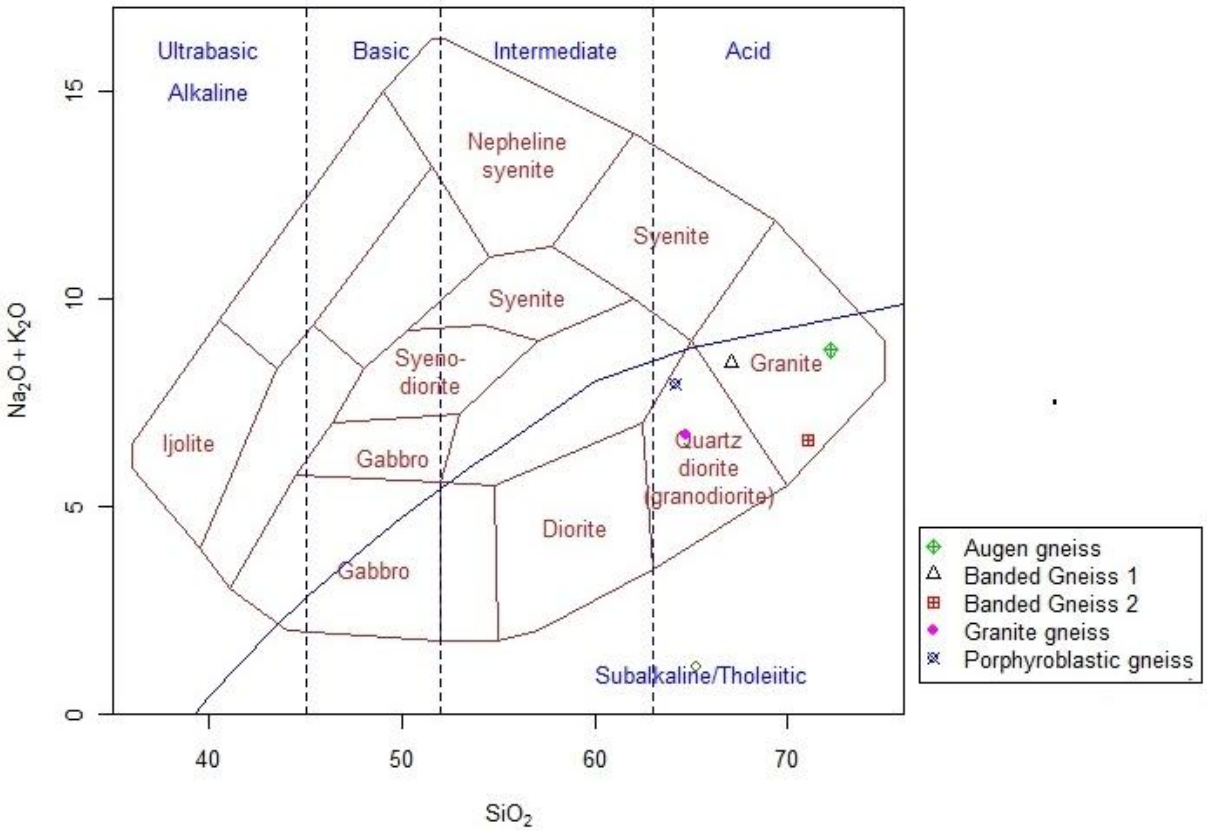


Fig. 5.7: Bivariate discrimination plot of SiO_2 versus Na_2O+K_2O of Cox *et al.,* 1979 showing chemical classification and nomenclature of gneisses and quartz-tourmaline rock.

Fig. 5.7 shows that the gneisses lie within the granodiorite to granite field.

Gneisses and Metasediments

On a TiO versus SiO_2 diagram of Tarney (1977), the gneisses dominantly plot in igneous field except granite gneiss that plotted in the sedimentary field. Also, the quartz-tourmaline rock plotted in the igneous field. The metasediments mainly plot in sedimentary field with an exception of the biotite schist 3 (Sample AA06) (Fig. 5.8).

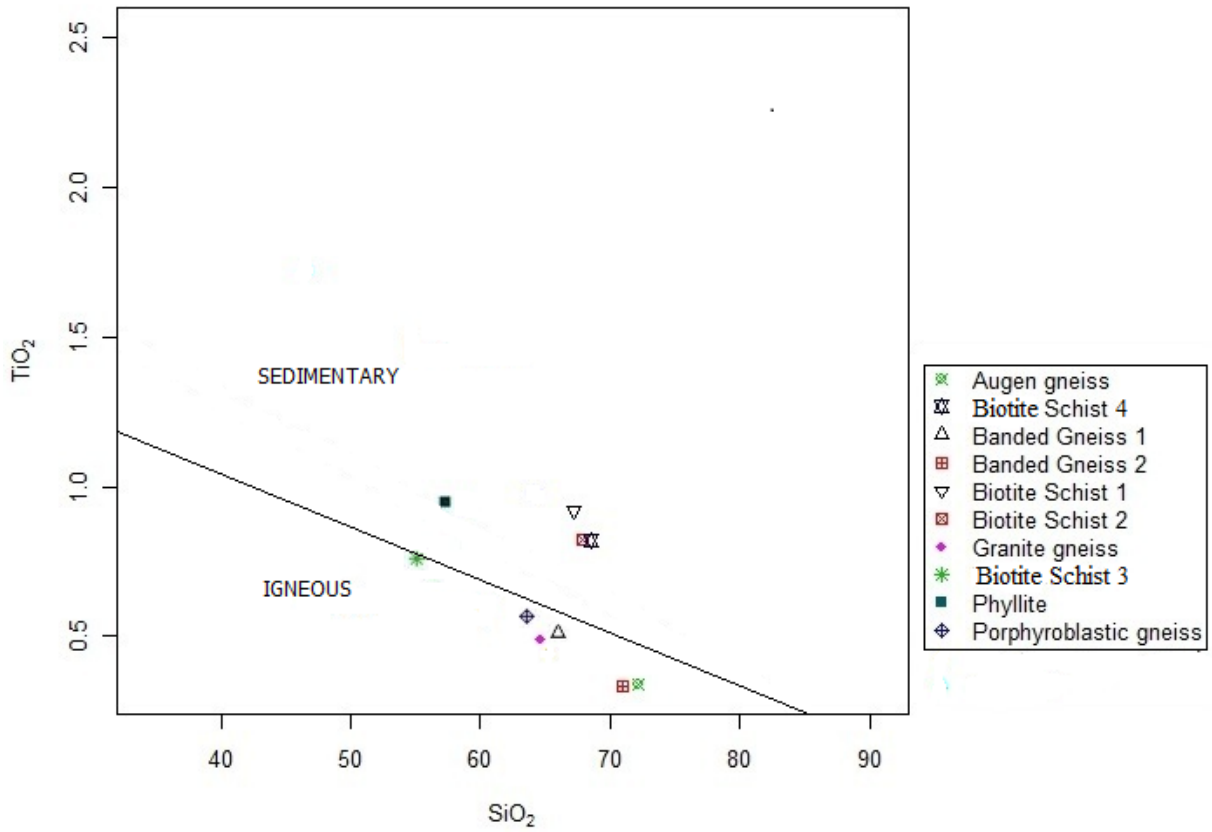


Fig. 5.8: Bivariate (TiO_2 versus SiO_2) discrimination diagram of Tarney, 1977 with a line that separates Igneous from Sedimentary fields for the rocks in the study area.

Truswell and Cope (1963), McCurry (1971), McCurry (1976), Ajibade *et al*. (1979), Adekoya (1998), Holt (1982), Fitches *et al.* (1985), Danbatta (2008), Danbatta (2010) have established sedimentary protolith for the younger metasediments. However, there are contrasting views concerning the evolution of the gneisses. Most authors believe that the gneisses are of igneous protolith while a few others noted that some gneiss evolved from granitization of pre-existing metasediments (e.g. McCurry, 1971).

Chemical characteristics of granitic rocks in Aderan area indicate they were derived from partial melting of mafic to semi-pelitic (metasedimentary) crustal rocks under conditions of intermediate oxygen fugacity and activities of H_2O (Okonkwo and Folorunsho, 2013).

The biotite schist 3 that plotted in igneous field was sampled close to contact with the intruding granites. Therefore, igneous precursor for the biotite schist 3 may result from contamination during magma emplacement.

5.4.7 Paleoweathering conditions and degree of maturity of metasediments

Molar proportions of Chemical Index of Alteration; CIA = $100[Al_2O_3/(Al_2O_3 + CaO^* + Na_2O + K_2O)]$ in molecular proportions, where CaO* is CaO in silicates only (Nesbitt and Young, 1982) and the Index of Compositional Variability, ICV of Cox *et al.* (1995) was calculated and presented in Table 5.6 below:

Table 5.4: Chemical Index of Alteration and Index of Compositional Variability of metasediments.

Lithology/Statistic	CaO*	CIA %	ICV
Biotite Schist 1	1.21	68.19	1.24
Biotite Schist 2	1.01	67.58	1.17
Mica Schist	1.36	72.10	1.22
Augen Schist	1.42	66.48	1.22
Phyllite	0.04	73.70	1.84
Xenolith	1.28	65.49	1.15
Range	0.04-1.42	65.49-73.70	1.15-1.84
Mean	1.05	68.92	1.31
SD	0.18	3.26	0.26

Where:
SD = Standard deviation

Chemical Indices of Alteration (CIA) of the rocks ranges from 65.5 - 73.7 with mean of 68.9% and standard deviation of ±3.3. These values point to relatively moderate to intense chemical weathering of the source rocks. The mean value is close to values for quartz schist (69.7%) but less than values of mica schists (85.9%) and quartzites (91.2%) from Okemesi fold belt,

southwestern Nigeria (Okunlola and Okoroafor, 2009). It is however higher than mean CIA of quartz schists from Igarra area– 53.9% (Okeke and Meju, 1985), Jakura area – 62.1% (Elueze and Okunlola, 2003) and Ibadan area – 57% (Okunlola *et al.*, 2009), southwestern Nigeria.

The medium to high degree of chemical weathering in the source area was possibly due to tectonic activity, which conforms to a tectonic setting in an active continental margin regime. Variable degrees of weathering in the source area led to relative depletion of alkali and alkali earth elements and enrichment in Al_2O_3 and TiO_2 in the resulting terrigenous sedimentary rocks (Nesbitt *et al.*, 1980).

Immature pelitic rocks or sediments will have high ICV (>1), whereas mature pelitic rocks with very little non-silicate clay minerals will possess low values (<0.6) (Elueze and Okunlola, 2003). In the present study, the ICV values of the metasediments range from 1.15 to 1.84 with an average of 1.31. These are higher than the values obtained for quartz schist (0.68), biotite-muscovite schist (0.85) and the quartzite (0.83) in Okemesi fold belt (Okunola and Okoroafor, 2009). This suggests that the protoliths of the metasediments are of low compositional maturity.

5.4.8 Spider diagrams for normalised trace elements

Metasediments

Spider diagram of trace element data for the metasediments was plotted in Fig. 5.9 using the normalizing values (CUB) of Taylor and McLennan (1995).

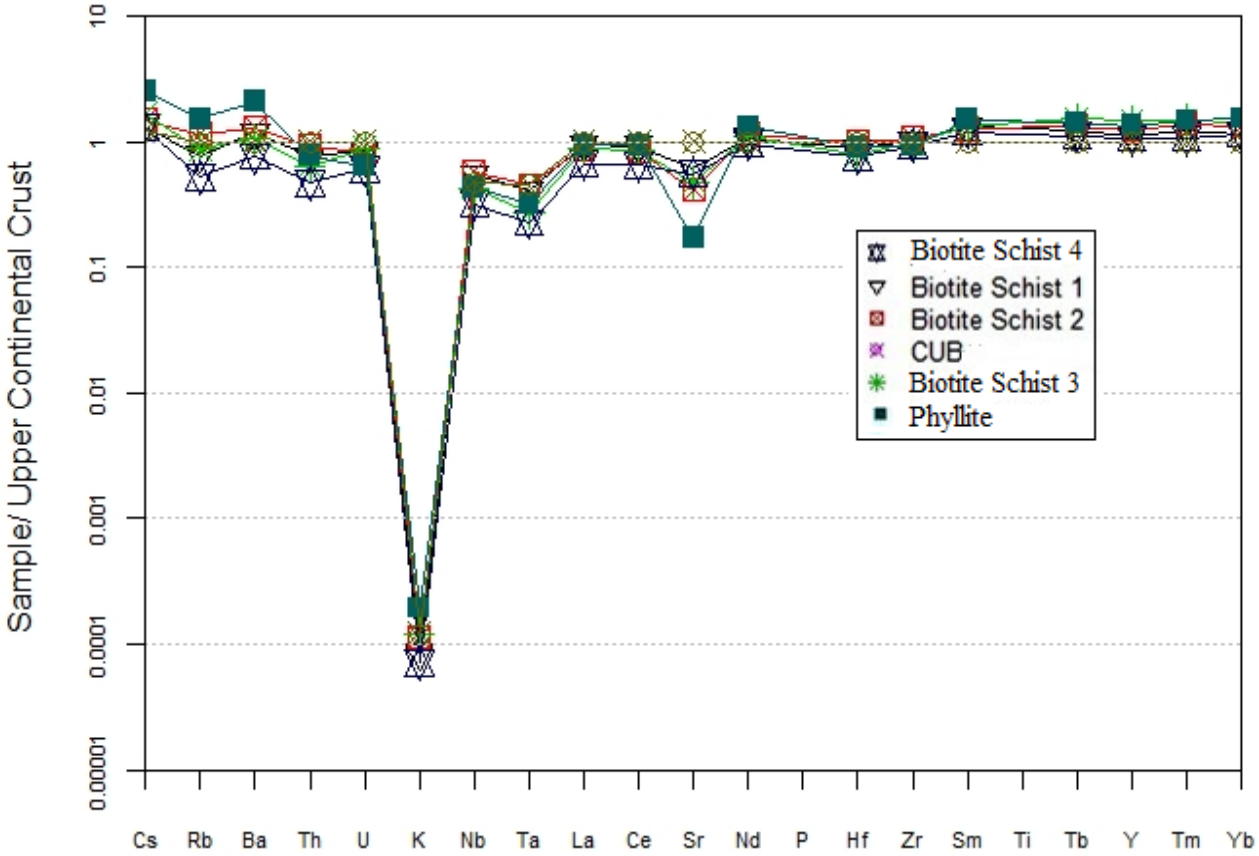


Fig. 5.9: Comparison of trace element of metasediments content with estimates (CUB) of Taylor and McLennan (1995) normalised to upper continental crust of Taylor and McLennan (1995).

There is striking parallelism between the contents in metasediments and the estimates of Taylor and McLennan (1995) except for slight to significant depletion of Sr in biotite schists and phyllite respectively. The alkali and alkali earth element (Rb, Cs and Ba) of the biotite schists scatter around the UCC but are slightly enriched in the phyllite. The high field strength elements (Ti, Hf, Nb, Ta and Zr) are not enriched in the metasediments. The actinide and heavy minerals are not enriched in the metasediments but there is slight depletion of Th and U (Fig. 5.9).

Gneisses

Trace element composition for the gneisses and quartz-tourmaline rock were normalised to the Bulk Continental Crust (BCC) data (ArC+An) of Taylor and McLennan (1995) in Fig. 5.10.

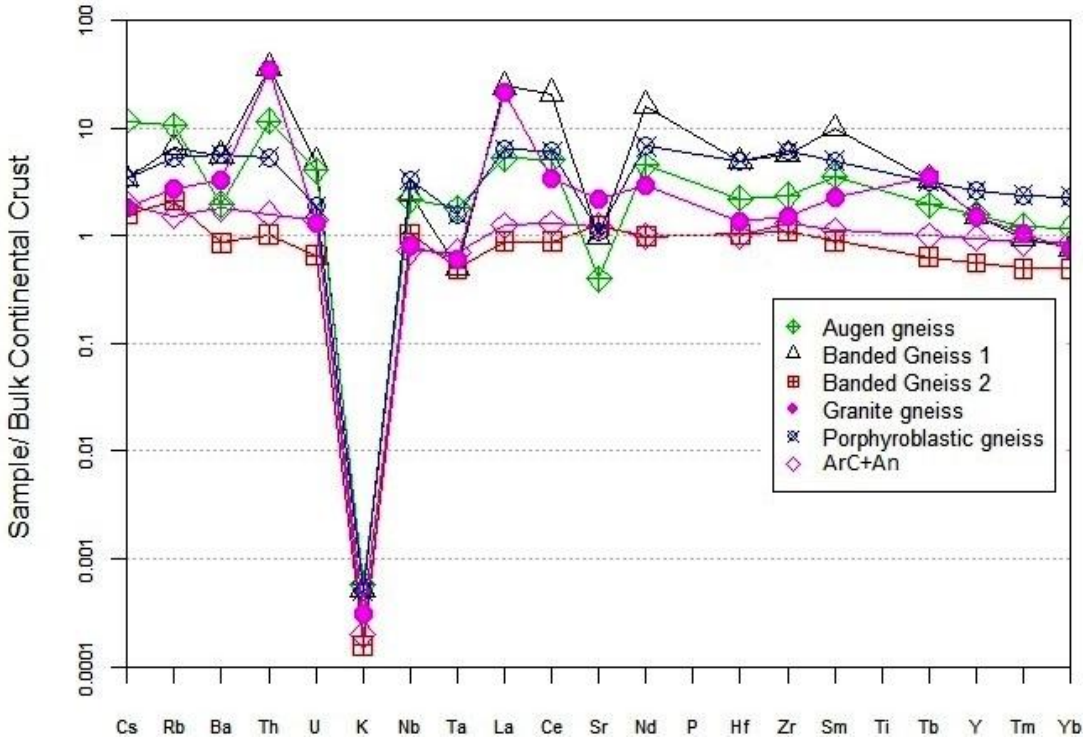


Fig. 5.10: Comparison of trace element estimate (ArC+An) of Taylor and McLennan (1995) with gneisses contents normalised to bulk continental crust of Taylor and McLennan (1995).

Trace elemental contents of the gneisses normalized to the BCC values (Taylor and McLennan, 1995) show that the alkali and alkali earth elements of the augen gneiss are significantly depleted in Sr. Sr content is remarkably coinciding for banded gneiss 1, banded gneiss 2 and porphyroblastic gneiss except for granite gneiss that is enriched in Sr. Ba and Cs also coincide in augen gneiss, granite gneiss and banded gneiss 2. There are varying degrees of enrichment of Rb in all gneiss samples. Ba is significantly depleted in banded gneiss 2 (Fig. 5.10).

The high field strength elements Nb, Ta, Hf and Zr are enriched in porphyroblastic and augen gneisses. Other gneisses remarkably coincide or moderately depleted in Nb, Ta, Hf and Zr relative to the BCC. The actinide and heavy minerals Th and U are enriched in the gneisses except banded gneiss 2. Also, the U in granite gneiss coincides with BCC (Fig. 5.10).

5.4.9 Chondrite normalised REE pattern

Chondrite normalised pattern show systematically varying fractionations (Table 5.7).

Table 5.5: Chondrite normalised elemental ratios for rocks in the study area using normalizing values of Nakamura, (1978).

Rock	Biotite schist				Phyllite	Banded gneiss		Augen gneiss	Porphyroblastic/Granite gneiss	
	BSch1	**BSch2**	**BSch3**	**BSch4**	**Phy**	**BGn 1**	**BGn 2**	**AGn**	**PGn**	**GGn**
Eu/Eu*	0.7	0.7	0.7	0.7	0.6	0.3	1.0	0.2	0.8	0.8
La_N/Yb_N	7.6	6.1	5.6	5.4	5.7	155.6	8.7	21.5	141.8	141.8
La_N/Sm_N	3.1	2.9	2.8	2.4	2.6	7.1	2.8	4.2	27.3	27.3
Ce_N/Yb_N	6.0	4.8	4.5	4.3	4.6	105.1	6.8	16.6	17.8	17.8
La_N/Lu_N	5.8	5.8	5.2	5.5	5.7	201.5	9.2	19.5	147.2	147.2

Metasediments

The chondrite normalised REE for the metasediments shows striking parallelism. The shape of the Rare Earth Elemnt (REE) distribution patterns are generally smooth as evident by decrease in REE values from light rare earth element (LREE) to heavy rare earth element (HREE) and negative Eu anomaly (Fig. 5.11).

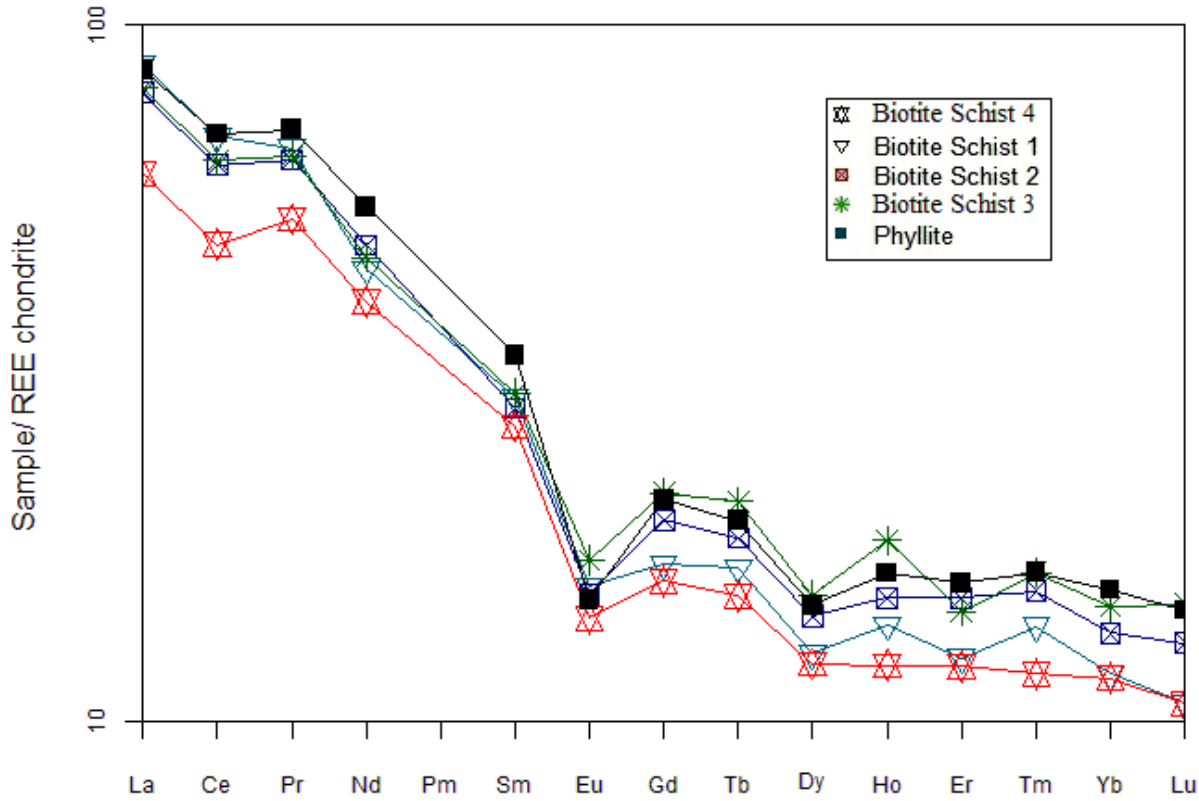


Fig. 5.11: Chondrite normalised (Nakamura, 1974) showing rare earth elements (REE) pattern in metasediments in the study area

Gneisses

Distribution pattern of gneisses show enrichment of LREE, prominent negative Eu anomaly (except banded gneiss 2 and granite gneiss) and HREE depletion. However, granite gneiss show moderate enrichment of Ho and Tm (Fig. 5.12).

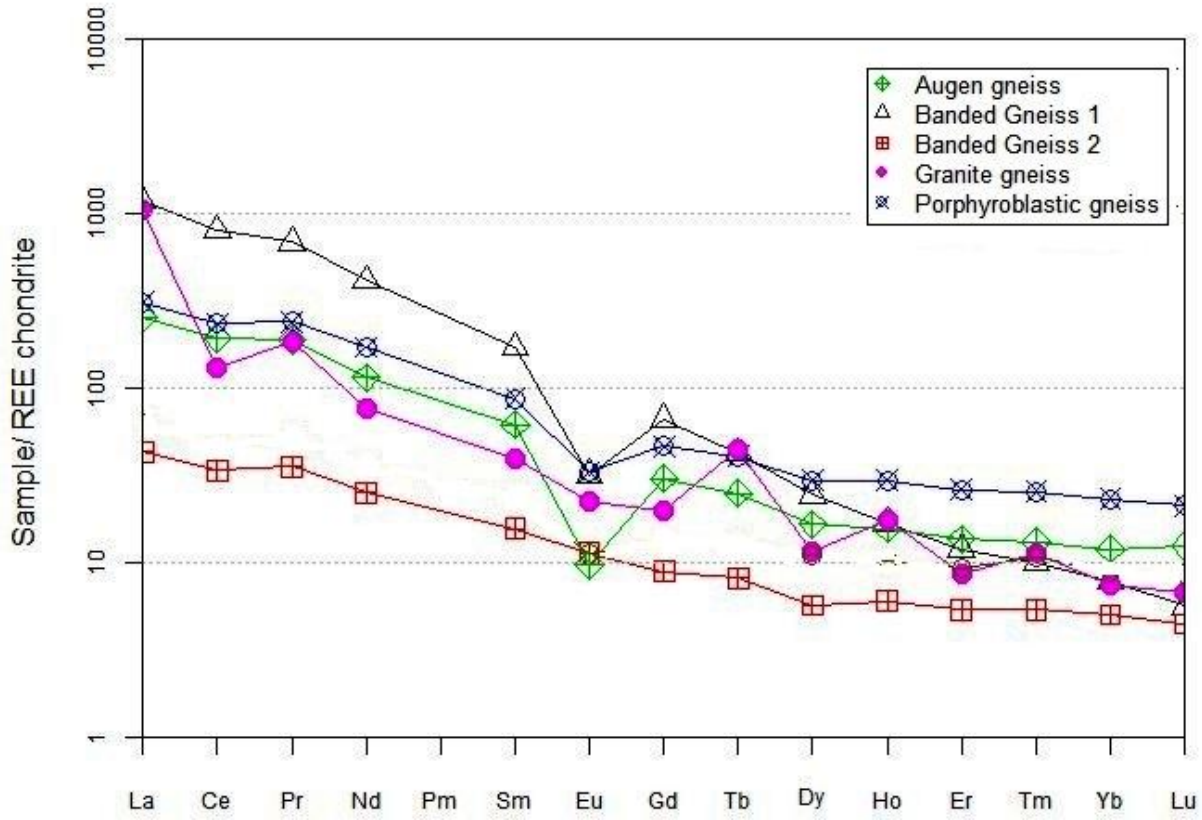


Fig. 5.12: Chondrite normalised (Nakamura, 1974) showing rare earth elements (REE) pattern in gneisses and quartz-tourmaline rock in the study area.

The shape of the Rare Earth Element (REE) distribution patterns in the metasediments and gneisses is generally smooth as evident from decrease in REE values from light rare earth element (LREE) to heavy rare earth element (HREE). The high values of the normalized ratios of La to Yb, Ce to Yb and La to Sm are evidence of high degree of fractionation in gneisses compared to metasediments, which show that the Rare-Earth Elements (REE) patterns are Light Rare-Earth Elements (LREE) enriched with the higher values recorded in the more fractionated gneisses than the metasediments. The enrichment in light REE relative to heavy REE could be caused by the presence of hornblende in the felsic melts of the protolith (Rollinson, 1993).

Striking parallelism of rare earth pattern of the metasediments except the schist xenolith and gneisses except granite gneiss imply an origin from the same source rock (thought to be co-genetic).

The REE contents are higher in gneisses than those of the metasediments by a factor of 4 to 10 except for banded gneiss 2. This pattern is similar to those of hornblende-biotite granitoids in Ityowanye and Katsina-Ala area (SE, Nigeria) (Obiora, 2012). Olanrewaju (1988) had reported similar variation for charnokitic rocks and granites from Ado-Ekiti. In the gneisses, the Eu anomaly expressed as Eu/Eu* ranges from 0.2 to 1.0 with high fractionation factor (La_N/Yb_N 8.7 to 155.6 ratios) compared to those from Katsina-Ala (SE, Nigeria) with Eu/Eu* ranges from 0.89 to 1.29 with lower fractionation factor (La_N/Yb_N ratios 39.22 to 67.97 ratios) in the gneisses (Obiora, 2012).

The relatively high abundances of light rare earth elements (LREE) in the gneisses are thought to be due to contamination with crustal sources. This is consistent with the conclusion of Rahaman *et al.,* (1988) on gneisses in Ile-Ife schist belt.

Enrichment or depletion of Eu is generally attributed to its tendency to be incorporated into plagioclase preferentially over other minerals (Weill and Drake, 1973). A negative Eu anomaly in metasediment indicates loss of plagioclase feldspar during fractionation (differential solubility during rock weathering). Negative Eu in gneisses probably resulted from low preferential concentration of plagioclase feldspar during magma crystallisation of the protolith. Normally, Ce is incorporated into zircon. Hence the negative anomaly of Ce displayed by granite gneiss is an indication of absence of zircon in the gneiss protolith. Negative Ce anomaly in the metasediments indicates anoxic to suboxic condition during metamorphism.

CHAPTER SIX

GOLD MINERALIZATION

6.1 GEOLOGICAL SETTING

A large scale mapping of the area was conducted to cover an area of about 86 km^2. This area is bounded by latitude 11° 48′ 00″ to 11° 53′ N and longitude 07° 00′ to 07° 05′ E and drained by river Yankuzau and its tributaries

Biotite schist (BSch) constitutes about 60% of rocks in the area. It covers the entire northwestern part, large proportion of the northeastern part and a cone shaped area in contact with porphyritic biotite granite in the southwest (Map in back pocket). The areas are low lying, light grey to brown and mainly covered by alluvium that supports vegetation (Plate LXXIII). Symmetrical folds with hinges at right angle to foliation pattern (NNE-SSW) were observed in places (Plate LXXIV). Joints parallel and perpendicular to foliation direction were also observed in places (Plate LXXV and LXXVI). Coarse grained quartz vein of different dimentions (≤1 to 7 cm) occur parallel to foliation pattern (Plate LXXVII and LXXVIII).



LXXIII



LXXIV

Plate LXXIII: Photograph of alluvium cover on biotite schists near Gidan Boss at 11° 51′ 42″ N and 07° 01′ 15″ E.
Plate LXXIV: Symetrical fold on biotite schist at 11° 52′ 01″ N and 07° 02′ 20″ E.



LXXV



LXXVI

Plate LXXV: Photograph of joint (k) that trends NW-SE on low lying biotite schist outcrop at the bank of stream Kaya at 11° 51′ 11.9″ N and 07° 01′ 13.0″ E.
Plate LXXVI: Photograph of joints that strikes NW-SE on biotite schist at 11° 52′ 00″ N and 07° 02′ E.



LXXVII



LXXVIII

Plate LXXVII: Photograph of thin quartz vein in brown coloured biotite schist around Gidan Boss at 11° 51′ 52″ N and 07° 01′ 10″ E.
Plate LXXVIII: Photograph of quartz vein in grey coloured biotite schist around Dutsen Burka at 11° 50′ 48″ N and 07° 01′ 12″ E.

In other places near Gidan Boss and Dutsen Burka, extensive quartz vein of broader width (Plate LXXIX and LXXX) abound. Samples of these vein were randomly sampled for geochemical analysis of target (Au) and pathfinder elements (Zn, Cu, Pb, Ag and Hg).



LXXIX



LXXX

Plate LXXIX: Photograph of quartz vein in biotite schist host rock of Dutsen Burka at 11° 50′ 53″ N and 07° 01′ 06″ E

Plate LXXX: Photograph of quartz vein in biotite schist host rock around Gidan Boss at 11° 52′ 10″ N and 07° 01′ 40″ E

The phyllite covers area around Gimba village in the northern edge of the northeastern quadrant of the area. It constitutes about 6% of rocks in the area (map in back pocket).

Porphyritic biotite granite (PBG) constitutes about 32% of rocks in the area. It outcrops mainly areas around Kutcheri village in southwestern part and most of the southeastern part (Map in back pocket). The PBG outcrops are mainly low lying, whale back. It is leucocratic, coarse grained with white to pink phenocrysts of feldspars. The longer axis of the phenocrysts mainly trend NNE-SSW (Plate LXXXI). Quartzofeldspathic pegmatites of varying width and length were observed on the PBG (Plate LXXXII).



LXXXI



LXXXII

Plate LXXXI: Photograph of PBG with feldspar phenocryst that trend NNE-SSW at 11° 49′ 18″ N and 07° 03′ 49″ E. Note pen length is 13 cm and its tip points NNE-SSW.
Plate LXXXII: Photograph of quartzofeldspathic pegmatite (50 cm width) in a whale-back PBG outcrop at 11° 49′ 17″ N and 07° 03′ 08″ E.

The remaining area (about 2%) is occupied by minor lithologies which include quartz vein (in metasedments) and quartzofeldspathic pegmatites within the porphyritic biotite granite.

6.2 GOLD OCCURRENCES

Active artisanal mining documented along stream channels that are tributaries to main river Yankuzau confirms the presence of placer gold occurrences (alluvial and eluvial) in areas near Gidan Chido (Plate LXXXIII), Gidan Boss (Plate LXXXIV) and Dutsen Burka (Plate LXXXV and LXXXVI).



LXXXIII



LXXXIV

Plate LXXXIII: Photograph of artisanal mining activities near Gidan Chido at 11°52′48″N and 07°03′15″E
Plate LXXXIV: Photograph of artisanal mining activities near Gidan Boss at 11°51′30″N and 07°02′55″E



LXXXV



LXXXVI

Plates LXXXV and LXXXVI: Photographs of active artisanal mining of placer deposits near Dutsen Burka at 11°51′22″N and 07°02′40″E

Artisanal miners are constrained to explore gold during raining season when seasonal stream channels are laden with water to pan for placer gold. To resolve this problem the local co-operative society (Kutcheri Cooperative Society) in the area in partnership with Chafe Local Government Council carried out reconnaissance sediment sampling and panning from pits around Gidan Boss (Plate LXXXVII) to determine/delineate area(s) of high placer gold occurrence.



LXXXVII

Plate LXXXVII: Photograph of a pit dug to pan sediments for placer gold around Dutsen Burka at 11° 51′ 16″ N and 07° 01′ 16″ E.

The area nicknamed “Gidan Boss” (local believe that gold is very valuable but difficult to get hence the nickname) was confirmed to be most prospective. Thus, mining site construction (Plate LXXXVIII) is underway with a plan to:

- Grade access road from Kutcheri to the mining site
- Install an excavator and mobile placer mining plant to mechanise sampling and panning.
- Drill borehole with a submersible to pump water into a water tank to ease access to water needed for panning.



LXXXVIII

Plate LXXXVIII: Photograph on mining site under construction showing by Kucheri Mining Co-operative Society in partnership woith Chafe Local Government Council to house A (Mobile placer plant) and B (Generator) around Gidan Boss at 11° 51′ 50.3″ N and 07° 01′ 49.9″ E.

6.3 SAMPLE COLLECTION AND ANALYSIS

6.3.1 Sediment sampling

20 kg each of sediments from pit close to banks of river Kaya (tributary to river Yankuzau), pits (about 6 m deep) around Dutsen Burka and Gidan Boss were sampled with shovel and pan. These were taken into the laboratory for panning to determine grain morphology.

6.3.2 Panning and grain morphology

The gold grains are denser and separates from other sediments by liquefaction during panning. The pan had concentric grooves that help trap denser gold grains upon shaking in water (Plate LXXXIX and XC).



LXXXIX



XC

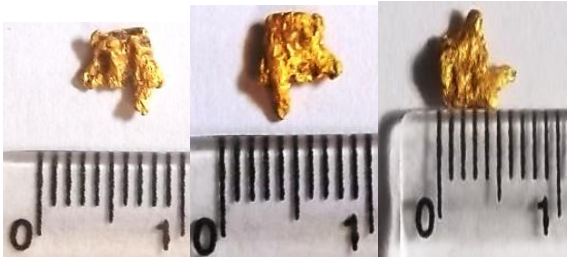
Plate LXXXIX: Photograph showing panning by liquefaction
Plate CX: Photograph showing concentric groove in panning plate. Observer points to a gold grain.

The panning of 20 kg sediments from pit close to river banks near Gidan Chido yielded no gold while 20 kg each from pits at Dutsen Burka and Gidan Boss (artisanal mining site) yielded 0.12 g and 0.16 g Au respectively.

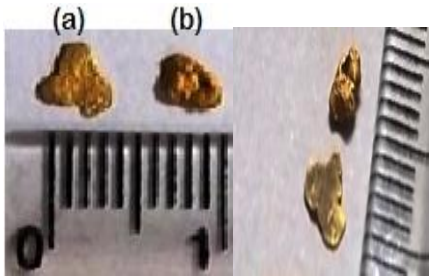
Diameters of grains range from ≤4 to 6 mm. The 6 mm grain has sharp tapering edges (Plate XCI) while some have smooth, curved edges and others tapering edge but flattened (Plate XCII). DiLabio (1990) devised a classification scheme in which gold grains are classified into three

categories: pristine, modified and reshaped. In pristine gold grains the primary shapes and surface textures are preserved. In modified gold grains some primary surface textures are preserved, however, the edges and protrusions have been damaged during transport. In reshaped gold grains the primary surface textures are destroyed and the original grain shape is no longer discernible.

Based on DiLabio (1990) classification, the 6 mm grain is thought to be pristine and alluvial (i.e probably resulted from decomposition or disintegration of rock in place). The material probably slumped or washed downslope for a short distance but has not been transported by a stream) while other grains thought to be modified to reshaped and elluvial (i.e probably resulted from action of running water in a stream channel). Hence, the grains (≤4 - ≥6.0 mm) in the sediments suggests ductile deformation of in-situ (proximal or far) quartz veins.



XCI



XCII

Plate XCI: Photograph showing different orientation direction of 6 mm grain with sharp tapered edges.
Plate XCII: Photograph of grains with (a) sharp edges but flattened and (b) smooth curved edges.

Garba (1990 and 2003) reported that Au mineralization in Nigerian basement is largely mesothermal. Nesbit (1991) geochemically charaterise mesothermal Au deposit greater than 1 ppm to be associated with Ag, Sb, As, W, Hg, Bi, Mo, Pb, Zn, Cu, Ba.

6.3.3 Chemical analysis and statistical relation

Thirteen samples of quartz vein samples were analysed to determine the variations in concentrations of target element (Au) and other indicator element (Hg, Ag, Cu, Zn and Pb).

The results show concentration of elements range as follows: Au (< 0.1-4.8 ppm), Hg (<0.05-0.42 ppm), Cu (6.2-61.4 ppm), Zn (<0.1-39.0 ppm), Pb (<0.03-28.00 ppm), Ag (<0.1-0.49 ppm) and Au (<0.1-1.8ppm), Hg (<0.05-0.44 ppm), Cu (4.80-8.80 ppm), Zn (6.00-30.00 ppm), Pb (<0.03-8.0 ppm), Ag (<0.1-0.42 ppm) for quartz vein samples around Gidan Boss and Dutsen Burka respectively (Table 6.1 and 6.2).

T-test (two tailed, assuming unequal variances)

Levels of significance of variation in concentration of elements were compared with two tailed t-test assuming unequal variances (Table 6.1 and 6.2). A null hypothesis (Ho) that there is significant difference in concentrations of target and pathfinder elements around Dutsen Burka and Gidan Boss at $\alpha = 0.05$ level of significance was set.

Table 6.1: Concentration of target and pathfinder elements around Gidan Boss and statistical relations

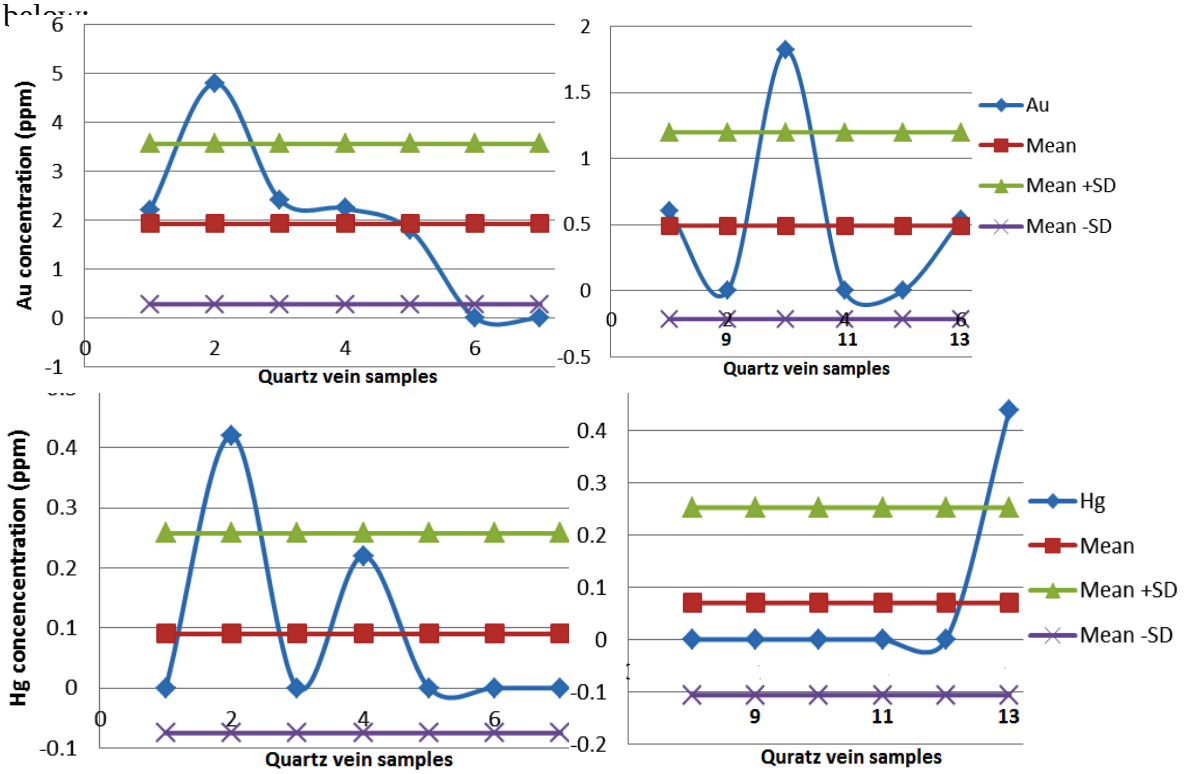
Location	**Element (ppm)**					
Gidan Boss	**Au**	**Hg**	**Cu**	**Pb**	**Zn**	**Ag**
AGQ1	2.21	0.00	40.30	18.20	23.00	0.20
AGQ2	4.80	0.42	61.40	28.00	39.00	0.49
AGQ3	2.41	0.00	26.20	12.00	12.00	0.34
AGQ4	2.24	0.22	8.80	10.40	4.00	0.24
AGQ5	1.80	0.00	7.60	10.20	0.00	0.32
AGQ6	0.00	0.00	7.20	0.40	12.00	0.00
AGQ7	0.00	0.00	6.20	0.00	0.00	0.00
Range	<0.1-4.8	<0.05-0.42	6.2-61.4	<0.03-28.00	<0.1-39.0	<0.1-0.49
Mean	1.92	0.09	22.53	11.31	0.23	12.86
Variance	2.68	0.03	458.87	95.91	0.03	199.48
SD	1.64	0.17	21.42	9.79	0.18	14.12
t Stat	2.09	0.19	1.95	2.00	0.51	-0.27
t Critical two tail	2.31	2.23	2.44	2.31	2.20	2.23
P ($T \leq t$) two tail	0.07	0.86	0.10	0.08	0.62	0.79

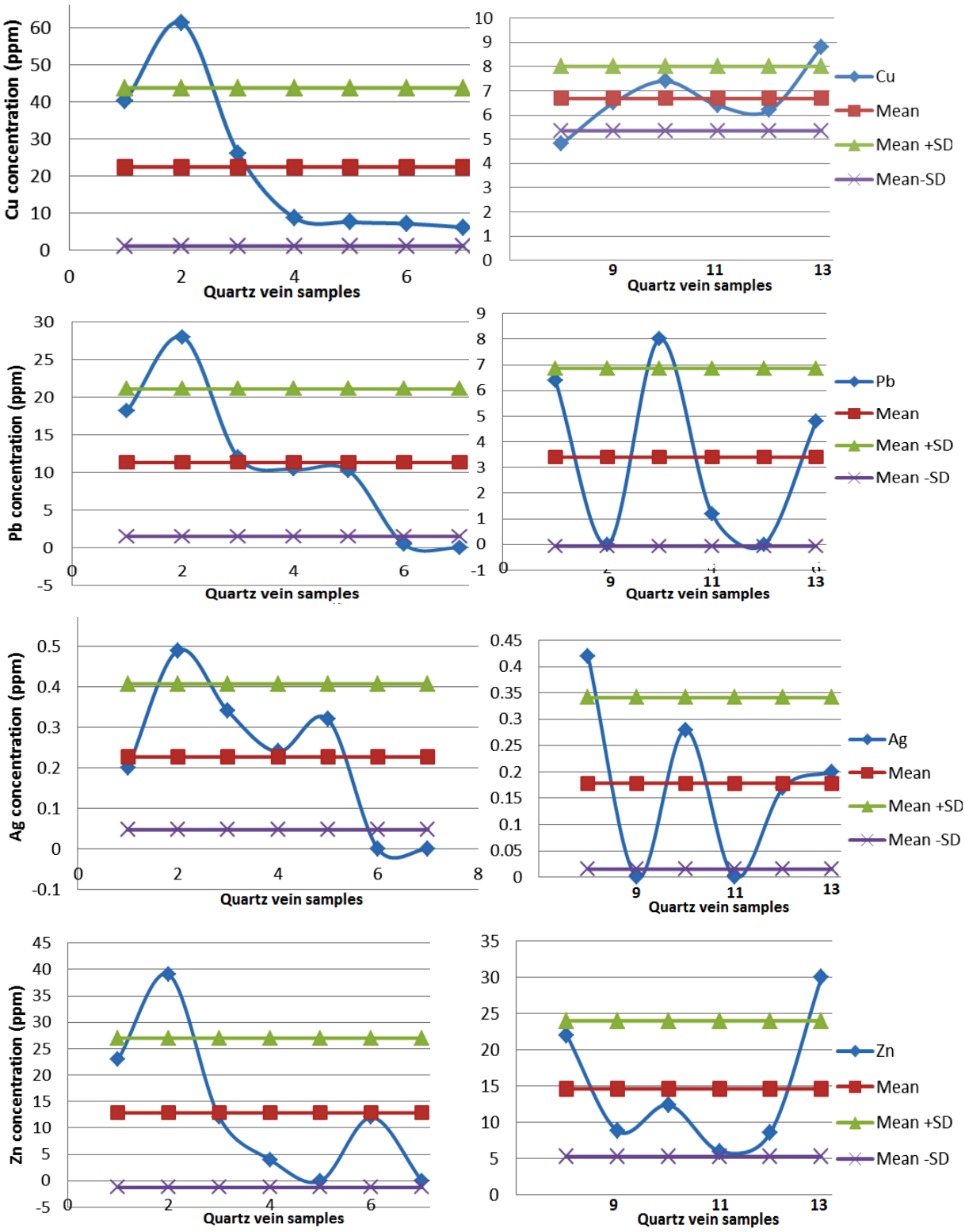
Table 6.2: Concentration of target and pathfinder elements around Dutsen Burka and statistical relations

Location	Element (ppm)					
Dutsen Burka	**Au**	**Hg**	**Cu**	**Pb**	**Zn**	**Ag**
AGq8	0.60	0.00	4.80	6.40	22.00	0.42
AGq9	0.00	0.00	6.50	0.00	8.80	0.00
AGq10	1.82	0.00	7.40	8.00	12.40	0.28
AGq11	0.00	0.00	6.40	1.20	6.00	0.00
AGq12	0.00	0.00	6.20	0.00	8.60	0.17
AGq13	0.54	0.44	8.80	4.80	30.00	0.20
Range	<0.1-1.8	<0.05-0.44	4.80-8.80	0.03-8.0	6.00-30.00	<0.1-0.42
Mean	0.49	0.07	6.69	11.31	14.63	0.18
Variance	0.50	0.03	1.78	12.02	88.07	0.03
SD	0.71	0.18	1.33	3.47	9.38	0.16
t Stat	2.09	0.19	1.95	2.00	-0.27	0.51
t Critical two tail	2.31	2.23	2.45	2.31	2.23	2.21
P (T ≤ t) two tail	0.07	0.86	0.10	0.08	0.79	0.62

Standard deviation plot

Standard deviation plot for samples around Gidan Boss and Dutsen Burka is shown in Fig 6.1 below:





(A) (B)

Fig. 6.1: Standard deviation plot for samples near (A) Gidan Boss and (B) Dutsen Burka area.

Generally, concentration of the target and pathfinder elements are higher than standard deviation of the mean near mining site (Gidan Boss) for quartz vein AGQ 2 while in other samples, concentration of these elements is within range except for quartz vein AGQ6 and AGQ7 in which have their concentrations are less than standard deviation of the mean for Au, Pb and Ag. Quartz vein samples near Dutsen Burka generally scatter around the range but had Au and Pb higher than the threshold for quartz vein AGq10. Also, a similar pattern is noted for quartz vein AGq13 for elements Hg, Cu and Zn.

The t Start value is generally less than the t Critical value for target and pathfinder element in all samples near Gidan Boss and Dutsen Burka. This means that the P values are greater than 0.05 for all the samples. Therefore, there is no significant statistical difference between the target and pathfinder element in Dutsen Burka and Gidan Boss area. The null hypothesis that there is significant difference in concentration of the tested contents around Dutsen Burka and Gidan Boss was rejected.

Correlation coefficient

All elements tested (Hg, Ag, Cu, Zn and Pb) positively correlate with Au at different levels, Au/Hg (r = 0.48), Au/Zn (r = 0.51), Au/Cu (r = 0.84), Au/Pb (r = 0.97), Au/Ag (r = 0.77) as shown in Fig. 6.2.

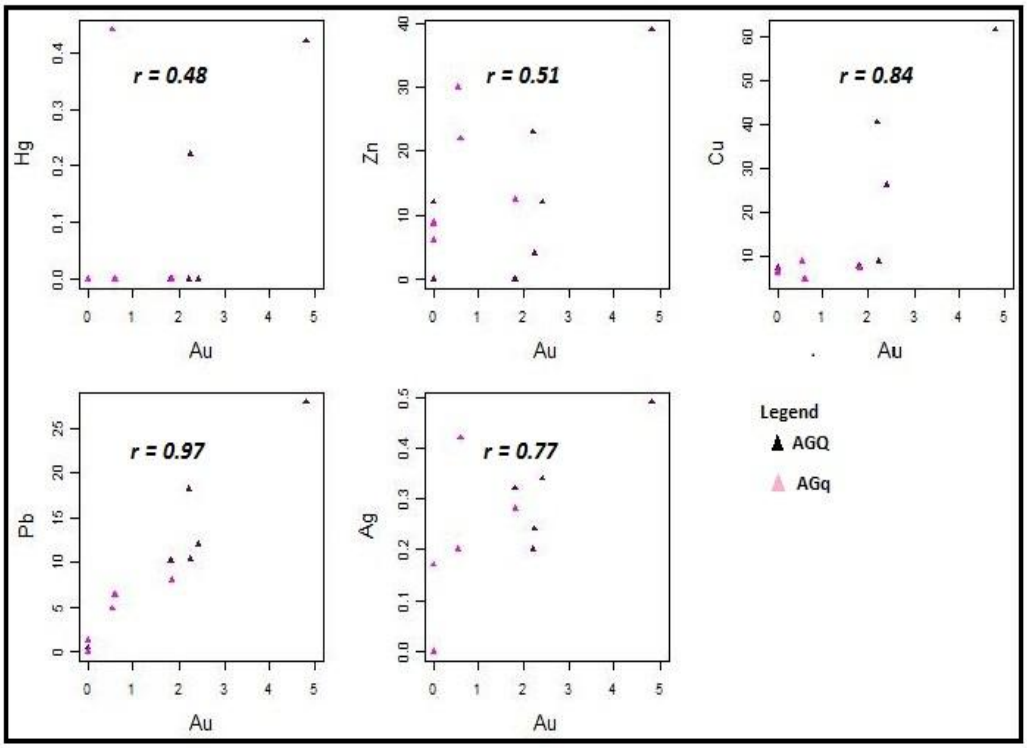


Fig. 6.2: Bivariate plot of Au against other trace element (Hg, Zn, Cu, Pb and Ag).

Pearson correlation coefficient shows the indicator elements Au for the area. Base metals Ag, Pb and Cu are chemically active while Au is a noble metal that is chemically inert (under most conditions). Resultant direct proportional relationship between Au/Pb, (r = 0.97) and Au/Cu, (r = 0.84) shows that Cu and Pb are indicator elements for Au in the area. Mobile elements Ni, Zn, Pb, As and Cu were used to locate buried gold mineralization in Essase Concession, Eastern Region, Ghana (Amedjoe and Adjovu, 2013).

CHAPTER SEVEN

SUMMARY, CONCLUSION AND RECOMMENDATION

7.1 SUMMARY AND CONCLUSION

Remote sensing studies with ASTER GDEM aided 3-D perspective view of the study area. Also, Band ratio, principal component analysis method, false color composit method and crosta technique from Landsat ETM+ aided qualitative discrimination of concealed lithologic boundaries, alteration mapping and automatic extraction of lineaments. The dominant lineament direction conforms to structure from field observations.

Field studies and petrographic analysis have shown that the major lithologies in the area include granitic gneiss (banded, augen and porphyroblastic), metasediments (biotite schist, phyllite) and granite (porphyritic and medium to coarse grained) while quartz-tourmaline rock, quartz vein, aplite dyke and quartzofeldspathic vein constitute minor rock types. The major minerals in the gneisses include quartz, biotite, plagioclase feldspar, microcline ± orthoclase, perthite, muscovite with opaque, ± pyroxene, zircon as accessories. The metasediments are composed of quartz, biotite ± plagioclase, muscovite, pyroxene and chlorite as the main minerals with opaque accessories. The serpentinite consist of olivine pseudomorph, anthophyllite and chromite.

The dominant foliation trend is NNE-SSW which follows the general trend of structures resulting from Pan-African Orogeny. Traces of other trend directions which include NNW-SSE and NW-SE thought to have resulted from other deformation processes that pre dates Pan-African Orogeny are also observed. Exfoliation and tectonic joints with non-orthogonal joint pattern predominates. The joint lengths are directly proportional to the aperture. Both dextral and

sinistral strike slip faults are common in the granites. All folds had NNE-SSW axial trend (attitude of hingeline).

Discrimination diagrams from geochemical analysis show that alkali elements in gneisses and schist have undergo varying mobility during metamorphism, thus confirming low grade metamorphism for the metasediments (greenschist facies) and low to medium grade for the gneisses (greenschist to lower amphibolite facies). The gneisses are of igneous parentage except granitic gneiss which may be sedimentary. Also, the metasediments are broadly of sedimentary origin. The gneisses are of continental origins that have granitic to granodioritic composition related to granite that originated from peraluminous magma involving some crustal material (continental).

Paleoweathering estimates point to relatively moderate to intense chemical weathering of the metasedimentary source rocks. Also, the protoliths of the metasediments are of low compositional maturity.

Trace element composition shows that the metasediments have pattern similar to the upper continental crust (UCC). The gneisses are more evolved.

There is variability in the total REE abundances, there is variation in pattern and degree of fractionation among the gneisses and the metasediments. Relative depletion of HREE and enrichment of LREE with significant negative Eu anomaly noted in the gneisses and metasediments shows that plagioclase feldspar fractionates. Negative Ce anomaly displayed by granite gneiss is an indication of absence of zircon in the gneiss protolith. Negative Ce anomaly in the metasediments indicates anoxic to suboxic condition during metamorphism.

Anomalous concentration of Au in most of quartz vein samples investigated confirm gold mineralization around Kutcheri. There is higher concentration of target and pathfinder elements (Au, Pb, Cu, Ag and Zn) in places at Gidan Boss relative to Dutsen Burka. However, it is not high enough to be considered statistically significant at least with the present number of samples. It is not possible to distinguish between mineralization reality and random chance.

7.2 RECOMMENDATIONS

I recommend the following:

i. Remote sensing of higher spatial and spectral resolution with Hyperspectral images to diagnostically delineate lithologic boundaries and highlight prospective mineralized areas.

ii. Representative systematic sampling of samples to diagnostically characterize the precursor of lithologies in the area.

iii. Representative systematic sampling of sediments to unequivocally determine gold grain morphology.

iv. Complementary small scale detailed grid sampling of core samples near Gidan Boss, Dutsen Burka and whole rock chemistry to discriminate the origin of the mineralizing fluid.

v. Fluid inclusion studies to confirm genetic models (metamorphic dewatering accompanied with low salinity CO_2 enrichment) proposed by other workers is recommended.

REFERENCES

Abdelhamid, G., Rabba, I., 1994. An investigation of mineralized zones revealed during geological mapping, Jabal Hamra Faddan-Wadi Araba, Jordan, using Landsat TM data Internation Journal of Remote Sensing 15, 1495–1506.

Abrams, M.J., Rothery, D.A. and Pontual, A. (1983). Mapping in the Oman ophiolite using enhanced Landsat Thematic Mapper images. *Tectonophysics* 151, 387–401.

Adekoya, J.A. (1998). The geology and geochemistry of the Maru Banded Iron-Formation, Northwestern Nigeria. *Journal of African Earth Sciences,* Volume 27, Number 2, pages 241-257.

Ajayi, J.A. (2003). Mineralogical studies of the gold ore of Ilesha area, southwestern Nigeria. *Journal of Mining and Geology,* Volume 39, Number 2, pages 63 – 65.

Ajibade, A.C. (1980). Geotectonic evolution of the Zungeru region, Nigeria. — Unpublished PhD thesis, University of Wales, Aberystwyth.

Ajibade, A.C. and Fitches, W.R. (1988). The Nigerian Precambrian and the Pan-African Orogeny. *A publication of the Geological Survey of Nigeria.*

Ajibade, A.C., Fitches, W.R. and Wright, J.B. (1979). The Zungeru mylonites, Nigeria: recognition of a major unit. Rev de Geol Geog Phys 21:359–363.

Ajibade, A. C. and Wright, J. B. 1988. Structural relationships in the schist belts of Northwestern Nigeria. In Precambrian Geology of Nigeria (Edited by Nigeria Geol. Surv. 103 -109.

Akande, S.O , Fakorede, O. and Mucke, A. (1988). Geology and genesis of gold bearing quartz veins at Bini Yauri and Okolom in the Pan-African domain of western Nigeria. *Geologie en Mijnbouw* 67:41-51.

Akande, A.O and Kinnaird, J. (1990). Characterization and origin of ore–forming fluids in the Nigerian mineral belts. *Proceedings of the Eighth Quadrennial IAGOD Symposium, Ottawa, Canada,* pages 199 – 218

Amedjoe, C.G and Adjovu, I.T. (2013): Application of the mobile metal ion geochemical technique in the location of buried gold mineralization in Essase Concession, Eastern Region, Ghana. *Journal of Geology and Mining Research.* Volume 5, Number 6, pages 147-160.

Amuda, A.K., Danbatta, U.A and Najime, T. (2014). Utilization of Landsat 7 ETM+ Multispectral Data and ASTERGDEM in Geological Investigation and Alteration Mapping around Yankara-Dan Sabo-Takulawa Area within Wonaka Schist Belt, Northwestern Nigeria. *Journal of Environment and Earth Sciences. Volume 4, Number 2. Pages 44 – 56.*

Bear, H.P. and Glaeser, R. (1981). The Mallam Tanko Serpentinites: Late Orogenic Ultramafic Intrussions in Pan-African Basement Complexes of NW-Nigeria. *A paper presented in Precambrian Geology of Nigeria symposium of the Geological Survey of Nigeria, held at Kaduna, 14th-17th October, 1986.*

Black, R. (1980). Precambrian of West Africa. *Episodes 4:3–8.*

Brown, M., Rushmer, T. & Sawyer, E. W. (1995b). Introduction to special section: mechanisms and consequences of melt segregation from crustal protoliths. *Journal of Geophysical Research 100, 15551–15563.*

Burke, K.C. and Dewey, J.F. (1972). Orogeny in Africa. *In: Dessauvagie TFJ, Whiteman AJ (eds), Africa geology. University of Ibadan Press, Ibadan*, pages 583–608.

Chica-Olmo, M. (2002). Development of a decision support system based on remote sensing and GIS techniques for gold-rich area identification in SE Spain. *International Journal Remote Sensing.* 23 (22), 4801–4814.

Condie, K.C. 1989. Plate tectonics and crustal evolution. Oxford: Peragamon. pages 160 – 186

Condie, K.C. (1993). Chemical composition and evolution of the upper continental crust: contrasting results from surface samples and shales. *Chem. Geol*.104, 1–37.

Cox, K.G., Bell, J.D. and Pankhurst, R.J. (1979). The Interpretation of Igneous Rocks. *George Allen & Unwin.*

Cox, R., Lowe, D.R. and Cullers, R.L. (1995). The influence of sediment recycling and basement composition on evolution of mudrock chemistry in the south-western United States. *Geochimica et Cosmochimica Acta* 59, 2919–2940.

Dada, S.S. (2006). Proterozoic evolution of Nigeria. In: Oshi O (ed) The basement complex of Nigeria and its mineral resources (A Tribute to Prof. M. A. O. Rahaman). *Akin Jinad and Company Ibadan*, pages 29–44.

Danbatta, U.A and Ike, E.C. (2001). Geochemistry and origin of metasediments from the Kazaure Schist belt in the Precambrian Basement of NW Nigeria. Nigerian Journal Chemical Research. *Volume 6, pages 31-36.*

Danbatta, U.A. (2002). Rb-Sr Isochron Dating of Granitoids from the Kazaure Schist Belts, NW Nigeria. Global journal of Pure and Applied sciences. *8 (3), pages 319 – 322.*

Danbatta, U.A. (2003). Structural framework underlyng the metamorphic evolution of the Kazuare Schist Belt, NW Nigeria. Global Journal of Geological Sciences. *1:1:82-83.*

Danbatta, U.A. (2008). Precambrian crustal development in the northwestern part of Zuru schist belt, northwestern Nigeria. *Journal of Mining and Geology*. 44 (1), pages 45-56 0

Danbatta, U.A. (2010). On the Evolution of the Kazaure Schist Belt of NW Nigeria: A Re-Interpretation. Global Journal of Geological Sciences. *Volume 8, Number 2.*

Danbatta, U.A. and Garba, M.L. (2007): Geochemistry and petrogenesis of Precambrian amphibolites in Zuru schist belt, northwestern Nigeria. *Journal of Mining Geology,* 43 (1), pages 23 – 30.

Danbatta, U.A and Ike, E.C. (2001). Geochemistry and origin of metasediments from the Kazaure Schist belt in the Precambrian Basement of NW Nigeria. *Nigerian Journal Chemical Resources, volume. 6, pages 31-36.*

DiLabio, R. N. W. (1990). Classification and interpretation of the shapes and surface textures ofgold grains from till on the Canadian Shield; Current Research, Part C, Geological Survey of Canada, Paper 90-1C, pages 323-329.

Drury, S. A. (1993). *Image interpretation in geology* (p. 283). London: Chapman and Hall.

Dunstan, W.R (1911): Reports on the results of mineral survey of Northern Nigeria, 1907 – 1908. *Colon. Rep. Miscel. Series* Number 79.

Egbuniwe, I.G. (1982). Geotectonic evolution of the Maru Belt, NW Nigeria. *Unpublished Ph.D. Thesis, University of Wales, Aberystwyth.*

Ekwueme, B.N. (1992). RbSr age of Pan-African migmatites in the Oban massif of southeastern Nigeria *Journal of African Earth Sciences, 15 (1), pages 65-72.*

Elueze, A. A., (1981a). Geochemistry and petrotectonic setting of metasedimentary rocks of theschist belt of Ilesha area S. W. Nigeria. *Journal of Mining and Geology. 18 (1), pages 194- 197.*

Elueze, A. A. (1981b). Dynamic metamorphism and oxidation of amphibolites of Tegina area, northwest Nigeria, Precambrian Res; 14, pp. 379 – 388.

Elueze , A. A & Okunlola , O. A. (2003). Petrochemical and Petrogenetic characteristics of metasedimentary rocks of Lokoja-Jakura schist belt, Central Nigeria. *Journal of Mining and Geol.*; Vol. 39 (1), pp 21–27.

Frei, M., & Jutz, S. (1990). Use of Thematic Mapper data for the detection of gold bearing formations in the Eastern Desert of Egypt. In *Thematic Conference on Remote Sensing for Exploration Geology- Methods, Integration, Solutions, 7 th, Calgary, Canada* (pp. 1157-1172).

Gad, S. and Kusky, T. (2006). Lithological mapping in the Eastern Desert of Egypt, the Barramiya area, using Landsat thematic mapper (TM). *Journal of African Earth Sciences, 44*(2), 196-202. http://dx.doi.org/10.1016/j.jafrearsci.2005.10.014

Garba, I. (1990): The Greenstone Belts. Unpublished M. Sc. Seminar, Ahmadu Bello University, Zaria, pages. 1 – 7.

Garba, I. (2000): Gold prospects of the Nigeria Pan African terrain of West Africa. Journal of Mining and Geology, Vol. 36 (2), pp. 123 – 135.

Garba, I. (2002). Late Pan-African tectonics and origin of gold mineralization and rare-metal pegmatites in the Kushaka schist belt, northwestern Nigeria. *Nigerian Journal of Mining and Geology*, 38, pages 1-12.

Garba, I. (2003): Geochemical characteristics of mesothermal gold Mineralization in the Pan African (600 $\pm$ 150 ma). Basement of Nigeria. Applied Earth Science, Volume 36 (2), pages 123 – 135.

Garba, I. and Akande, S.O. (1992). Origin and significance of CO2 bearing fluid inclusion in the Bin Yauri gold quartz veins of Northwestern Nigeria. Mineralium Deposita, 27, pages 249-255.

Grant, N.K. (1978). Structural distinction between a metasedimentary cover and an underlying basement in the 600 m.y old Pan-African domain of Northwestern Nigeria. *Geological Society of America Bulletine 89:50–58.*

Harper, C.T., Sherrer, G., McCurry, P. and Wright, J.B. (1973). K-Ar retention ages from the Pan-African of Northern Nigeria. *Geological Society of Amererica Bulletine 84, 919-926.*

Holt, R.W. (1982). The Geotectonic Evolution of the Anka Belt in the Precambrian Basement Complex of N.W. Nigeria. *Unpublished Ph.D. Thesis, The Open University.*

Ibrahim, A.A. (2008). Petrography, geochemistry and origin of banded iron-formation of the Kazaure schist belt, Western Nigeria. *Journal of Mining and Geology* 44 (1), pages 13-20

James, R.S., Grieve, R.A.F and Paul, L. (1978). The petrology and cordierite-anthophyllite gneisses and associated mafic and pelitic gneisses at Manitouwadge, Ontario: American Journal of Science, volume 278, pages 41-63.

Johnson, S.E., Dupee, M.E. and Guidotti, C.V. (2006). Porphyroblast rotation during crenulation cleavage development: an unequivocal example from the aureole of the Mooselookmeguntic pluton, Maine, USA. *Journal of Metamorphic Geology. 24, 55-73*.

Jingyuan, E.A. and Xucman, M. (1991). Using remote sensing and GIS to analyse land cover change and its impacts on the regional sustainable development. *International Journal of Remote Sensing, 23(1), 107-114.*

Kaufmann, H. (1988). Mineral exploration along the Aqaba-Levant structure by use of TM data; concepts, processing, and results. *International Journal of Remote Sensing*, volume 9, 1639-1658.

Kusky, T. M. and Ramadan, T. M. (2002). Structural controls on Neoproterozoic mineralization in the South Eastern Desert, Egypt: an integrated field, Landsat TM, and SIR-C/X SAR approach. *Journal of African Earth Sciences, 35*(1), 107-121.

Marc, D. (1992). Granites and rhyolites from the northwestern USA: temporal variation in magmatic processes and relations to tectonic setting. Transactions of the Royal Society Edinburgh, Earth Sciences 83, 564.

McCurry, P. (1971). Pan-African Orogeny in Northern Nigeria. *Geological Society of America Bulletine 82: 3251-3263.*

McCurry, P. (1973). Geology of degree sheet 21, Zaria, Nigeria. *Overseas Geol Mineral Resources 45:1–30.*

McCurry, P. (1976). The geology of the Precambrian to Lower Palaeozoic Rocks of Northern Nigeria – A Review. *In: Kogbe CA (ed) Geology of Nigeria. Elizabethan Publishers, Lagos, pages 15–39.*

McCurry, P. and Wright, J.B. (1977). On Place and Time in Orogenic Granite Plutonism. *Journal of Geological Society of America.* Volume 82, number 6 pages 1713-1716.

Middelburg, J.J., Van der Weijden, C.H and Woittiez, J.R.W (1988). Chemical processes affecting the mobility of major, minor and trace elements during weathering of granitic rocks. *Chemical Geology, 68 (1988), pp. 253–273*

Mucke, A. (2005). The Nigerian manganese-rich iron-formations and their host rocks – From sedimentation to metamorphism. *Journal of African Earth Sciences, 41 (5), 29p.*

Mucke, A., Annor, A. and Neumann, U. (1996). The Algoma-type iron-formations of Nigerian metavolcano-sedimentary schist belts. *Mineralium Deposita 31: 113-122.*

Nakamura, N. (1974). Determination of REE, Ba, Fe, Mg, Na and K in Carbonaceous and ordinary Chondrites. Geochim. Cosmochim. Acta volume 38, pages 757-775.

Nesbitt, B.E. (1991): Phanerozoic gold deposits in tectonically active continental margins. *In:* Foster, R.P. (ed.), Gold metallogeny and exploration, Blackie and Son, Glasgow and London, 104-132

Nesbitt , H. W. & Young , G. M. (1982): Early Proterozoic Climates and Plate Motions Infered from Major Element Chemistry of Lutites. *Nature 199*; pages 715–717.

Nesbitt, H.W., Markovics, G. and Price, R.C. (1980). Chemical processes affecting alkaliesand alkaline earths during continental weathering. Geochimica et Cosmochimica Acta 44, 1659–1666.

Obaje, N. G. (2009). Geology and Mineral Resources of Nigeria. Springer-Verlag Berlin Heidelberg, Page 15.

Obiora, S C. (2012). Chemical characterization and tectonic evolution of hornblende-biotite granitoids from the Precambrian Basement Complex around Ityowanye and Katsina-Ala, Southeastern Nigeria . Journal of Mining and Geology Volume 48(1), pages 13–29

Odeyemi, I.B. (1977). On the petrology of the basement rocks around Igarra, Bendel state, Nigeria. Unpublished Ph.D. Thesis, University of Ibadan, 223 pages.

Ogezi, A.E.O. (1977). Geochemistry and Geochronology of Basement Rocks from Northwestern Nigeria. Unpublished Ph.D. Thesis, University of Leeds.

Ogezi, A.E.O. (1988). 'Origin and evolution of the Basement Complex of northwestern Nigeria in the light of new geochemical and geochronological data'. *Precambrian Geology of Nigeria. A publication of the Geological Survey of Nigeria*, edited by P.P. Oluyide and others. Pages 301-312.

Okeke, P. O. and Meju , M. A. (1985). Chemical evidence for the sedimentary origin of Igarra Supracrustal rocks S.W. Nigeria. *Journal Mining and Geology*; Volume 22 (1 and 2), pages 97–104.

Okonkwo, CT and Folorunso I.O, (2013). Petrochemistry and Geotectonic Setting of Granitic Rocks in Aderan area, S.W. Nigeria. *Journal of Geography and Geology; Volume 5, Number 1*. Published by Canadian Center of Science and Education

Okonkwo, C.T and Ganev, (2012). U-Pb Geochronology of the Jebba Granitic Gneiss and its Implications for the Paleoproterozoic Evolution of Jebba Area, Southwestern Nigeria. *International Journal of Geosciences, 1065-1073*

Okonkwo, C. T. and Winchester . J. A. (1996). Geochemistry and Geotectonic Setting of Precambrian Amphibolites and Granititc Gneisses in the Jebba Area, Southwestern Nigeria. *Journal of Mining and Geol*olgy. Volume 32(1), pages 11–18.

Okunlola, O. (2008). Deformation and mineralisation in the Basement Complex of Nigeria. *33rd International Geological Congress, Oslo.* http://www.cprm.gov.br/33IGC/1199807.html

Okunola, O.A and Okoroafor, R.E. (2009).Geochemical and petrogenetic features of schistose rocks of the Okemesi fold belt, Southwestern Nigeria. Materials and Geoenvironment, Volume 56, Number 2, pages 148-162, 2009 148

Okunlola, O.A; Adeigbe, O.C and Oluwatoke, O.O. (2009). Compositional and Petrogenetic Features Of Schistose Rocks Of Ibadan Area, Southwestern Nigeria. Earth Science Researcch Journal Volume 13, Number 2: 119-133.

Olade, M.A., (1978). General features of a Precambrian iron ore deposit and its environment at Itakpe ridge, Okene, Nigeria. Intitute of Mining and Metallurgy. Volume 87. pB1-B7.

Olade, M,A, and Elueze, A.A. (1979). Petrochemistry of the Ilesha amphibolite and Precambrian crustal evolution in the Pan-African domain of SW Nigeria. Precambrian Res 8:303–318.

Olanrewaju, V.O. (1981). Geochemistry of the charnockitic and granitic rocks of the basement Complex around ado-Ekiti-Akure, S.W. Nigeria. Unpubl. Ph.D. thesis, University of London. 383 pages.

Olanrewaju, V.O. and Rahaman, M.A. (1982). Petrology and geochemistry of the Older Granites from some parts Northern Nigeria. Journal Mining and Geology Volume 17 Number 2.

Olujide, P. O. and Udoh, A. N. (1989). Preliminary comments on the fracture systems of Nigeria. *In Proceedings of the National Seminar on earthquakes in Nigeria (Ed.) Ajakaiye D. E; Ojo S. B. and Daniyan M. A. 97-109.*

Oluyide, P.O. (1988). Structural Trends in the Nigerian Basement Complex. In: P.O. Oluyide. Precambrian Geology of Nigeria. *Geol. Surv. Nigeria: Lagos, Nigeria. 93-98.*

Onyeagocha, A. C., 1979. The Mallam Tanko Serpentinite Petrology and Economic Implication, Journal of Mining and Geology 16(1)37-40.

Onyeagocha, A.C. (1986). Geochemistry of Basement granitic rocks from northcentral Nigeria. *Journal of Mining and Geology,* 19/2, pages 62–68.

Oyawoye, M.O. (1972). The basement complex of Nigeria. In: T. F. J. Dessauvagie and A. J. Pan-African Orogeny in Northern Nigeria. *Geological Society of America Bulletin, November 1971, volume 82, pages 3251-3262.*

Pearce, M., Gorman, B.E. and Birkett, T.C. (1975). The Relationship between Major Element Chemistry and Tectonic Environment of basic and intermediate Volcanic Rocks. *Earth Science Letter*; Volume 36, pages 121–132.

Rahaman, M. A. (1976). Review of the basement complex of Nigeria in: Kogbe, C. A. (ed) Geology of Nigeria. *Elizabethan publishing Lagos, Nigeria, 514.*

Rahaman, M.A. (1981). Recent advances in the study of the basement complex of Nigeria. *Abstract, 1st Symposium on the Precambrian Geology of Nigeria.*

Rahaman, M.A. (1988). Recent advances in the study of the basement complex of Nigeria. *In: Geological Survey of Nigeria (ed) Precambrian Geology of Nigeria, pages 11–43.*

Rahaman, M.A., Ajayi, T.R., Oshin, T.O. and Asubiojo, F.O.I. (1988). Trace Element Geochemistry and Geotectonic setting of Ile-Ife Schist Belt. In Precambrian Geology of Nigeria. Geology Survey of Nigeria, Kaduna. pages 241-256.

Rahman, A.M.S., Ekwere, S.J., Azmatullah, M, and Ukpong, E.E. (1987). Petrology and geochemistry of granitic intrusive rocks from the western part of the Oban Massif, southeastern Nigeria. *Journal of African Earth Sciences*, 7 (1), pages 149-157.

Rollinson, H. R. (1993). Using Geochemical Data: Evaluation, Presentation and Interpretation. Longman, UK, 352 pages.

Rowan, L.C. and Bowers, T.L. (1995). Analysis of linear features mapped in Landsat Thematic Mapper and side-looking airborne radar images of the Reno, Nevada 1° by 2° quadrangle, Nevada and California-implications for mineral resource studies. *Photogrammetric Engineering and Remote Sensing*, Volume 61, 749-759.

Rudnick, R.L. and Gao, S. (2003). The Composition of the Continental Crust, pp. 1-64. In The Crust (ed. R.L. Rudnick) Vol. 3, Treatise on Geochemistry (eds. H.D. Holland and K.K. Turekian), Elsevier-Pergamon, Oxford.

Russ, W. (1957). The geology of parts of Niger, Zaria and Sokoto Provinces. *Geological Survey of Nigeria Bulletine 27:1–42.*

Shalaby, M.H., Bishta, A.Z., Roz, M.E. and El Zalaky, M.A. (2009). Singh A, Harrison A, Standardized principal components. International Journal of Remote Sensing 6, 883–896.

Shand, S. J. (1943). Eruptive Rocks. Their Genesis, Composition, Classification, and Their Relation to Ore-Deposits with a Chapter on Meteorite. *New York: John Wiley & Sons*.

Shaw, D.M. (1972). The origin of the Apsley Gneiss, Ontario. Canadian Jour. Earth Science 9, pages 18-27.

Shibayan, Y. (1985). Investigation of possible Chromite bearing Serpentinites and associated rocks of NW Nigeria. Unpublished MSc Thesis, Ahmedu Bello University, Zaria, Nigeria.

Sultan, M., Arvidson, R. E., Sturchio, N. C. and Guinness, E. A. (1987). Lithologic mapping in arid regions with Landsat thematic mapper data: Meatiq dome, Egypt. *Geological Society of America Bulletin, 99*(6), 748-762.

Talaat, M.R and Mohammed, F.A. (2010). Characterization of gold mineralization in Garin Hawal area, Kebbi State, NW Nigeria, using remote sensing. The Egyptian Journal of Remote Sensing and Space Science. Volume 13, Issue 2, Pages 153–163.

Taylor S.R, and McLennan S.M. (1995). The geochemical evolution of the continental crust. Rev. Geophys. 33, 241–265.

Tarney, J. (1977). Petrology, mineralogy and geochemistry of the Falkland Plateau basement Rocks, site 330, deep sea drilling project. Init. Rep. 36, p.893-921. .

Truswell, J.F. and Cope, R.N. (1963). The geology of parts of Niger and Zaria Provinces, Northern Nigeria. *Geol Suvey Nigeria Bull* 29:1–104.

Turner, D.C. (1983). Upper Proterozoic schist belts in the Nigerian sector of the Pan-African Province of West Africa. *Precambrian Res 21:55–79.*

Udo, R.K (1978). A Comprehensive Geography of West Africa. New York : Africana: Publishers and Company.

Ukwang, E.E., Ekwueme, B.N., Horsley, R.J. (2003). Petrology of granulite facies rocks in Ukwortung area of Obudu Plateau, southern Nigeria. — *Global Journal of Geological Sciences, 1/2, pp. 159–168.*

Weill, D.F, Drake, M.J. (1973). "Europium Anomaly in Plagioclase Feldspar: Experimental Results and Semiquantitative Model". Science 180 (4090): 1059–1060.

van de Kamp, P.C. and Leake, B.E. (1985). Petrography and geochemistry of feldspathic and mafic sediments of the northeastern Pacific margin. Transactions of the Royal Society of Edinburgh: Earth Sciences 76, 411–449.

Weaver, C.E. (1989). Clays, muds and shales. *Elsevier*; Amsterdam, 820 pages.

Wilson, M. (1989). Igneous Petrogenesis. London: Unwin Hyman.

Woakes, M., Rahaman, M.A. and Ajibade, A.C. (1987). Some metallogenetic features of the Nigerian basement. Journal of African Earth Sciences 6:54–64.

Wright, J.B. (1985). Geology and mineral resources ofWest Africa. George Allen & Unwin, London, 187 pages 111-123.

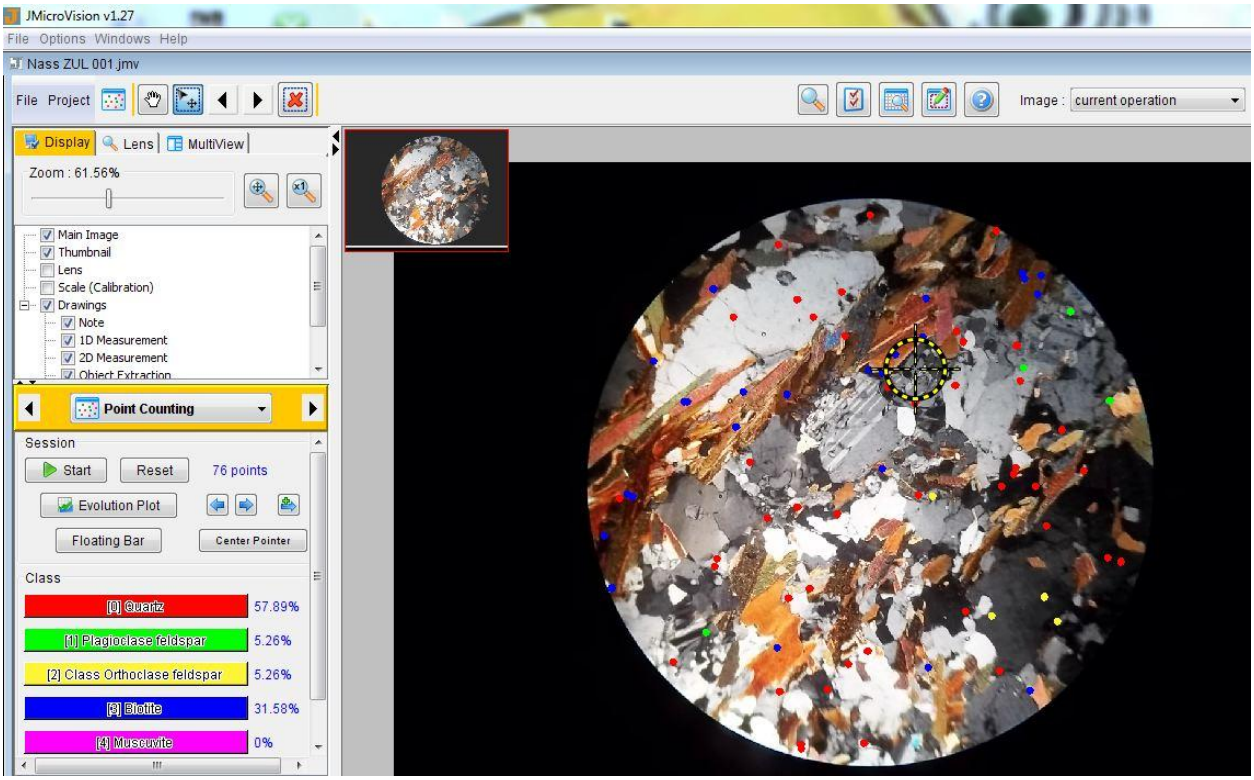
Yousif, M.S.M. and Shedid, G.A. (1999). Remote sensing signature of some selected basement rock units from the central eastern desert of Egypt.*Egypt. Journal of Remote Sensing and space Science*, volume 1, 132-141. 515-517.

Zoheir, B. and Emam, A. (2012). Integrating geologic and satellite imagery data for highresolution mapping and gold exploration targets in the South Eastern Desert, Egypt. Journal of African Earth Sciences 66–67, 22–34.

APPENDIXES

APPENDIX I

Point counting with JMicrovision software



APPENDIX II

Trend of foliation in gneisses in degrees (°)

022	018	020	024	010	022	022	024	030	040	032	032	034
046	116	120	160	162	176	178	178	022	020	032	020	018
034	038	040	028	022								

APPENDIX III

Trend of foliation in metasediments (mica schist and phyllite) in degrees (°)

046	044	060	058	098	146	178	040	032	032	034	028	026
026	024	028	020	018	020	010	010	012	016	030	030	038

APPENDIX IV

Trend of longer axis of phenocrysts in porphyritic biotite granite in degrees (°)

046	022	024	058	020	040	032	032	034	028	026	026
024	028	020	018	020	010	010	012	016	030	030	

APPENDIX V

Joints on gneisses in degrees (°)

180	184	182	168	170	090	094	092	090	096	094	350	354
048	050	054	080	082	010	012	014	350	350	090	088	100
010	020	098	102	182	184	014	050	054	184	016	010	046
088	086	190	192	036	046	010	018	022	016			

APPENDIX VI

Joints on schists in degrees (°)

090	092	090	094	176	170	090	090	092	180	092	094	120
090	092	094	082	096	090	182	176	180	098	092	094	270
276	280	280	176	172	180	180	170	180	172	360	80	090
090	350	360	360	210	260	260	270	340	350	350		

APPENDIX VII

Joints on granites in degrees (°)

090	088	086	092	046	044	136	138	140	136	140	138	086
134	136	088	090	092	094	090	092	130	136	136	138	182
122	138	140	090	092	092	094	092	046	044	092	094	088
088	048	100	036	036	038	030	032	034	034	036	040	040
050												